

DISSERTATION

THE TOPOLOGY AND ECOHYDROLOGY OF RIVER CORRIDORS
IN MOUNTAIN RIVER NETWORKS

Submitted by

Alexander C. Brooks

Department of Ecosystem Science and Sustainability

In partial fulfillment of the requirements

For the Degree of Doctor of Philosophy

Colorado State University

Fort Collins, Colorado

Spring 2022

Doctoral Committee:

Adviser: Tim Covino

Ryan Morrison

Chuck Rhoades

Matt Ross

Ellen Wohl

Copyright By Alexander C. Brooks 2022

All Rights Reserved

ABSTRACT

THE TOPOLOGY AND ECOHYDROLOGY OF RIVER CORRIDORS IN MOUNTAIN RIVER NETWORKS

River corridors are comprised of the river, the surrounding valley and riparian areas, and subsurface hyporheic zones. River corridors have the potential to regulate hydrological, biogeochemical, and ecological processes and patterns from reach to watershed scales. Within mountainous landscapes, narrow sections of the river corridor are often interspersed within wider, yet less frequent, river corridor sections. Reach-scale studies (i.e., 1 km) suggest that wide river corridors, also referred to as river-floodplain systems and river beads in this dissertation, have disproportionate impacts on river network behavior. In chapter one, I introduce the concept of river corridors, briefly review the history of the concept's development, the hydrologic and eco-geomorphic factors that drive functioning in these systems, and alterations driven by anthropogenic activities.

In chapter two, as a first step to deepening understanding of the influence of river network valley morphology on watershed process, I quantify the spatial distribution of wide and narrow river corridor segments in twenty river networks in the Southern Rockies Ecoregion. I then characterize the spatial configuration of river beads including their frequency, abundance, and spacing. These results reveal variable network topology of river beads in the region and illustrate the need to consider network position when investigating functioning in these systems. I conclude that characterizing river bead configurations can improve river network understanding and aid decision making in prioritizing conservation and restoration efforts.

In chapter three, I explore water-mediated linkages, termed hydrologic connectivity, that connect landscape components within an intact beaver mediated river-floodplain system in Rocky Mountain National Park. I evaluate surface water hydrologic connectivity using field indicators and develop a continuous connectivity metric that represents a vector strength between a source along the North St Vrain river to ten surface water target sites within the river-floodplain system. To measure this connectivity strength, I analyzed hydrometric, injected conservative tracers, and natural occurring geochemical and microbial tracers across streamflows in 2018. I developed empirical models of surface water hydrologic connectivity as a function of river stage to predict daily connectivity strength across multiple floodplain sites for 2018 and assessed the sensitivity of surface connectivity to inter-annual streamflow variability between 2016-2020. At the river-floodplain system scale, I found hydrologic connectivity always increased with streamflow while across-system variance in connectivity peaked at intermediate streamflow. At sites with intermittent connections to the river, river stage disconnection thresholds were variable and their connectivity dynamics were sensitive to inter-annual variation in streamflows, suggesting that future connectivity behavior under climate change will depend on how flow durations change across a range of flow states. These results suggest that the intermediate flows are critical periods for understanding seasonal connectivity within river-floodplain systems. Accordingly, our results suggest that alteration to connectivity regimes as dictated by future hydrologic change will be in part a function of the speed at which streamflow moves from peak to low flow states.

In chapter four, I examine the spatial patterns in land cover within the Southern Rockies Ecoregion and assess the implications of wetland cover on river corridor productivity and the sensitivity of productivity to inter-annual climate variability across geographic and climatic gradients in the region. We found that wetlands, which comprise today only around a third of river corridor area, maintain high productivity even in river corridor segments within water limited landscapes. However, degradation in wetlands and the loss of woody cover create river corridors with high sensitivity to climate variability,

particularly in areas with lower climatic water availability. Wetlands with woody cover were clustered in proximity to rivers and maintain relatively low climate sensitivity even in more water limited landscapes. Vegetation productivity and sensitivity patterns in river corridors without wetlands were largely driven by climatic water availability. Areas with high water availability generally contained forested cover with high productivity and low climate sensitivity while water limited areas generally contained shrub lands and grasslands cover with low productivity and high climate sensitivity. These results suggest that wetland loss and/or degradation have resulted in losses in productivity and climate resilience, particularly within more water limited portions of the region.

ACKNOWLEDGMENTS

I am deeply fortunate to have the support and guidance of many during my dissertation work. Many thanks to my PhD advisor, Tim Covino, for being a patient, steady guiding force in this research, and for giving me the funding, opportunities and space to explore new ideas while also being there to help me pull all those ideas into cohesive results and manuscripts. Thank you to Matt Ross, for being a mentor and friend throughout my graduate experience and for input along the way that has greatly improved this work through our many walks, meetings and brainstorming sessions. Thank you to Ellen Wohl, for providing ideas and questions about the functioning of river corridors that sparked my interest in the subject and underpinned many of the ideas explored in this dissertation. Thank you to both Ryan Morrison and Chuck Rhoades for contributing many ideas that added to the research and for connecting me to resources that made this work possible. Thank you to my collaborators and co-authors. Ed Hall, thank you for the ideas and support that made possible the work on microbial indicators of hydrologic connectivity. Thanks to Xiao Yang and Antonino Annis for developing tools and providing technical assistance that were essential to this research. Thank you to Tim Fegel, Kristen Otto and the Rocky Mountain Research Station lab for your assistance with chemical and microbial analyses. Thank you to my many field volunteers and especially to my undergrad technicians and mentees Danielle Palm, Spencer Rhea, Connor Lockwood, Chris Sunblade, Evan Mann who tackled whatever challenges I threw at them and inspired me with their curiosity and dedication to the work. Thank you to Scott Esser and the rest of the team at Rocky Mountain National Park for your logistic support, housing and permission to conduct our field research in the national park. Thank you to funders including a NASA National Earth and Space Science fellowship (#80NSSC18K1348), and grants from National Science Foundation Division of Earth Sciences (#1632798 & #1945504), the United State Department of Energy Subsurface Biogeochemistry Research (#0000241776) and the Colorado Water Center. A great thanks to the many

dog-sitters who took great care of our dog Louie while I was off doing field work. To my fellow grad students, John, Tristan, Abby, Karin, Allie, Eric, Juli, Rosie, Ethan, Beth, et al., nothing has been more fun these past years than grabbing a beer and nerding out with all of you about science. Thank you to my family including my parents Sandra and Dana, my brothers Daniel & Jonathan, and my aunts, uncles, and in-laws, whose love, support and curiosity inspired me and kept me motivated even when the end seemed a long ways off. Finally, thank you to my wife, Natalia for supporting me through the ebbs and flows of my graduate school journey, and making my life outside of work full of joy, fulfillment and love.

DEDICATION

To the many generations of my family who fostered my love of science, exploration, critical thinking and justice and taught me to love the world while remaining curious about its truths. To my daughter Raffaella. May this work inspire you to pursue your interests wherever they take you and give you the confidence to share those efforts with the world.

TABLE OF CONTENTS

ABSTRACT..... ii

ACKNOWLEDGMENTS..... v

DEDICATION vii

CHAPTER 1 – INTRODUCTION 1

 1.1 Background on the development of the river corridor concept..... 1

 1.2 Geomorphology and Hydrology within River Corridors..... 2

 1.3 Anthropogenic Impacts on River Corridors..... 4

CHAPTER 2 - RIVER BEADS IN THE NETWORK: IDENTIFYING THE SPATIAL CONFIGURATION OF WIDE RIVER CORRIDORS IN MOUNTAIN RIVER BASINS 6

 2.1 Introduction 6

 2.2 Methods..... 8

 2.2.1 River Corridor Delineation 9

 2.2.2 River Corridor Width Measurement 10

 2.2.3 Landcover Extraction 11

 2.2.4 River Bead and Bead Type Identification 12

 2.2.5 River Bead Statistics 13

 2.2.6 Comparison to Field Mapped River Beads..... 14

 2.2.7 Predicting Basin-Scale Bead Network Statistics Using River Gradient..... 15

 2.2.8 Metrics for Assessing Network Context and Relative Influence of River Beads..... 16

 2.3 Results..... 17

 2.3.1 River Bead Network Position 18

 2.3.2 Spacing and Length of River Beads 19

 2.3.3 Spacing and Length of Wetland Beads..... 20

 2.3.4 Predicting River Bead Configurations at the Basin Scale 20

 2.3.5 Network Context of River Beads Along Poudre Mainstem..... 21

 2.4 Discussion..... 22

 2.4.1 Methodological Considerations 23

 2.4.2 The Role of Network Context and River Bead Configuration 25

 2.5 Conclusion..... 27

CHAPTER 3: EVALUATING SPATIAL AND TEMPORAL DYNAMICS OF RIVER-FLOODPLAIN CONNECTIVITY SURFACE WATER USING HYDROMETRIC, GEOCHEMICAL AND MICROBIAL INDICATORS.....	43
3.1 Introduction	43
3.1.2 Study Overview	44
3.2 Methods.....	45
3.2.1 Site Description	45
3.2.2 Hydrometric Field Measurements and Conservative Tracer Injection	46
3.2.3 Incorporating Microbial Indicators of Hydrologic Connectivity.....	47
3.2.4 Field Sample Collection and Lab Analysis	48
3.2.5 Connectivity Strength Metrics	49
3.2.6 Metric Evaluation	52
3.2.7 Sensitivity Analysis of Surface Connectivity to Inter-Annual Variability in Streamflow	53
3.3 Results.....	54
3.3.1 Hydrometric Monitoring and Tracer Experiment:	54
3.3.2 Seasonal Dynamics in Aqueous Geochemistry and Microbiome Membership	57
3.3.3 Comparison of Connectivity Metrics.....	59
3.3.4 Connectivity Regimes.....	60
3.3.5 Sensitivity of Floodplain Surface Connectivity to Inter-Annual Variability in Streamflow .	61
3.4 Discussion.....	62
3.4.1 Connectivity Strength as a Continuous Measure.....	63
3.4.2 Microbiomes as Complementary Sources of Connectivity Information.....	64
3.4.3 Connectivity Regimes: Scaling from Site to System Scales	66
3.4.5 Inter-Annual Variability in Connectivity at Site-Specific and River-Floodplain System Scales	67
3.4.6 Limitations and Recommendations for Future Research	68
3.5 Summary	70
CHAPTER 4: ECOHYDROLOGY IN THE RIVER CORRIDOR: INVESTIGATING THE INTERDEPENDENT EFFECTS OF WETLANDS, CLIMATE, HUMAN DISTURBANCE AND TOPOGRAPHY ON PRODUCTIVITY AND CLIMATE SENSITIVITY OF VEGETATED MOUNTAIN RIVER CORRIDORS	83
4.1 Introduction	83
4.2 Methods.....	85
4.2.1 Study Region	85
4.2.2 River Corridor Delineation and Generation of River Corridor Polygon Segments.....	86
4.2.3 Land Cover, Climate and Elevation	87

4.2.4	Identifying Trends in River Corridor Land cover Patterning	88
4.2.5	Productivity and Climate Sensitivity in Wide River Corridors.....	89
4.2.6	Productivity and Sensitivity in Wetland and Vegetated Non-Wetland RC Segments.....	90
4.2.7	The Role of Compounding Historic Disturbances: A Case Study in Rocky Mountain National Park.....	92
4.3	Results.....	93
4.3.1	Productivity and Climate Sensitivity in Wide River Corridors.....	95
4.3.2	River Distance Structuring of Wetlands, Productivity and Climate Sensitivity in Wide River Corridors at Segment Scales	96
4.3.3	Rocky Mountain National Park Case Study.....	97
4.4	Discussion.....	98
4.4.1	The Implications of Wetland Occurrence on Productivity and Resilience in River Corridors	98
4.4.2	Spatial Patterning in River Corridors.....	101
4.5	Conclusion.....	102
CHAPTER 5 – CONCLUSION.....		115
5.1	Key Findings and Implications.....	115
5.2	Opportunities for Future Research.....	117
REFERENCES.....		119
APPENDIX 1 - SUPPLEMENTAL INFORMATION – CHAPTER 2		130
APPENDIX 2 - SUPPLEMENTAL INFORMATION – CHAPTER 3		132

CHAPTER 1 – INTRODUCTION

River corridors are comprised of rivers, adjacent riparian areas and subsurface hyporheic zones. Collectively, these zones form alluvial habitats that influence both aquatic (Harvey and Gooseff, 2015) and terrestrial systems (Hauer et al., 2016). Along mountainous river networks, river corridors can be confined to narrow valley bottoms with limited floodplains or extend laterally in lower gradient valley bottoms that enable the development of broad floodplains, hyporheic zones, and river corridor wetlands (O'Brien et al., 2019; Wohl et al., 2017). This research will focus primarily on these wider zones in river corridors, which I will refer to in this research as wide river corridors, river-floodplain systems or river beads.

While all three terms are mostly interchangeable, in this research, I will use wide river corridors as a generic term, while I use river-floodplain system and river beads in different chapters to emphasize differing aspects of river corridor functioning. River-floodplain system is a term that emphasizes that functioning within rivers and floodplain ecosystems are regulated by their lateral hydrologic connectivity (Junk et al., 1989). In contrast, the term river bead describes the longitudinal patterning of narrow and wide river corridor segments. From a planform perspective, wide river corridor segments appear 'like beads on a string' (Stanford & Ward, 1993a). Thus, the term river bead places an emphasis on network scale patterning and longitudinal impacts of wide river corridors (Wohl et al., 2017). Through this research, I will emphasize both the lateral and longitudinal relationships within river corridors and thus use both terms when appropriate.

1.1 Background on the development of the river corridor concept

The concept of the river corridor is rooted in three theoretical developments of the late 1980s. In this era, river scientists were beginning to incorporate the role of floodplains into ecologic conceptual

models of longitudinal patterns in stream networks (Junk et al., 1989), began to recognize the role of connectivity between rivers and their landscapes on river ecology (Ward , 1989), and began to view streams in a hierarchical framework that highlighted how river habitats are strongly associated with the geomorphic features of their watersheds (Frissell et al., 1986). These concurrent conceptual advances were all evolving from and responding to both Hynes' view that the river channel both influences and is influenced by other components within the catchment (Hynes, 1975) and to the River Continuum Concept (RCC) (Vannote et al., 1980) which describes broad longitudinal resource patterns along river networks from headwaters to outlets. Building on these concepts, the hyporheic corridor concept was developed that added stream-aquifer interactions to this list of key interactions affecting longitudinal river network patterns (Stanford & Ward, 1993a). These new perspectives collectively argued that geomorphic features and processes within river networks can drive interactions between rivers and floodplains and/or groundwater that can modulate or even override spatial patterns predicted by the RCC. Collectively, they also highlighted the disproportionate effects of wider, alluvial segments and floodplains (aka river beads) on river network dynamics. Thereby spearheading work starting in the 1990s that continues today to understand, predict and restore geomorphic, hydrologic and ecologic structures, processes and functions within river corridors (Harvey & Gooseff, 2015; A. S. Ward & Packman, 2019; Wohl et al., 2017).

1.2 Geomorphology and Hydrology within River Corridors

The key morphological feature of wide river corridors is the presence of a river segment with an unconfined valley bottom with low lying, less steep terrain compared to nearby topography (Gallant & Dowling, 2003). There are multiple, interacting geologic processes that can generate un-confinement in valley bottoms including longitudinal variation in bedrock lithology, jointing, responses to base level changes, glaciation, confluences and inherited landscapes (Belmont, 2011; Ferguson et al., 2006;

Notebaert & Piégay, 2013; Wohl, 2014; Wohl et al., 2021). As these geologic processes occur at long timescales relevant to present-day processes, spatial configuration of wide corridors within river networks are largely invariant except for the influence of anthropogenic disturbances. Despite an understanding of the geomorphic factors creating wide river corridors, their spatial configuration and topology in river networks is not well understood at regional scales. In chapter two, I address this gap by quantifying the width of river corridors and developing an approach to identify the configuration of river beads throughout river basins in the Southern Rockies Ecoregion.

Hydrologic and eco-geomorphic interactions between the river and the floodplain generate highly variable surface topography and subsurface stratigraphy in intact river-floodplains (Poole et al., 2002). Channel migration, bank avulsions, and flooding occur repeatedly in these systems, causing net aggradation and sporadic erosional events that create complex surface geomorphology (Wohl & Iskin, 2019). These processes often bury and uncover relic surface water features. In glaciated gravel and cobble-bed rivers, this process generates paleochannels, which are a lattice of high porosity subsurface layers that rapidly route water and materials through the subsurface, creating expansive hyporheic zones (Stanford and Ward 1993). Feedbacks between geomorphologic process and vegetation also result in a tight coupling between the geomorphic evolution of these systems and the development of patchy mosaics of vegetation and wetlands that exhibit highly variable hydrologic conditions (Bywater-Reyes et al., 2017; Loheide & Gorelick, 2007; Poole et al., 2002) .

In many river basins including those of the Southern Rockies Ecoregion, two key biotic mechanisms also generate and maintain geomorphic heterogeneity and lateral connectivity: large wood and beaver activity. In rivers flowing through forested ecosystems, wood loads delivered to streams form channel spanning log jams that can act as agents of storage and geomorphic change (Collins et al., 2012). Log jams can correspond to more physical diversity of channel planforms, increase hyporheic exchanges, promote overbank flow, retain sediments and organic matter , reduce stream power, and

increase water tables in adjacent floodplains (Doughty et al., 2020; Lininger et al., 2019; Livers & Wohl, 2016; Wohl, 2013a).

Beavers, through their dam building and channel digging activities, create similar effects in channels while also shaping river beds into a distinct landform known as beaver meadow complexes (Pollock et al., 2014; Polvi & Wohl, 2012). These complexes, which form from repeated cycles of beaver activity and subsequent abandonment (C. J. Westbrook et al., 2011) create a mosaic of surface features including anastomosing channels, river connected and isolated ponds, wetlands, and spring brooks. Hydrologically, these complexes often force bi-directional flows of water between the river and the floodplain that regulate physical, biogeochemical (Covino, 2017) and biological processes (Amoros & Bornette, 2002). Characterizing this hydrologic connectivity requires approaches that can identify connectivity across single or multiple dimensions and identify the strength, directionality and duration of connectivity between portions of the landscape (Ali et al., 2018). In chapter three, I develop new approaches using hydrologic, geochemical and microbial indicators to quantify the spatial and temporal dynamics of surface hydrologic connectivity within a beaver-influenced river-floodplain system.

1.3 Anthropogenic Impacts on River Corridors

Anthropogenic activities have caused alterations to river corridors with as much of 90% of floodplains 'functionally extinct' due to water management of river systems and cultivation within floodplain areas in Europe and the United States (Tockner & Stanford, 2002a). In mountainous regions where unconfined river corridors are relatively rare, degradation in river corridors has been compounded by both legacy and ongoing impacts including the extirpation of beaver and predators from the landscape (Beschta & Ripple, 2012), flow and sediment regulation (Kuiper et al., 2014), agriculture and ranching (Trimble & Mendel, 1995), placer mining, development and related infrastructure including levees, ditches, roads and railways (Karpack et al., 2020; Wohl, 2006). One of

the consequences of such impacts has been the widespread loss of wetlands and lateral hydrologic connectivity within these river corridors (Krause et al., 2011; Lee Foote et al., 1996; Rajib et al., 2021). As the ecosystem services provided by wetlands and connected floodplain have been more widely understood (Wohl et al., 2021), there has been growing interest in restoring functionality in more degraded river-floodplain systems (Fesenmyer et al., 2018; Pollock et al., 2014; Silverman et al., 2019). Within this context, in chapter four, I examine the spatial patterns in land cover within the Southern Rockies Ecoregion and assess the implications of wetland cover on river corridor vegetation productivity and climate sensitivity across geographic and climatic gradients in the region.

CHAPTER 2 - RIVER BEADS IN THE NETWORK: IDENTIFYING THE SPATIAL CONFIGURATION OF WIDE RIVER CORRIDORS IN MOUNTAIN RIVER BASINS¹

2.1 Introduction

River corridors are comprised of rivers, adjacent riparian areas and subsurface hyporheic zones. Together they form alluvial habitats that influence hydrologic process, water quality, and provide important ecosystem services (Harvey & Gooseff, 2015). Shaped by interactions between fluvial and terrestrial systems, river corridors simultaneously act as zones that regulate transport, storage and reactions of water, solutes, sediment in river networks (Pinay et al., 2018; Wohl & Scott, 2017) and serve as critical habitat that promotes both aquatic and terrestrial biodiversity (Amoros & Bornette, 2002; Hauer et al., 2016). River corridor functions and influence are controlled by interactions between their geomorphology, hydro-climatic setting, landscape position and degree of anthropogenic influence (Montgomery, 1999; Steiger et al., 2005; Tomscha et al., 2017). One of the key geomorphic constraints on river corridor function is the valley width (Bellmore & Baxter, 2014; Livers & Wohl, 2016), which sets a maximum constraint on river corridor size and is related to river size, planform, and slope (Belmont, 2011; Brierley & Fryirs, 2000). These corridor controls are commonly modified by people through interventions such as terrain modification, levees, channelization and flow regulation (Gendaszek et al., 2012; Nardi et al., 2018; Wohl, 2006). Historically, functioning in river corridors was also related to the widespread presence and persistence of wetlands that often occur in wider, unconfined reaches with high lateral hydrologic connectivity and elevated water tables (J. V Ward & Stanford, 1995). However, wetland pervasiveness has been greatly diminished by anthropogenic disturbances, resulting in the widespread alteration of river corridor functioning (Wohl et al., 2021).

¹ This chapter is in review at *Earth Surface Processes and Landforms*: Brooks, A.C., Covino, T., Ross, M.R.V, Morrison, R.M., Yang, X., Wohl, E. (2022). *River Beads in the Network: Identifying the Spatial Configuration of Wide River Corridors in Mountain River Basins*

River networks are generally thought to exhibit broad longitudinal patterns, with river corridor widths scaling with river size. Superimposed on this scaling pattern are local discontinuities that can generate segments with river corridor widths that are substantially narrower or wider than neighboring portions of the river network (J. V. Ward & Stanford, 1995). Increasing river width and discharge of downstream rivers generally result in wider river corridors, as does concavity in longitudinal river profiles that generate steeper segments in headwaters and flatter valleys lower in the river network (Khan et al., 2021). Local deviations from this broader trend can be the product of interactions between: longitudinal variation in bedrock lithology, jointing, responses to base level changes, glaciation, confluences and inherited landscapes (Belmont, 2011; Ferguson et al., 2006; Notebaert & Piégay, 2013; Wohl et al., 2021), as well as human modifications which can generate additional spatial variability or conversely homogeneity in longitudinal patterns within river corridors (Nardi et al., 2018; Scheel et al., 2019; Wohl, 2006).

In mountain river networks that are comprised predominantly of low-order, high-gradient streams, the alternating pattern of narrow segments and relatively rare wider segments has been described as analogous to beads on a string (Stanford & Ward, 1993b). Recent conceptual and empirical work has reinforced focusing on these wide segments (henceforth referred to as river beads) in contrast to narrow segments (henceforth referred to as river strings) because of the disproportionate role of wide segments in influencing critical ecosystem services such as flood control, water quality and ecosystem health (Wohl et al., 2017). Many initial research efforts have focused on quantifying specific hydrologic, geomorphic and biogeochemical functions within a single river bead (eg. Helton et al., 2014); among several river beads across different branches of a river basin (eg. Lynch et al., 2019), between beads to string segments (eg. Bellmore & Baxter, 2014; Livers & Wohl, 2016; Sutfin et al., 2021), or pre/post restoration efforts in river beads (eg. Hunt et al., 2018; Roley et al., 2012; Sparacino et al., 2019). These efforts typically do not consider interactive effects between bead segments, leaving a gap

in our understanding of how river bead functions accumulate and interact across the full river network (Wohl et al., 2017). Similarly, river restoration efforts often target a single or a select number of reaches for restoration without considering the context of how reaches interact with the upstream and downstream portions of the network (Bernhardt & Palmer, 2011). This lack of considering network and cumulative impacts of river beads partially comes from the fact that we don't have basic understanding of how beads and strings are structured. As such, better approaches are needed to both describe configurations of river beads in a river network and how a single or multiple river beads might be important within restoration or management contexts.

Quantifying river corridor widths across the network is a first step toward moving past the single segment scale toward conceptualizing how the spatial structure and topology of widths may influence larger scale process and pattern. Previous efforts that focus on river corridor width (or similar metrics including floodplain and valley bottom width) have been focused on understanding regional and local controls on width (Belmont, 2011; Notebaert & Piégay, 2013) and/or on describing scaling behavior (Gangodagamage et al., 2007; Nardi et al., 2006). Very few studies have attempted to characterize river corridor widths, including their distribution patterns, throughout a large-scale river network (although see Notebart & Piegay, 2013).

Here we develop a methodology using currently available geospatial tools to identify river beads from a river corridor width dataset. We then use the methodology to describe river bead distributions within 20 mountain river networks in the Southern Rockies Ecoregion.

2.2 Methods

To identify river beads, we first needed to generate a definition of a river bead that could be operationalized through a geographic information systems (GIS) approach at network scales. As such, we defined river beads as a *contiguous longitudinal segment of a river network with river corridors*

above a specified width threshold. We further differentiated two types of river beads. Hydro-geomorphic beads include all sections of the river network that exceed the specified width threshold. Wetland beads exceed the width threshold but simultaneously exceed a specified wetland cover threshold. River strings were defined as all river network segments below the specified *river corridor width threshold.* Identifying river bead locations and types required four steps in our GIS workflow: (1) delineation of the river corridor, (2) measurement of river corridor widths, (3) extraction of river corridor land cover, and (4) identification of rivers beads in the network using river corridor width and landcover thresholds (Figure 1).

To apply our developed river bead identification workflow and assess spatial patterns across different network configurations, we delineated river beads and river bead type within twenty river basins of the Southern Rockies Ecoregion (Figure 2). The Southern Rockies Ecoregion encompasses 138,854 km² of mountainous terrain within Colorado, New Mexico and Wyoming in the United States, with terrain ranging from foothills to high peaks. In the region, there are large gradients in elevation (1142 m to 4399 m), precipitation (250-1000 mm) and a large diversity in geologic history relating to the evolution of seven predominantly north-south mountain ranges (Drummond, 2012). Basins for this study were chosen to represent a range of basin sizes, lithology and climate and all had mainstream rivers that were 4th order or larger at the intersecting boundary of the ecoregion.

2.2.1 River Corridor Delineation

River corridors were delineated using the GFPLAIN tool, a hydro-geometric approach that relies on terrain analysis of a digital elevation model (DEM) and scaling behavior between flood height and catchment area (Nardi et al., 2006, 2019). Given this specified flood height above the stream, GFPLAIN identifies the spatial extent of flooded areas. Although this and similar hydro-geomorphic delineation

approaches have been used to delineate floodplains with specified flood magnitudes and/or full valley bottom extents (Gilbert et al., 2016; Nardi et al., 2018), our goal was instead to delineate regions that are likely to be hydrologically connected to a river, which we will here refer to as the river corridor (RC).

We used a USGS 3DEP 1/3 arc-second DEM that we conditioned for hydrologic routing with manually corrected flowlines from the National Hydrography Dataset Plus Version 2 (NHDPLUSv2) into the DEM, using a decay coefficient that imposes a gradient towards the stream (Lindsay, 2018). Prior to conditioning, NHDPLUSv2 flowlines were filtered for stream and artificial paths. Also, where multithread segments were present, the main flowpaths were simplified to a single flowline. Flowlines were also manually corrected using visual comparisons to satellite imagery to correct major misalignments with the river network, which is a known problem with the NHDPLUSv2 dataset (Hughes et al., 2011). This conditioned DEM was used only for the portion of GFPLAIN tool that identifies the stream network. The raw DEM was then used as input for the flooding extent procedure because elevations of the conditioned DEM are modified to unrealistic values by the conditioning process. River corridors were then delineated for all portions of the river networks that had catchment areas above 5 km² (Figure 3). Following Annis et al. (2019), we chose scaling parameters for the flood height function that elsewhere represented a 500-1000 yr flood and varied the parameters based on stream order (1st-3rd order streams: $a = 0.01$, $b = 0.33$, 4-6th order streams: $a = 0.01$, $b = 0.30$). We then visually inspected the results to ensure the appropriateness of these values to our study system.

2.2.2 River Corridor Width Measurement

Once RCs were delineated, we adapted the RivWidthCloud tool (X. Yang et al., 2020) to automate extraction of centerlines and measure cross-sectional RC widths at points every 200 m along the centerlines throughout the delineated river corridors. RivWidthCloud identifies the centerline within

the delineated polygons using a skeletonization process and then prunes the resulting centerline to remove spurious branches. While beneficial, this process generated some gaps along the river network, particularly at locations with complex river corridor geometries, such as confluences. These gaps were filled later in the analysis through interpolation of measured values. Once centerlines were extracted, RivWidthCloud calculated the direction orthogonal to the local centerline, generated a cross-sectional line across the river corridor polygon, and calculated width along these orthogonal cross-sections. Width values were then assigned to the RC width points that were generated along the centerline (Figure 3).

2.2.3 Landcover Extraction

To extract landcover within the river corridor, we buffered the cross-sections by 75 m at every measured RC point (at 200 m intervals), generating a polygon that was 150 m in the longitudinal direction of the local centerline and had a variable width that was equal to the 1.5x the RC width at the measurement point to ensure the resulting polygon captured the full river corridor. The polygons were then intersected with the river corridor polygon to exclude area outside the RC (Figure 3). While the 75 m buffer was chosen to minimize overlap between polygons, due to the sinuosity of the RC centerline and/or at confluences of centerlines of two river corridor branches, polygon overlap did occur and thus we removed any polygon that overlapped with more than 5 other polygons. For each polygon, we extracted land cover from the 2016 National Land Cover Dataset (NLCD) (L. Yang et al., 2018) and extracted the water occurrence map from the Joint Research Center (JRC) Global Surface Water layer (Pekel et al., 2016).

At water bodies within the river networks, we observed elevated RC width measurements because RC width values reflected the water body width. While water bodies are important to river network functioning, to focus on non-inundated river corridors and to remove bias associated with the

inflated values of these areas, we removed any RC width measurements taken at areas with above 15% water coverage based on the JRC water layer, which was 2.7% of the total RC width measurements, resulting in a final RC width dataset with 97,785 measurements.

To consider RC characteristics as well as RC width, we calculated the wetland coverage (% of each buffered segment), including both woody wetlands and emergent herbaceous wetlands landcover classes in the NLCD dataset. Wetland cover is generally associated with lower human modification, and higher hydrologic connectivity and spatial heterogeneity and thus provides a good proxy for overall condition within RCs (Karpack et al., 2020; Wohl et al., 2021).

2.2.4 River Bead and Bead Type Identification

To move from point-based measurements of RC width to identification of river beads and strings, we needed to operationalize our definition of a river bead as a contiguous longitudinal segment of a river network with a wide river corridor. This required a multi-step process. We first generated a networked dataset using our RC width points, then we defined each point as a river bead or string using a chosen RC width threshold. Points were then aggregated longitudinally as contiguous bead or string reaches, with each reach assigned a unique ID. This procedure was then repeated at each of the 20 study basins.

To transform RC width points into a networked dataset, we snapped points with RC width and wetland coverage to the nearest flowline in the NHDPLUSv2 dataset. To ensure evenly spaced measurements along the network and reduce effects of outlier measurements, we linearly interpolated snapped RC width and wetland coverage measurements to points at every 100 m along each path level in the NHDPLUSv2 network and then smoothed the dataset by taking a rolling average with a 500 m window along each path level. Path levels were assigned using the `nhdplusTools` R package (Blodgett,

2018) and represent a hierarchy of main paths of water flow in the network (Whitaker et al., 2002). The result is that at each confluence in the network, there exists a major branch where the path level value propagates to the reach below the confluence and a minor branch whose path level value ends at the confluence (Figure 4).

In order to identify beads and strings, we used thresholds in RC width (T_{wid}) to classify all points as either a bead (width $> T_{wid}$) or a string (width $< T_{wid}$). We then classified points as wetland beads if they exceeded T_{wid} and also exceeded the specified wetland coverage threshold (T_{wet}). Longitudinally consecutive points with the same classification along each path level within stream orders were aggregated to reaches which were assigned a unique ID and classified as a river bead or sting. A reach ended where the following point was either the opposite classification, when the following point belonged to a higher stream order, or when the path level ended at a confluence with a more major branch of the river network (Figure 4). The procedure was repeated varying T_{wid} between 25 m to 1000 m while also varying T_{wet} between 0% to 80% (Figure 5).

2.2.5 River Bead Statistics

For every unique bead and string reach, we generated a dataset of attributes that describe the reach size (length, width, and area), network position, and their geomorphic attributes. The reach length was calculated as the length of the NHDPLUSv2 flowline through the reach, the mean RC width was the mean of the interpolated RC width measurements, and the reach RC area was the product of reach length and mean width. NHDPLUSv2 attributes were used for parameters including stream order, elevation, distance to outlet, and slope. Mean annual river discharge and river width were collected from the US Stream Classification System (US SCS) dataset (McManamay & Derolph, 2019). NHDPLUSv2 and US SCS contain attributes that are calculated for each COMID, which is a uniquely identified flowline

segment that typically represents the flowline between two confluences in a stream network. River bead and string reaches identified in our analysis can contain multiple COMIDs. As a result, for continuous parameters such as slope, elevation, distance to outlet, and mean annual river discharge, we calculated a mean value for each reach weighted by the flowline distance of COMID flowlines within the reach. For stream order, which is categorical, we assigned the reach with the stream order that was most prevalent by flowline length in the reach.

To further describe the spacing of river beads, we also calculated the downstream distance along the river network between river bead reaches. We used the *igraph* R package (Csardi et al., 2006) to generate a new directional network graph where additional network nodes were generated at the top and bottom of each bead and string reach. We then measured the distance along edges between nodes at the bottom of each river bead to the node at the top of the nearest river bead downstream in the network. If a river bead on a path level ended at a confluence where the path level or stream order also ends, the distance to the next downstream river bead can equal zero if the reach below the confluence is also a river bead (Figure 4).

In order to summarize basin scale network attributes of river beads, we calculated median, mean and skewness of distributions of reach length and network distance between beads for each basin. We then calculated the overall proportion of bead length to the overall network length. Finally, we calculated bead density as the count of beads in the basin divided by the overall network length. To identify how river bead configurations change by network position, we also calculated network attributes for each stream order in each basin.

2.2.6 Comparison to Field Mapped River Beads

We compared our results to a previously published dataset of river beads delineated using field surveys in portions of the St. Vrain and Big Thompson river networks within Rocky Mountain National Park (Wohl, 2013b) to better understand how our GIS approach compares to field-scale efforts. We made two comparisons with the field dataset. First, we compared our bead delineations to 11 beaver meadows identified through field mapping on the eastern side of the Rocky Mountain National Park. Second, we compared our results to an inclusive effort that mapped all river beads along 1st-3rd order streams in the North St. Vrain basin, which were defined through surveying as river corridor segments with widths 4x or greater than river width. To compare datasets, we calculate true positive rates (TPR) and false positive rates (FPR) across varying T_{wid} values. Note that despite the language of true and false positive, both datasets contain error and the analysis should be considered comparative rather than a validation of model performance.

2.2.7 Predicting Basin-Scale Bead Network Statistics Using River Gradient

We also explored whether the spatial distribution and configuration of beads in our study basins could be predicted with descriptors of basin-scale river gradient distributions. Because lower river gradient is commonly associated with wider river corridors, we hypothesized it may be a strong predictor of river bead network statistics. Using multiple linear regression, we modeled four bead network attributes including the bead length as percent of network length, bead density, median bead length and median distance between beads. We developed models individually for each predictor and each unique combination of the three predictor's variables: mean basin river gradient, the coefficient of variation of river basin gradient, and basin area. We hypothesized that the mean river gradient would be a strong predictor for metrics relating to the overall prevalence of river beads, and that including the coefficient of variation of the gradient would improve prediction of metrics relating to the alternating

pattern between bead and strings. Basin area was included to account for the expected pattern of increasing river corridor width at higher stream orders which are more likely to occur in larger basins. To identify the best model for each metric, we selected the set of predictor variables that minimized Akaike information criterion (AIC), which is an estimate of prediction error. To assess the model accuracy across metrics with differing scales, we compared the normalized root mean square error percentage (NRMSE%) using the mean of the observed response variable for normalization. To simplify this analysis, we only conducted the model fit on the results from a RC width threshold of 100 m ($T_{wid} = 100$) and included all hydro-geomorphic beads ($T_{wet} = 0$).

2.2.8 Metrics for Assessing Network Context and Relative Influence of River Beads

To evaluate the potential for river beads to affect river network processes, we quantified five metrics that may help describe the context of a river bead in the network and its potential influences on local and network scale dynamics: (1) river bead area; (2) river bead area normalized by upstream accumulate catchment area (RI_UAA); (3) river bead area normalized by mean annual flow (RI_QNA); (4) the ratio of river bead area to the total river bead area upstream in the network (RI_UBA); and (5) a ratio of unconfinement, calculated as $1 - \text{confinement}$ where confinement is defined as the ratio between river width and RC width (Roux et al., 2015)). We evaluated these five metrics using a case study along the mainstem of the Cache la Poudre River basin in Colorado, with a single set of bead delineation thresholds ($T_{wid} = 100$, $T_{wet} = 0$). Along the mainstem of all basins, we also evaluated the ratio of upstream accumulated bead area to upstream accumulated catchment area to identify if there were consistent scaling behavior in the total bead area as a proportion of catchment area.

All statistical analyses and figures were generated and conducted in R version 4.0.5. Geospatial analysis was conducted using ArcGIS Pro (GFPLAIN tool), Google Earth Engine (RivWidthCloud) in

combination with the sf (Pebesma, 2018) and raster R packages (Hijmans, 2021) and maps were generated with the tmap R package (Tennekes, 2018).

2.3 Results

River corridors were delineated for all 20 basins using the GFPLAIN tool for all portions of the stream network with catchment areas above 5 km². Total delineated river corridor area was 2817 km², which represents 4% of the total land area within the study basins. This matched well with a previous independent effort that found riparian zones accounted for 3.1% of the Southern Rocky Ecoregion land area (Salo & Theobald, 2016). As a result of the 5 km² minimum catchment size, river corridors were delineated for only 60% of the first-order stream network in the NHDPLUSv2 dataset, 96% of second-order streams and 100% of third and higher stream orders.

Distributions of RC widths were highly variable across the region and within individual basin river networks but also followed broad longitudinal trends with increasing RC width in lower portions of the network (Figure 5 & 6). Across the region, RC widths distributions were skewed right with a median width of 62 m and the interquartile range (IRQ) within 39 m to 114 m (Figure 6a). RC width distributions were variable between basins in the region with the smallest median RC widths in La Plata basin (med: 40 m, IRQ: 26-65 m) and the widest median RC widths in the North Platte basin (med: 118 m, IRQ: 65-259 m) (Figure 6b). RC widths also generally increased with catchment area up to 1000 km², above which no trend with RC width was observed. (Figure 6c). Despite this broad trend, there was high RC width variability across all catchment areas, reflecting the impact of local controls of RC width in river networks that are superimposed on the longitudinal patterns. RC width also generally decreased with increasing river slope but again substantial variability in RC width at a given slope was observed (Figure 6d).

Given the variability in RC widths, identification of river bead and string reaches in the network was highly sensitive to varying the width threshold that defined a river bead. Total river bead count and river bead densities varied over two orders of magnitude between the lowest threshold value ($T_{wid} = 25$ m, 6333 beads, 1.92 beads per 10 km) and the highest threshold value ($T_{wid} = 1000$ m, 64 beads, 0.0194 beads per 10 km), declining exponentially as T_{wid} increased (Figure 7a&b). Overall, beads accounted for between 0.5% ($T_{wid} = 1000$ m) and 90.1% ($T_{wid} = 25$ m) of the overall network length across all basins. Median reach length of beads was less sensitive to T_{wid} , with median lengths of between 1 km and 1.7 km for T_{wid} ranging from 50-1000 m, with a higher length of 3.5 km at $T_{wid} = 25$ (Figure 7c). The median distance between beads rose approximately linearly with T_{wid} from near 0 km at $T_{wid} = 25$ m to 3 km at $T_{wid} = 1000$ m (Figure 7d).

By contrasting delineated beads to the field mapped dataset, we found that our delineation approach agrees best with the field datasets when using T_{wid} values of 75 or 100 m and when identifying larger sized river beads and/or river beads at higher stream orders (Figure 8a). Using our geospatial delineation with T_{wid} values lower than 75 m, identified many river corridor segments as beads that were mapped as strings in the field dataset. In contrast, at T_{wid} values above 200 m, very few river beads were identified in our delineation as compared to the field datasets (Figures 8a & 8b).

For the remaining analyses, we either chose to use a set of three T_{wid} values [75,100,200] across which bead length as a proportion of network length varied substantially (38.3%, 27.5%, 12.1%, respectively) or simply a value of $T_{wid} = 100$ to explore in more detail the configuration and condition of river beads in the river networks.

2.3.1 River Bead Network Position

Across the study basins, 1st order followed by 2nd order streams dominated the river network length but the relative abundance of river beads in the upper portion of the network was dependent on the chosen T_{wid} (Figure 9). With a 75 m T_{wid} , in low order streams, bead length comprised a relatively high proportion of the low stream orders' network length (1st order: 23%, 2nd order: 37%), resulting in high total bead length relative to downstream portions of the network. Conversely, with a 200 m T_{wid} , beads were proportionally very rare in low order streams (1st order: 4%, 2nd order: 8%) while higher order streams maintained a relatively higher proportion of river beads and therefore river beads by total length were most abundant at 3rd and 4th order streams (Figure 9). Fifth and sixth order streams comprise far less of the total network length and thus despite having high RC widths, across all three chosen T_{wid} values (i.e., 75, 100, and 200m), total bead length in these higher order streams remained a small proportion of overall network's total bead length (Figure 9).

2.3.2 Spacing and Length of River Beads

The distributions of spacing of river beads within the study basins demonstrated strong positive skews that indicate high spatial variability in bead configuration in the river networks (Figure 10). Using the 100 m T_{wid} , within basins, median spacing (range: 0 to 1.5 km) was substantially lower than mean spacing (0.7-3.7 km) with all basins exhibiting strong positive skews in their distributions (skewness range: 1.5-4.7). One reason for this unevenness in spacing is that river beads are more common near confluences. Nearly 40% of beads had a distance of 0 km to the next bead, which indicates the bead ended at a confluence with a downstream bead. If beads were all equal sizes and equally spaced throughout the full network, bead spacing would have ranged between 2.8 to 12 km depending on the study basin. This is 2-13x higher than the observed mean spacing in the study basins and results from many upper portions of the river network containing no river beads.

Distributions of river bead lengths within the study basins also demonstrated strong positive skewness (skewness range across basins: 1.2-5.8) that indicate a high number of relatively short river beads and a small number of very long river beads (Figure 10). Using the 100 m T_{wid} , within basins, median bead length (range: 0.6 to 2.1 km) was substantially lower than mean bead length (1.2-3.7 km). As a result of the strong positive skew, a small number of long beads comprise a large portion of the overall bead length. Across the twenty study basins, the largest 9% to 18% of beads account for 50% of the total bead length in each river network.

2.3.3 Spacing and Length of Wetland Beads

We also evaluated the loss of wetland cover in wide valley segments by quantifying how river bead distributions change in the basin river networks when we eliminate beads below a wetland cover threshold (T_{wet}). To simplify the analysis we used a constant 100 m T_{wid} for this assessment. Only 1513 river beads met the strictest definition of wetland beads ($T_{wet} \geq 80\%$), a 59% decline from the total number of beads defined hydro-geomorphically (3712 beads when $T_{wet} = 0\%$). Similarly the proportion of total bead length to network length declined from 27.5% to 4.2% of the network (Figure 11). This results in a 225% increase in median distance between beads from 0.4 km to 1.3 km. The reduction from geomorphic to wetland beads is most dramatic in higher order streams where the proportion of wetland bead length to network length within the stream order falls most sharply as higher wetland thresholds are applied (Figure 11).

2.3.4 Predicting River Bead Configurations at the Basin Scale

Our efforts to predict across basin trends in river bead abundance and spacing suggest that basin scale metrics like river slope can describe broad trends in river bead abundance and length but may not be appropriate for describing spacing and patterning within the basins (Table 1, Figure 12). Our regression models that incorporated basin river slope and basin area performed well for predicting basin scale river bead statistics that relate more directly to RC width distributions within basins (% of network: NRMSE%: 20.6%, $R^2=0.78$; Bead Density: NRMSE%: 15.1%, $R^2=0.57$) but performed more poorly in predicting bead attributes that describe bead size and spacing (Median Bead Length: NRMSE%: 26.4%, $R^2=0.34$; Median Distance Between Beads: NRMSE%: 55.7%, $R^2=0.25$) (Figure 12, Table 1). None of the final models included basin area as a predictor variable. The highest performing model for bead length as percent of network length and bead density included both the mean slope and slope CV as predictor variables while the slope CV was the sole variable kept for the median bead length model and the mean slope was the sole predictor variable in the median bead distance model (Table 1). This ran counter to our hypothesis that including information about both mean slope and variability would be mostly likely to improve our ability to predict attributes like river bead size and spacing.

2.3.5 Network Context of River Beads Along Poudre Mainstem

In a case study along the mainstem of the Poudre River, we found that while bead area is not strongly associated with network position along the mainstem, other metrics of river bead relative influence are positively associated with headwater proximity as measured by distance to outlet (Figure 13). The area of river beads along the mainstem (mean 0.44 km^2 , range: $.01 - 4.25 \text{ km}^2$) was not associated with distance to outlet ($r = .02$) with several large river beads ($>2 \text{ km}^2$) in the middle and lower positions of the network and many smaller river beads ($<2 \text{ km}^2$) distributed throughout the network. In contrast, our relative influence metrics all were moderately positively correlated with distance from the outlet including bead area normalized by annual flow ($r = .41$), bead area normalized by upstream catchment area ($r = .53$), bead area normalized by up-network bead area ($r = .59$) and unconfinement

($r=.42$). Despite general trends, the largest river beads by area, which were lower in the network also had moderate to large relative influence values due to their large size (Figure 13).

2.4 Discussion

Defining river beads using thresholds in river corridor width enabled us to implement a methodology to identify river beads in Southern Rocky Ecoregion river basins. Beyond river corridor width being useful because it is measurable at regional scales, it serves as a good metric for river bead identification because it acts as a control on important river bead attributes, including the development of unconfined channel planforms, setting the maximum potential extent of river-wetland habitats, and influences the potential for subsurface hyporheic and surficial perirheic river-floodplain exchanges and the storage of water, sediment and carbon along the reach (Van Appledorn et al., 2019; Stanford & Ward, 1993b; Sutfin et al., 2021; Wohl et al., 2021). Our delineation of river beads using solely the river corridor width metric can therefore be thought of as the maximum current potential distribution of river bead segments in the river network.

Due to human alterations within river beads, the abundance of river beads segments actually contributing to riparian functioning in the river network are much more sparse (Wohl et al., 2017). For example, Sano et al. (2016) estimated that human activities have caused loss of 21% of all riparian zones in the Southern Rocky Ecoregion. Thus, delineations of rivers beads also need to consider metrics that describe river corridor integrity. Complete measures of river corridor integrity require multi-metric approaches because river bead functioning results from interactions of hydrologic, geomorphic and ecologic processes (Karpach et al., 2020). However, we find here that even a single simplified integrity metric such as wetland cover can provide insights into broad patterns of river bead disturbance and captures the uneven impacts of human activities on the landscape. For example, here we found that

excluding river beads with wetland cover below 50% resulted in losses of approximately 85% of river bead length in sixth-order rivers compared to somewhat smaller losses of approximately 60% in second-, third- and fourth-order rivers.

2.4.1 Methodological Considerations

As our methodology and analysis developed here were oriented towards identifying river beads using currently available datasets and tools at a regional scale, the accuracy of our results are reliant on the correct delineation of river corridors and width measurements. Despite using the best available datasets, there remains considerable uncertainty due to coarse resolution input datasets (DEM: ~10 m resolution, NLCD: 30 m resolution), problems in NHD alignment, and uncertainty in choosing the correct parameters for the GFPLAIN and RivWidthClouds tools. While the 10 m DEM represents the best continuous elevation dataset across the full region, it is too coarse to identify many smaller scale features driving flow routing in river corridors that may be more apparent in higher resolution topography datasets obtained by LIDAR which are not currently available across the full region (Grau et al., 2021). Similarly, 30 m resolution landcover datasets are too coarse to depict much of the heterogeneity in river corridor landscapes.

The limitations in resolution help explain why many of the smaller river bead features in the field mapped dataset were not observed in our river bead delineation while there was better agreement with the field dataset at longer and higher-order river beads (Figure 8). Further it likely explains why agreement between the two datasets improved for 3rd order stream over 1st and 2nd order because flow routing and river alignment is better in larger watersheds. Finally, these data limitations are linked to the high false positive values observed in the comparison at low T_{wid} values between 25 and 50 m (Figure 8a). With a ~10 m DEM, even with correct river alignment, in sub 10 m wide rivers, the elevation

of the DEM at the river pixel will at least partially reflect the floodplain elevation not just the stream elevation. Therefore, when applying the GFPLAIN algorithm, the initial elevation upon which the flood height is added will be inflated with corresponding inflated results for the modeled river corridor width. As a result, we believe that in most of the network, very narrow river corridors were assigned values of between 25 to 50 m. Despite differences with the field scale dataset, this comparison builds trust in our methods ability to describe broad differences in river bead configuration and condition across different basins and network positions. As an alternative to field scale mapping, our approach is easier to scale and replicate and reduces subjective decision-making. The approach can also be optimized for efforts targeting smaller scales such as individual river networks by incorporating higher resolution topographic and land cover datasets when available. At smaller scales, we also suggest following Nardi et al.'s (2018) approach of incorporating stream gage data to help determining scaling parameters for the GFPLAIN tool.

Defining river beads with a static RC width rather than using a scalable metric like (un)confinement creates trade-offs between information requirements and improving the ability to define river beads from a process perspective. One limitation of a static RC width is that it doesn't account for changing river widths and how rivers of differing sizes will interact with the same-sized river corridor. For example, at a given RC width, the zone of active erosion/sedimentation could be anywhere from a small fraction to the entire width of the river corridor depending on the river size and lateral connectivity (Khan et al., 2021). On the other hand, river confinement when described as the ratio between river width and valley width or as the proportion of the river touching confining boundaries can be scalable and provides information on valley setting and riparian process zones (Fryirs et al., 2016; O'Brien et al., 2019). However, river confinement requires additional data such as river width and/or accurate mapping of river segments that are not always readily available at the river network scale. While advances have been made in delineating rivers and measuring river width in larger rivers (>30 m

width, X. Yang et al., 2020), characterizing geospatial information like river width across large regions in smaller rivers remains a challenge (Allen & Pavelsky, 2015). For example, datasets used here including NHDPLUSv2 flowlines and the SCS river width measurements both contain major observable inaccuracies in our study basins that limit their utility in measuring river confinement without additional verification.

2.4.2 The Role of Network Context and River Bead Configuration

Patterns observed in river bead abundance, spacing and configuration also highlight how context matters when considering river bead influence on river networks. For example, in the Cache la Poudre Basin, with a 100 m T_{wid} , river beads follow the characteristic alternating pattern described by Stanford & Ward (1993) with river beads sporadically distributed between narrow string segments in the network (Figure 5a). However, with the same 100 m T_{wid} , river bead configuration in the North Platte basin is quite different, with broad zones of the lower portion of the river network all classified as continuous river beads, and river strings only abundant in the upper, low stream order portions of the network (Figure 5b). Such differences in river bead topology between basins is also observed in scaling behavior of the proportion of catchment area that is comprised of river beads as catchment area increases (Figure S1). While some basins demonstrate peak ratios at moderate catchment area sizes, other display monotonically increasing or decreasing relationships suggesting that basins are quite variable overall in their river bead topologies.

Such differences in configuration and spacing of river beads likely influence the net impact of river beads on network process yet there is little understanding of how the impacts of river beads accumulate at the network scale. This is despite the increasing evidence that at the scale of individual segments, river beads act as ecologic control points (*sensu* Bernhardt et al. (2017)), disproportionately

impacting a range of network scale processes. For example, individual river beads have been found to store 1.8 times more organic carbon per hectare than adjacent narrower riparian zones (Sutfin et al., 2021), host 1.8 times more salmonid biomass by length of valley (Herdrich, 2016), contain 1.6 times more invertebrate taxa (Bellmore & Baxter, 2014), have higher stream metabolism and reduced particulate organic matter travel distances (Bellmore & Baxter, 2014).

Functions in river beads are both dependent on network scale dynamics that regulate processes such as fluxes of water, carbon, sediment, and biota but also modify these fluxes by acting as sources, sinks and transformative zones within the network. As a result, the functioning of any single river bead can be influenced by the functioning of other beads in the network while also influencing other beads further downstream. A single river bead's influence on other river beads will likely decay with network distance as its impact is overwritten by increasing accumulation of additional river corridor and watershed influences. Thus, we speculate that tightly spaced configurations of river bead or continuous long segments of wide river corridors will have strong interactive effects that need to be considered to describe bead functioning while sparsely configured river beads will act more independently as individual control points along the network.

Beyond understanding broad network scale patterning, mapping river beads also can provide contextual information on particular river segments that can improve prediction of their influence on the network scale processes and their restoration potential. How one defines the potential influence of a river bead will depend on the processes of interest and on the scale of the river network being considered. To explore this idea, here, we conducted an exploratory analysis of five descriptive metrics along the Poudre River basin mainstem (bead area, ratio of bead area to total up network bead area (RI_UBA), ratio of bead area to annual volumetric streamflow (RI_QNA), ratio of bead area to accumulated catchment area (RI_UAA), and unconfinement) that help identify the network context of individual river beads (Figure 13). From the analysis, it becomes clear that network position is a key

factor in river bead influence. In the upper portion of the Poudre River, relatively small river beads generate large RI_UBA and RI_QNA values because, as compared to lower portions of the network, river size and flow are small relative to the width of the river corridor and the river beads comprise a significant portion of the total upstream river corridor and catchment area (Figure 13). Lower in the network, the RI_UBA and RI_QNA values are smaller despite larger river bead area due to larger river flows and accumulation of more river corridor area. However, somewhat offsetting this trend in the Poudre is that river beads tend to be more abundant and densely spaced in the lower portion of the Poudre mainstem, such that the accumulated influence of multiple river beads in the lower network collectively may still be significant in influencing landscape- or network-scale processes (Figure 13). Based on this initial analysis, we suggest that mapping of these metrics is a first step toward more rigorous assessments of how individual river beads influence behavior across river networks.

2.5 Conclusion

We develop and demonstrate an approach to identify wide river corridors, here termed river beads, along river network segments and analyze their network configuration in a case study of twenty basins in the Southern Rockies Ecoregion. Understanding the topology of river beads is a first step towards greater understanding cumulative effects of river corridors on network scale processes relevant to water resources and ecosystem management. In our case study, differences in river bead network configuration are evident both between basins and within differing stream orders in individual river networks. Longitudinal patterns of increasing river corridor widths with larger catchment areas and lower slopes result in increasing densities, widths and lengths of river beads in higher-order streams. However, as low-order streams comprise a greater portion of the network, substantial numbers of river beads are prevalent within lower-order portions of the networks. River beads along lower-order reaches tend to be smaller than those along higher order rivers, however the ratio of their size to local

streamflow are larger than at down-network river beads, suggesting lower-order river beads may play important roles in regulating signals and processes observed in higher order segments downstream. Most river beads at all network positions lack high wetland cover, suggesting human disturbance and alteration of river and floodplain ecosystems has led to the widespread loss of wetland habitat along river corridors in the Southern Rockies Ecoregion. Quantifying the configuration and vegetation cover of river beads is a first step toward restoring hydrological and ecological function along river networks of the Southern Rockies Ecoregion and beyond.

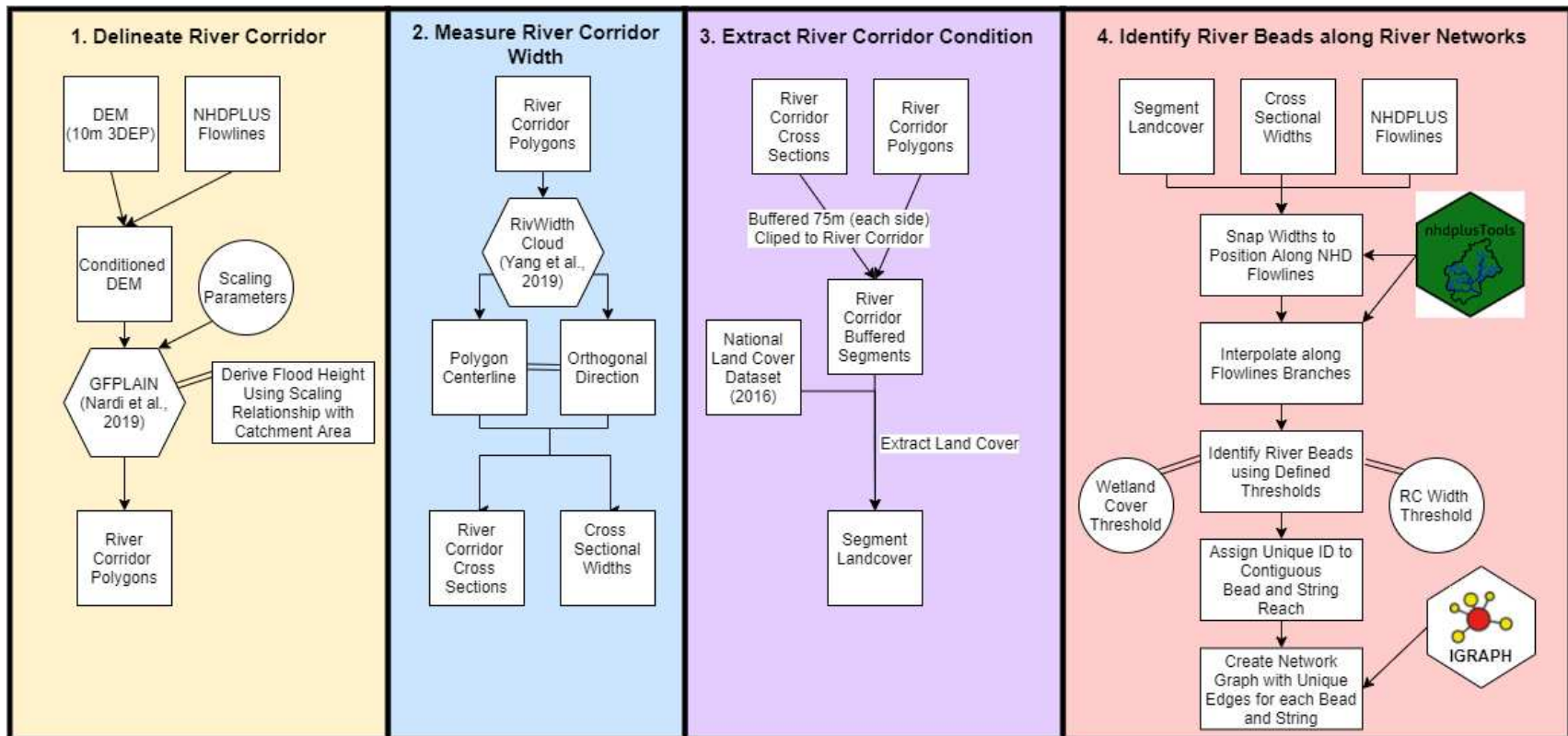


Figure 2.1: Process diagram illustrating major steps in river bead and string identification and analysis

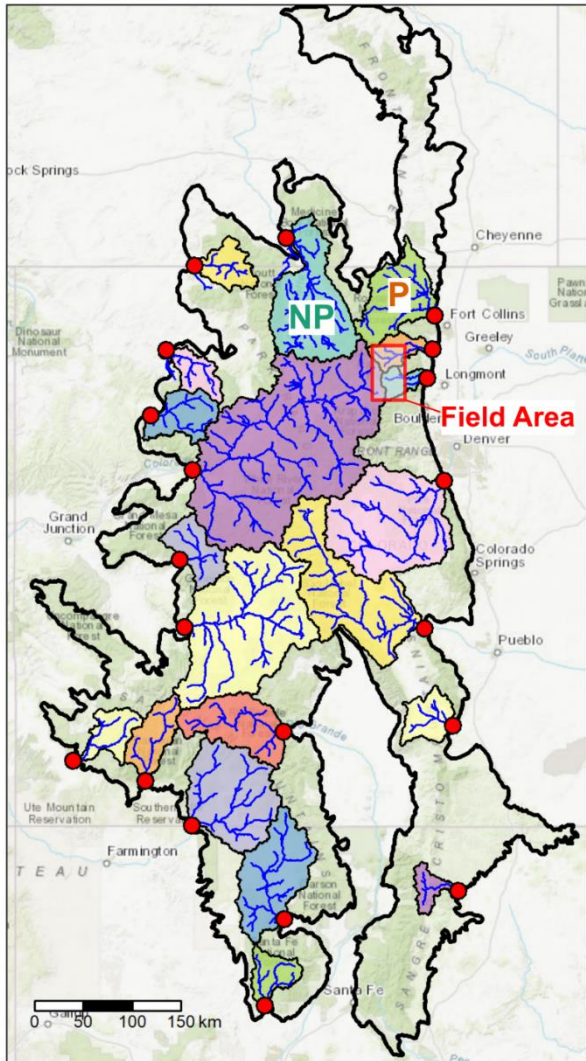


Figure 2.2: Map of study basins and NHD river network in the Southern Rockies Ecoregion. Red dots are basin outlet points. Example basins including the Poudre (P) and North Platte (NP) are labeled. The red box indicates the area from which the comparative field dataset was collected.

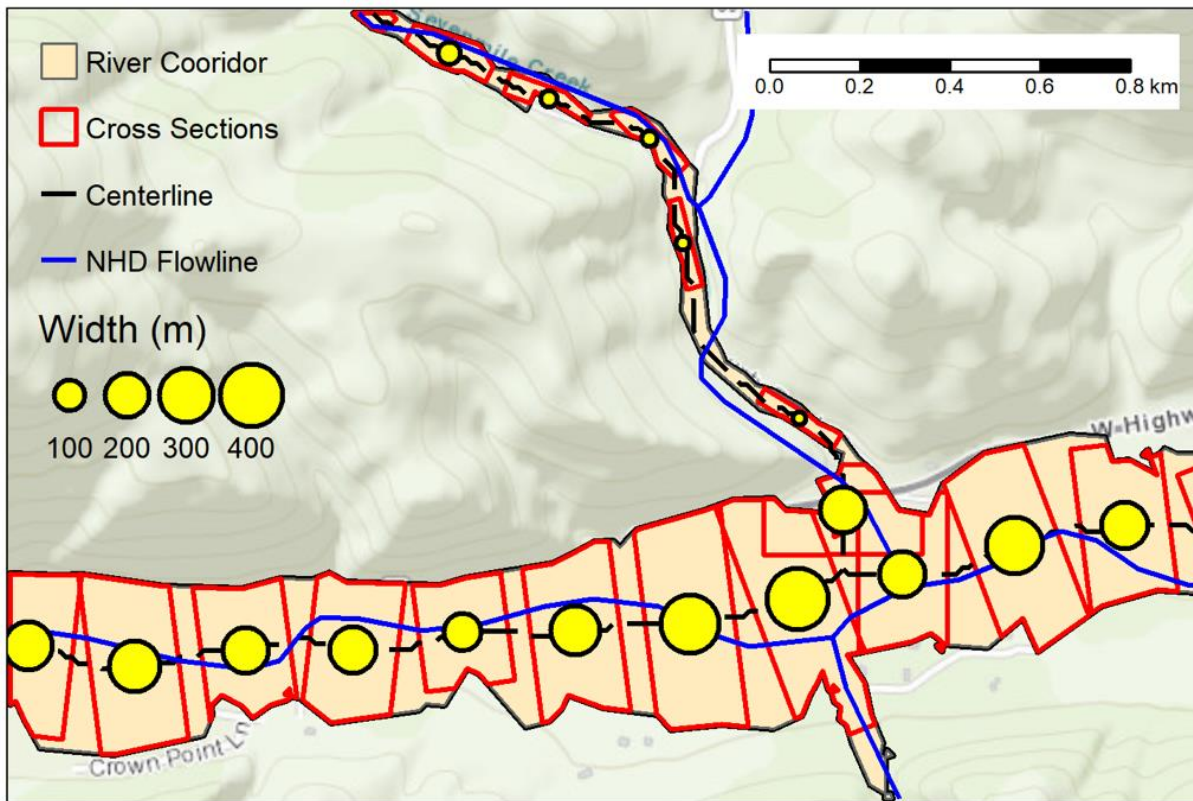


Figure 2.3: Illustration of delineated river corridor (RC) polygons (tan areas), RC width calculation (yellow points) and buffered cross sections (red outline) used for land cover analysis. Widths are measured along RC polygon centerlines (dotted black line) and then later snapped (not depicted) to the nearest NHD flowline (blue line).

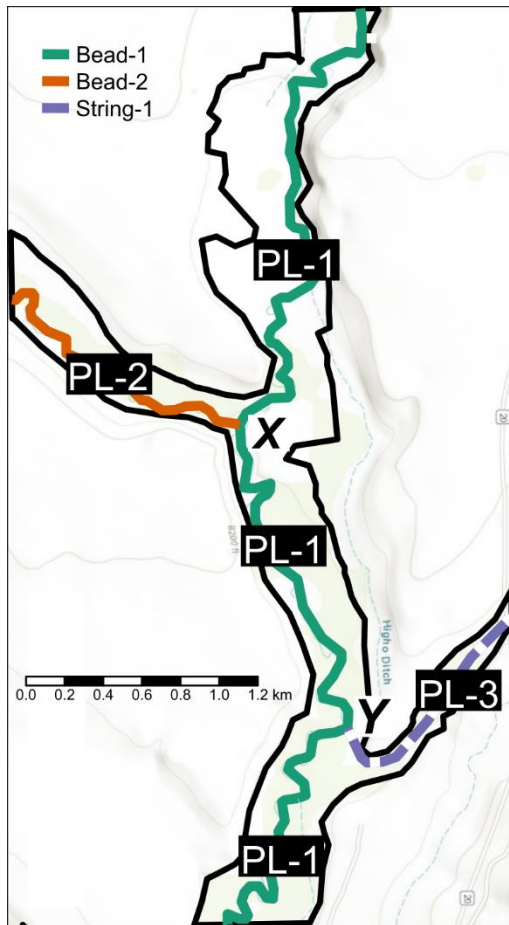


Figure 2.4: Example of river bead (solid line) and string (dashed line) delineation at confluences with the delineated river corridor (black line) from the North Platte basin. Unique colors represent individual bead or string segments and 'PL' label is the hierarchical NHD path level of each flowline. At confluence X, both upstream branches and the downstream branch have been identified as beads. In this case, the PL-1 bead (green) continues while the PL-2 bead (orange) ends because the lower path level value of PL-1 identifies it as a more major branch. At confluence Y, a string segment (purple) meets PL-1 flowline and ends. The PL-1 bead (green) continues downstream because beads are identified both above and below the Y confluence along the PL-1 flowline.

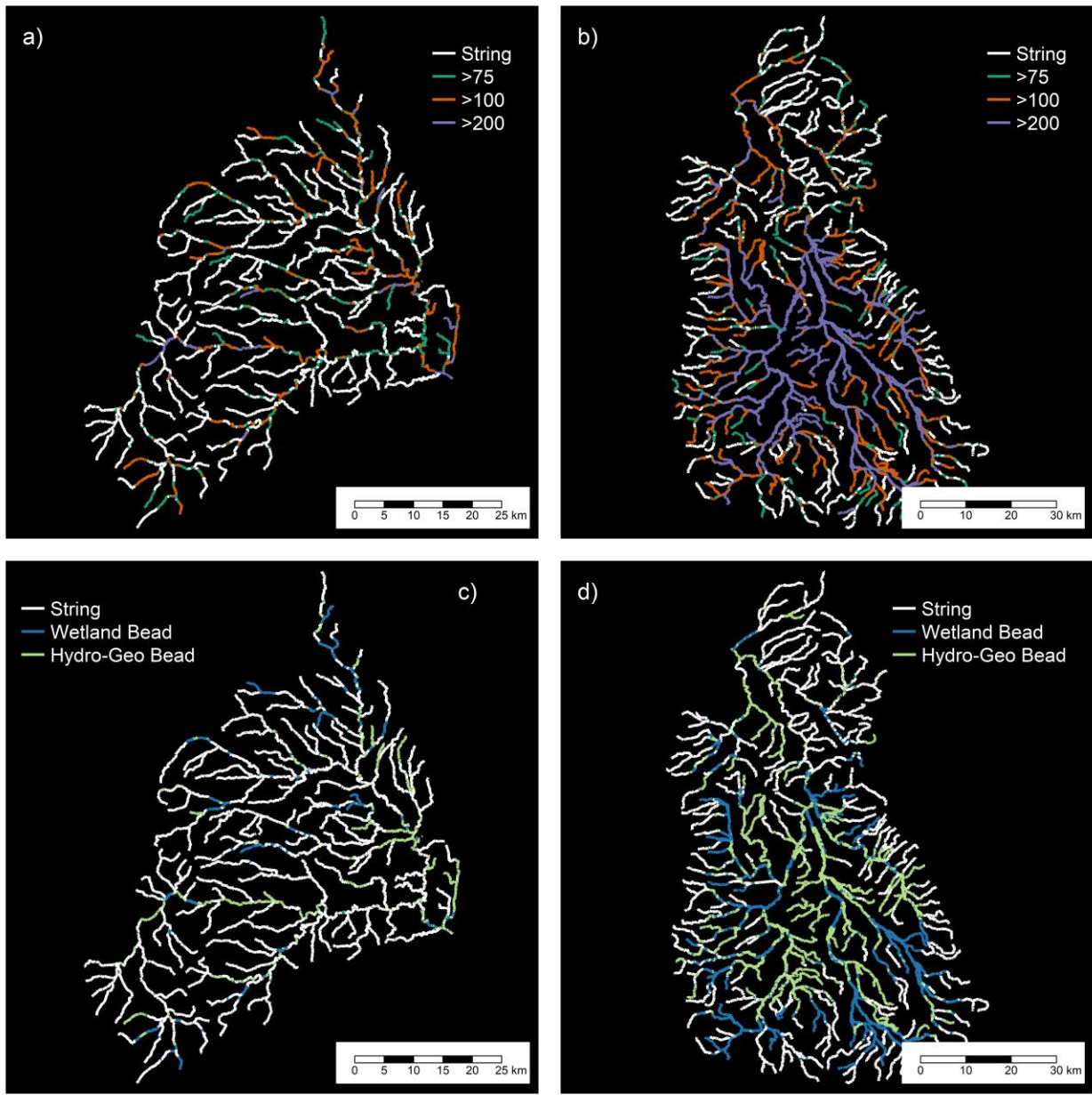


Figure 2.5: River bead delineations using different river corridor (RC) width thresholds (a & b) and river bead type (c & d) in Poudre (a & c) and North Platte (b & d) river basins. In a & b, bead delineations were conducted using 75, 100 and 200m width thresholds and are colored using the highest threshold exceeded. White segments are strings with RC width <50m. In c & d, bead type was delineated using a 100m width threshold and a 50% wetland cover threshold. Wetland bead segments (>100m width & >50% wetland cover) are in magenta, hydro-geomorphic segments (>100m width & <50% wetland cover) are in orange and strings (<100m width) are in white.

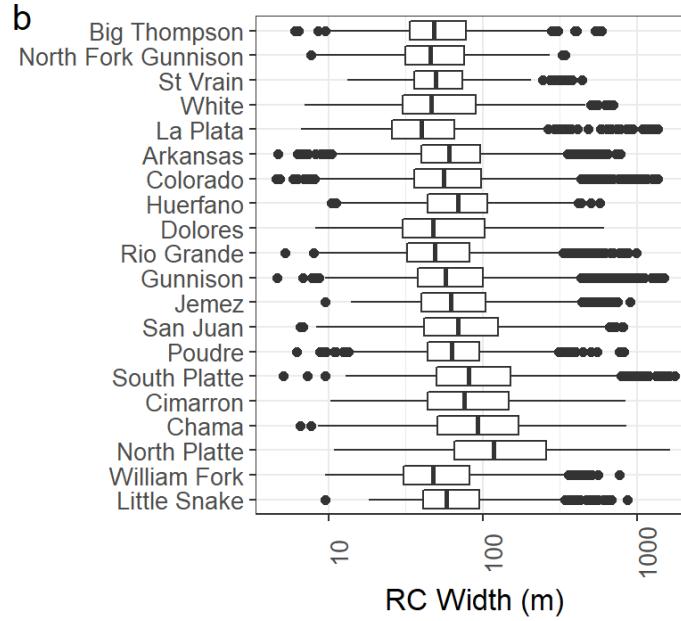
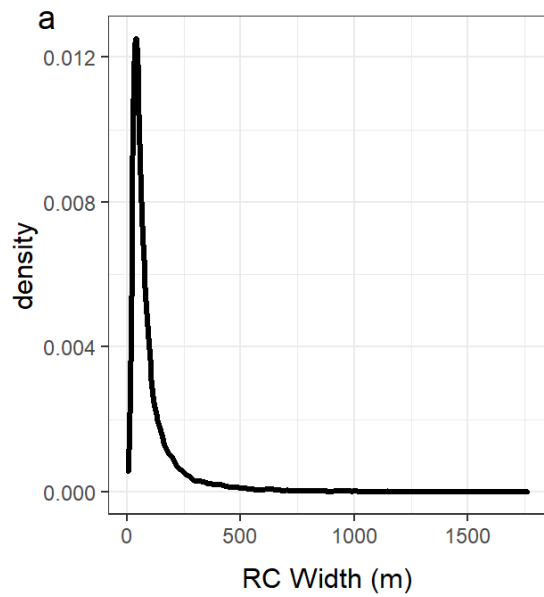
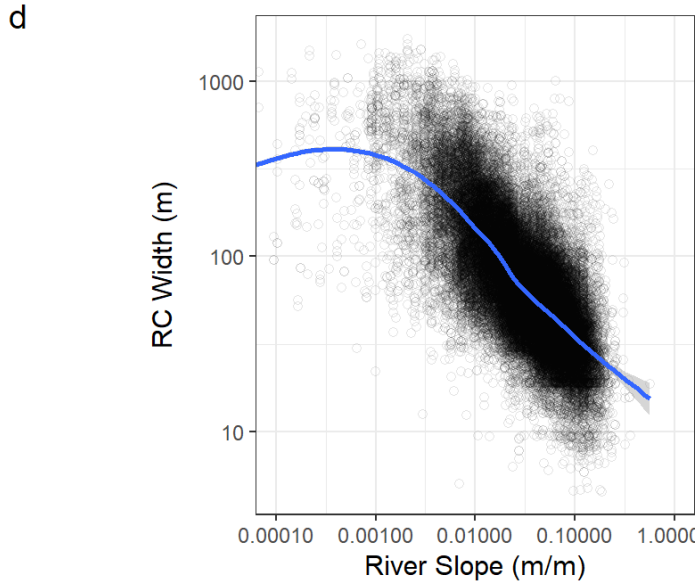
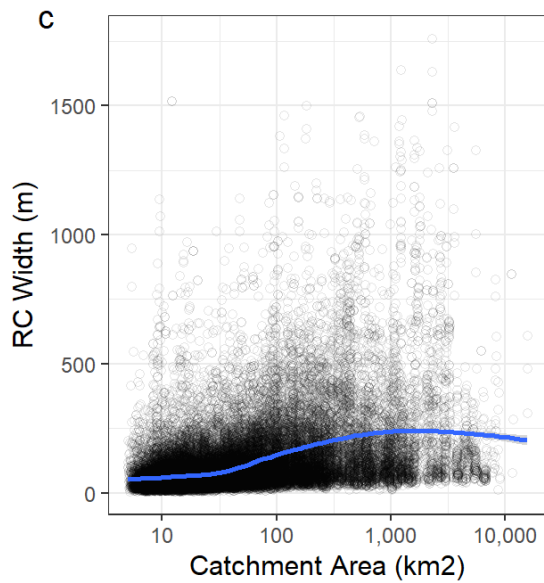


Figure 2.6: River corridor (RC) widths density plot (a), RC widths by basin (b), and RC width relationship with catchment area (c) and river slope (d). In (b), basins are ordered top to bottom from highest to lowest median slope. Smoothing curves (in blue) in (c) and (d) are fit with a generalized additive model



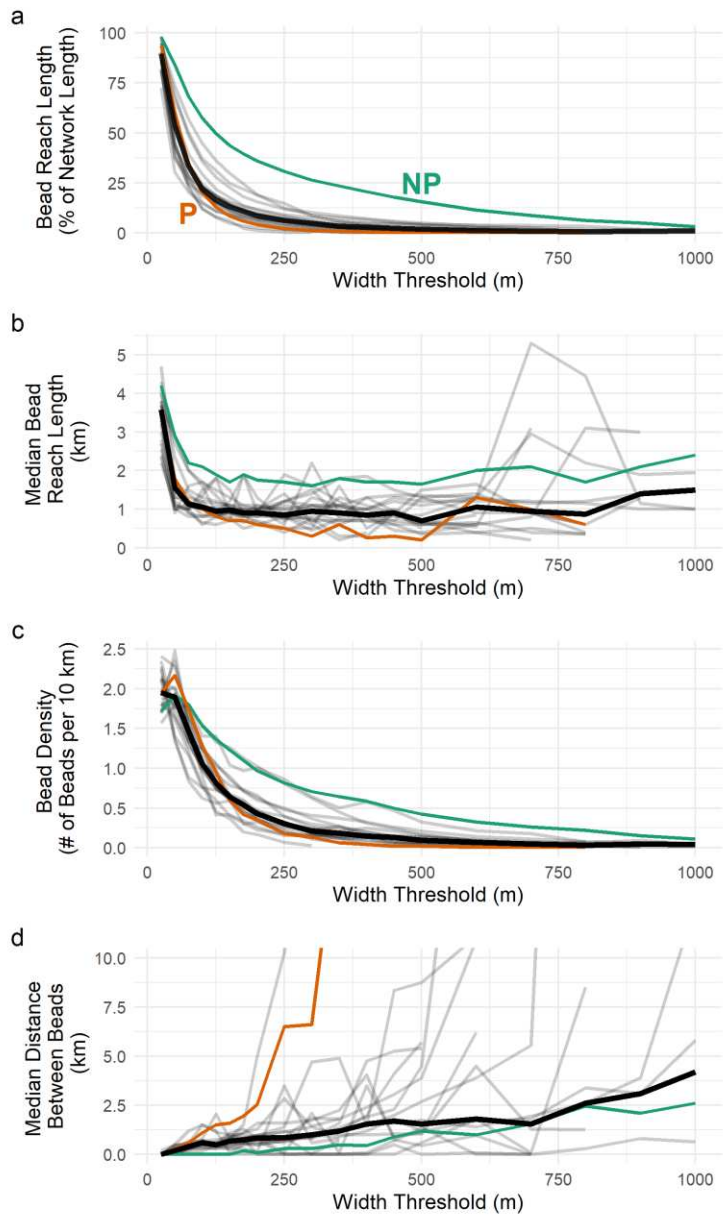


Figure 2.7: River bead network statistics with varying river corridor width thresholds including the bead reach length as % of network length (a), median bead reach length (b), bead density (c) and median distance between beads (d) for individual basins (light grey lines) and median value across basins (black line). The Poudre (P, orange) and North Platte (NP, green) are highlighted in color as examples. Values above 10km for median distance between beads are not displayed.

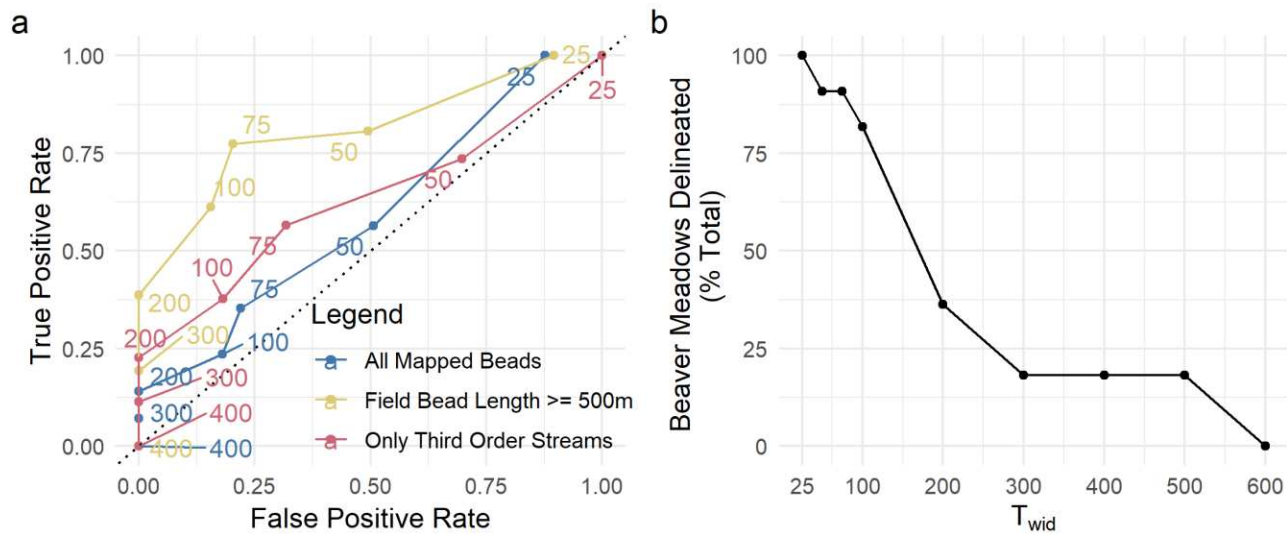


Figure 2.8: Comparison of field mapped river beads to GIS delineated results. a) Receiver operating characteristic (ROC) curves showing classification agreement with the intensive dataset at North St Vrain using varying RC width thresholds (T_{wid}). Numbered point reflect classification results with specified T_{wid} value and higher true positive rates with lower false negative rates reflect better agreement between the two datasets. Agreement between the datasets is best when including only field mapped beads with lengths above 500m (yellow), followed by including only third order streams (red), as compared to including all field mapped beads (blue). b) The proportion of field mapped beaver meadows where some part of the meadow is identified as river beads in the GIS based dataset across differing T_{wid} values.

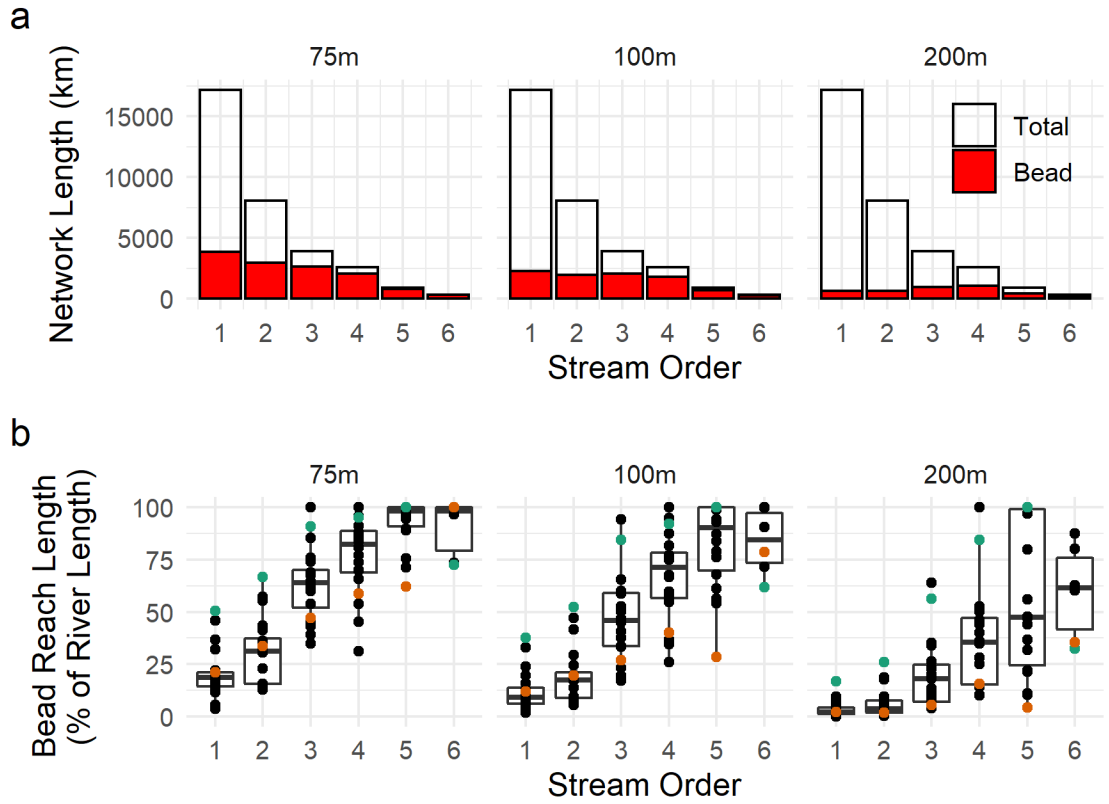


Figure 2.9: Proportionality of total river bead reach length to network length by stream order across 75,100 and 200 meter width thresholds. In (a), total network length (black outline) and total bead length (red fill) are displayed for each stream order. In (b), boxplots of the proportion of total bead reach length to stream order length calculated at each basin. Points are individual basins with Poudre (orange) and North Platte basins (green) highlighted in color. Note that 40% of 1st order stream network is excluded from analysis because streams with contributing area <5km were not considered in the study.

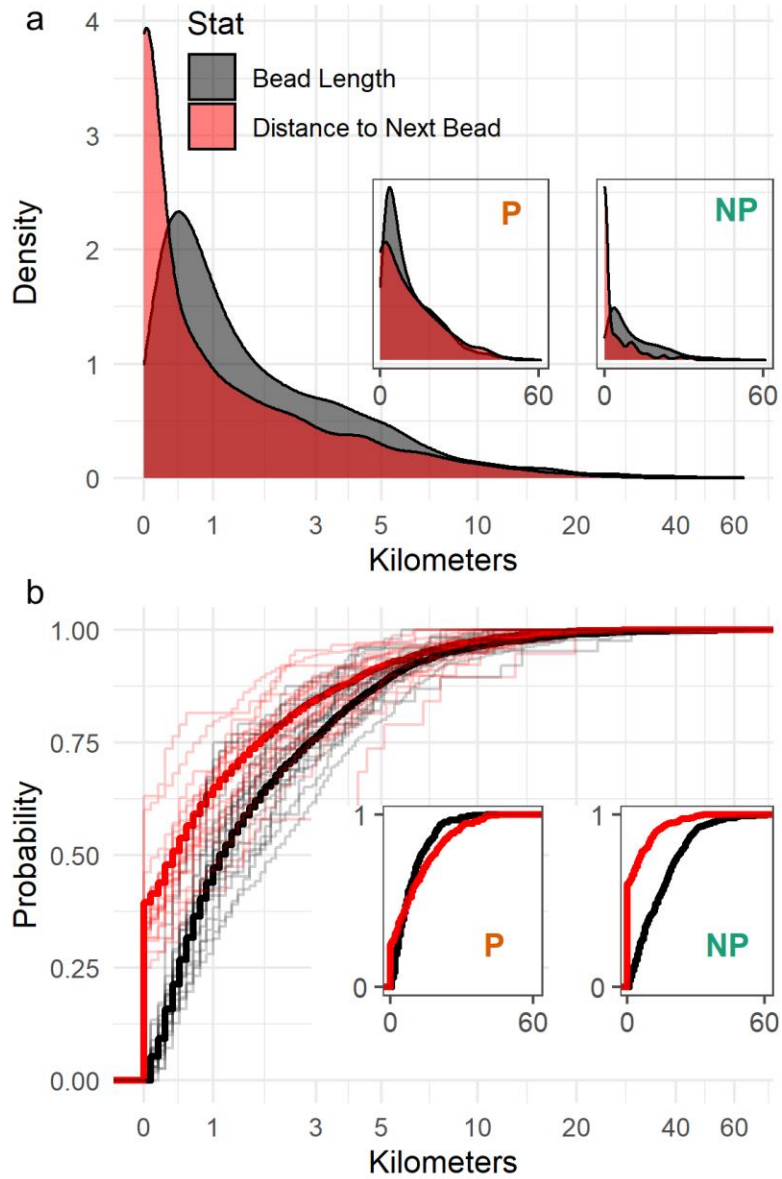


Figure 2.10: Density plots (a) and empirical CDFs of bead length (black) and distance to next bead (red) statistics using 100m width threshold. In (b), CDFs are also plotted for every basin for both statistics (light black and light red). Insets show distributions for Poudre (P) and North Platte (NP) basins

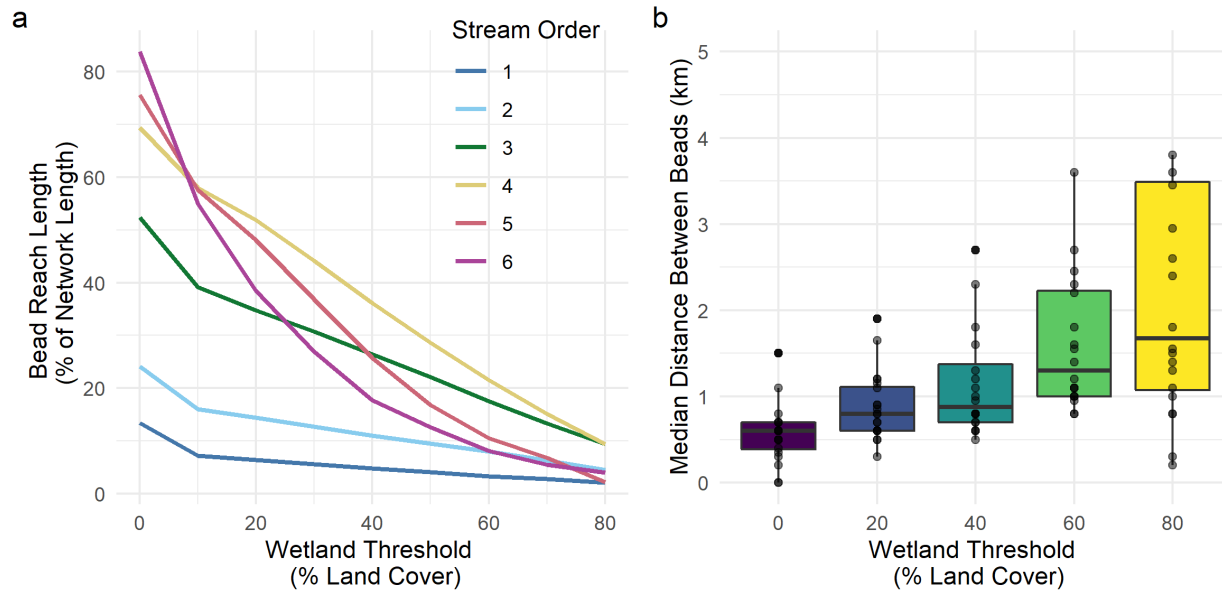


Figure 2.11: Impact of wetland cover threshold on river bead network statistics using constant 100m width threshold including a) proportion of total bead reach length to network length within each stream order and b) boxplot of median distance between beads, calculated individually for each basin.

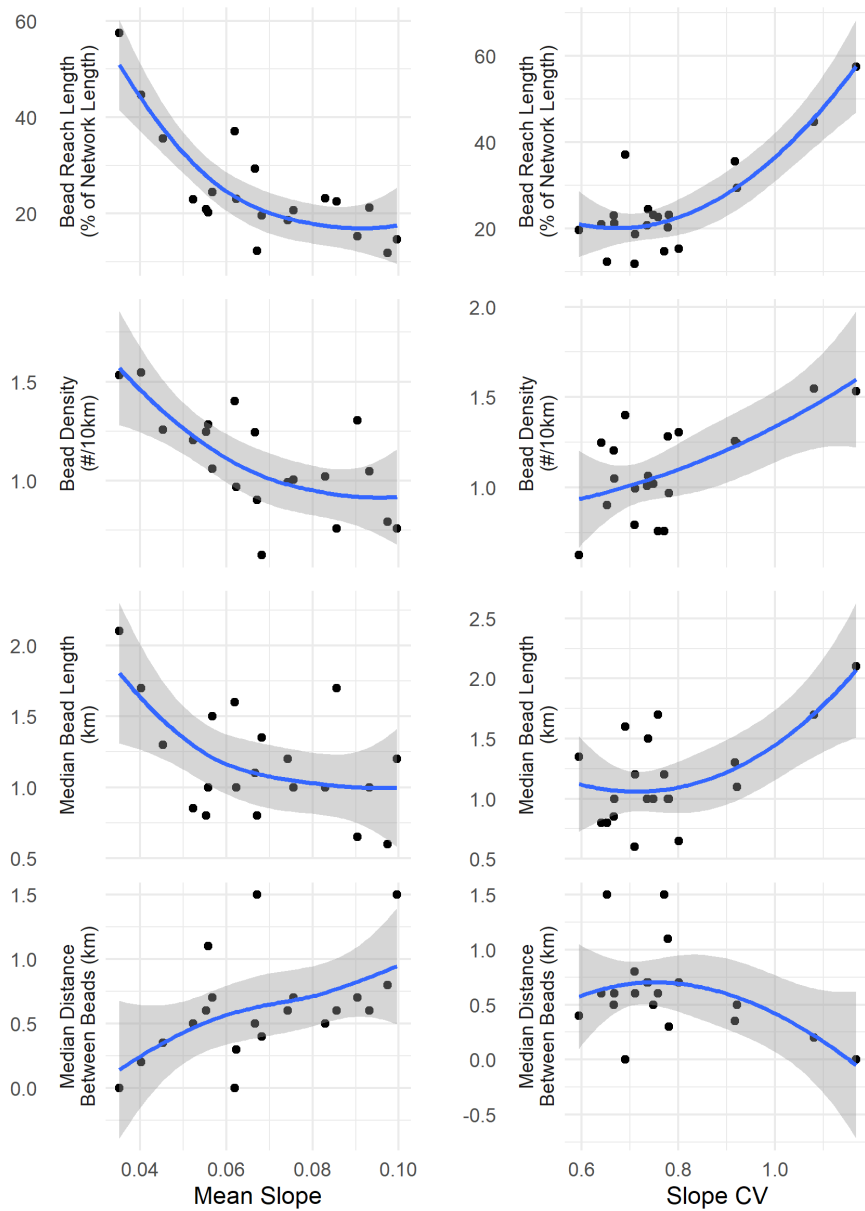


Figure 2.12: Scatterplot and loess regression line between basin slope characteristics and river bead network statistics using 100m width threshold.

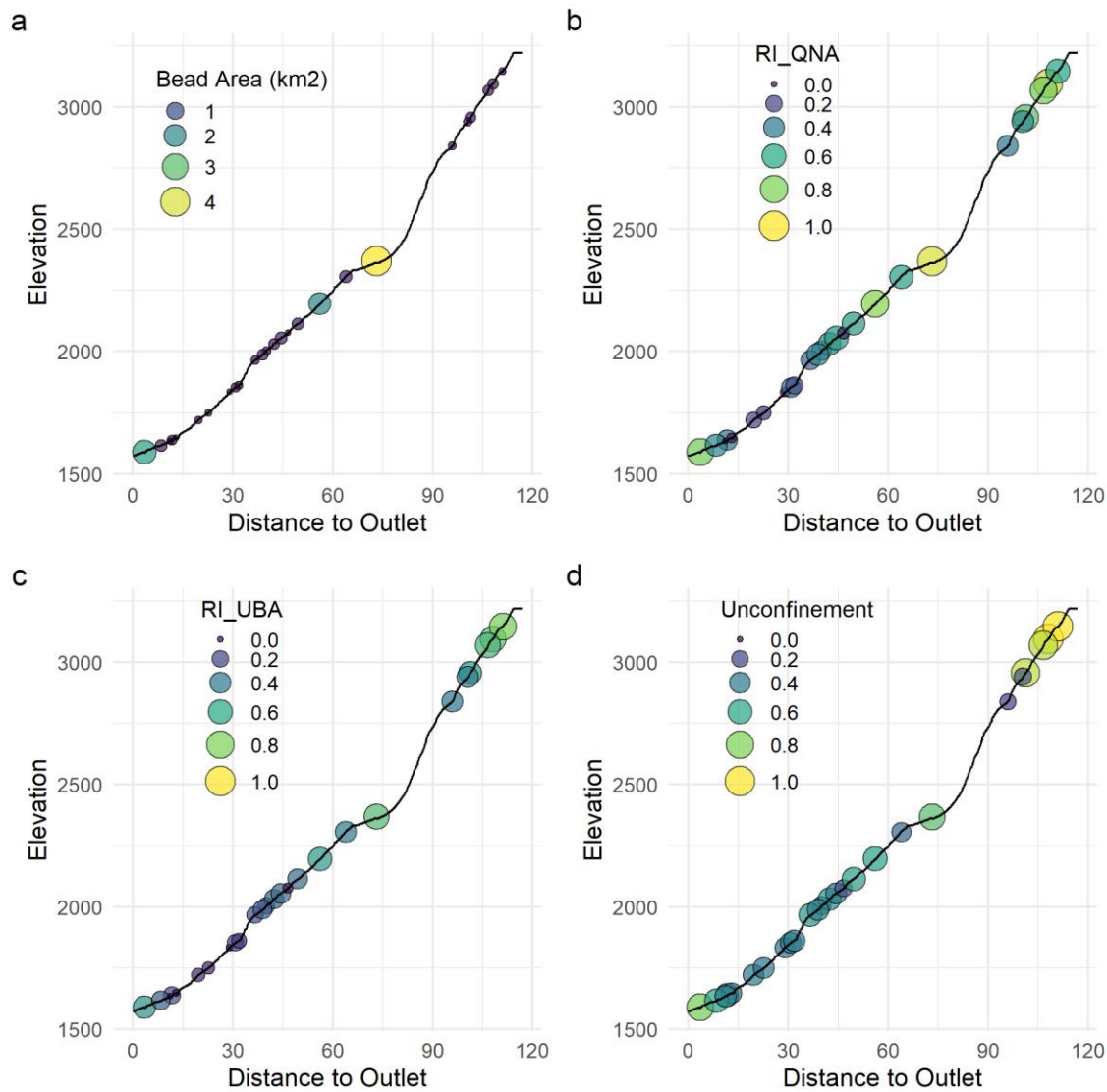


Figure 2.13: Contextual metrics at individual river beads (points) along the mainstream of the Poudre basin. Bead area (a) is approximated as bead length * mean bead width. Relative influence (point size and color) is calculated using two methods: (b) RI_QNA is calculated as the logged ratio of bead area to the annual volumetric flow (Q , m³). (c) RI_UBA is calculated as the logged ratio of bead area to the total bead area upstream in the network. Both b & c metrics are rescaled to between 0 and 1 for improved visualization. (d) Unconfinement is calculated as $1 - (\text{river width} / \text{RC width})$. The full longitudinal profile of the mainstem is displayed as the black line. RI_UAA is not shown in figure because metric is strongly correlated to RI_QNA ($r=0.95$) and patterns are nearly identical.

Table 2.1: Results for multiple linear regression models. Models selected for predictors that minimize AIC. NRMSE% is the mean normalized root mean square error expressed as percentage. CV stands for Coefficient of Variation.

Response Variable	Best Predictors	NRMSE%	R²
<i>Bead Length (% of Network Length)</i>	mean slope & slope CV	20.6	0.78
<i>Bead Density</i>	mean slope & slope cv	15.1	0.57
<i>Median Bead Length</i>	slope CV	26.4	0.34
<i>Median Distance Between Beads</i>	slope CV	55.7	0.25

CHAPTER 3: EVALUATING SPATIAL AND TEMPORAL DYNAMICS OF RIVER-FLOODPLAIN CONNECTIVITY
SURFACE WATER USING HYDROMETRIC, GEOCHEMICAL AND MICROBIAL INDICATORS.²

3.1 Introduction

Hydrologic linkages of matter and energy within landscapes are important regulators of physical (Bracken & Croke, 2007), biogeochemical (Covino, 2017) and biological processes (Amoros & Bornette, 2002). These linkages, defined as hydrologic connectivity, are an emergent landscape property that connect multiple landscape components (e.g., uplands, streams, floodplains, hyporheic zones, and groundwater). Hydrologic connectivity emerges from complex interactions of topographic, climatic, geologic, biotic, and anthropogenic controls (Leibowitz et al., 2018). Hydrologic connectivity has gained popularity as a conceptual and quantitative framework because it enables description of patterns in hydrologic function without requiring the full quantification of underlying processes and controls (Wohl et al., 2019). Despite this popularity, there remains a need to quantify hydrologic connectivity across spatial and temporal scales to facilitate inter-study comparisons, inform landscape restoration, and more directly translate assessments of connectivity to policy and management decisions (Roni et al., 2019; Wohl et al., 2019).

River-floodplain systems are formed by interactions between rivers and adjacent landforms that support important ecologic and hydrologic services (Opperman et al., 2010) and have highly variable surface topography and subsurface stratigraphy (Poole, 2002). Within these systems, hydrologic connectivity results from surficial flow and flood pulses (Junk et al., 1989; Tockner et al., 2000) as well as subsurface hyporheic exchange (Stanford & Ward, 1993a). Variable hydrologic dynamics generate patchy mosaics of aquatic habitats, which tend to be most heterogeneous at low flow and most

² This paper is in review at *Water Resources Research*: Brooks, A.C., Covino, T.P., Hall, E.K., 2022. Evaluating spatial and temporal dynamics of river-floodplain connectivity using hydrometric, geochemical and microbial indicators.

homogenous at high flows (Thomaz et al., 2007). The degree of surface and subsurface connectivity also influences downstream fluxes and concentrations of organic matter, sediment, nutrients and heavy metals (Bellmore & Baxter, 2014; Briggs et al., 2019; Tockner et al., 2002; Wohl et al., 2017). Controls on downstream concentrations and fluxes are influenced by both connectivity or disconnectivity, often described as hydrologic isolation (Cohen et al., 2016; Rains et al., 2016). Isolation plays a critical role in water chemistry (Cheng & Basu, 2017), and in the maintenance of floodplain habitat complexity and biodiversity (Amoros & Bornette, 2002).

The potential hydrologic connections in river-floodplain systems are known as structural connections or structural connectivity (Bracken & Croke, 2007), while the degree to which material and/or energy is transferred within the landscape is known as functional connectivity (Bracken et al., 2013; Turnbull et al., 2008). For functional connectivity to be achieved, flow must overcome resistance, impedances, and losses along structurally connected pathways (Ali et al., 2018). Functional connectivity only occurs under specific hydrologic conditions driven by internal (e.g., antecedent moisture conditions and geomorphic structure) and external (e.g., river flow state, local precipitation) factors (Fritz et al., 2018). Field methods to measure functional connectivity, including hydrometric measurements and end-member mixing analyses, often consider connectivity as a categorical or binary attribute (i.e., connected or isolated) (Cabezas et al., 2011; Jones et al., 2014; Rinderer et al., 2018). However, surface and subsurface hydrologic connections can generate spatial and temporal gradients in hydrologic conditions in fluvial networks (Garbin et al., 2019). As such, we developed an approach for quantifying connectivity as a continuous, as opposed to binary, value to describe spatio-temporal patterns of hydrologic connectivity across a river-floodplain system.

3.1.2 Study Overview

In this study we quantified temporal patterns of hydrologic connections as a continuous value between 0 and 1 from a source (the river at the upstream boundary of the study system, see Figure 1) to target sites (sites located both on the floodplain and downstream on major channel braids of the river, see Figure 1). To do this, we combined data from a network of continuous water level sensors, conservative tracer injections, and weekly sampling for aqueous geochemistry and microbiome membership in order to quantify connectivity of surface water features within the montane river-floodplain system. We also assessed the potential for microbiomes to be used as indicators of connectivity strength and identify whether they provide complementary information to more traditional hydrologic and geochemical connectivity indicators. We then generate site-specific empirical models of connectivity strength for each target site based on streamflow at the source and predict daily connectivity strength at each site. From this developed connectivity dataset, we seek to understand:

- 1) How does hydrologic connectivity differ within the river-floodplain system?
- 2) Does connectivity demonstrate binary or continuous behavior?
- 3) How does site-level connectivity aggregate to system-wide dynamics?
- 4) How sensitive is floodplain connectivity to inter-annual variability in streamflow?

3.2 Methods

3.2.1 Site Description

This study occurred in a river-floodplain system along the North St. Vrain River, Colorado (Figure 1). The river drains an 84km² watershed within Rocky Mountain National Park and has a snowmelt driven hydrograph with late spring/early summer snowmelt peak flows and summer streamflow recession (Figure 1). The river has a multi-thread anastomosing planform within the river-floodplain system which is 1.5km long, 200m to 300m wide with an area of 0.47km². The floodplain has high spatial

heterogeneity with a mosaic of beaver ponds, side channels and wetlands (Laurel & Wohl, 2019). Beaver colonies are active within the reach and geomorphic structures in the floodplain are strongly impacted by historic and current beaver activities including dam construction, channel dredging and pond creation. The floodplain is vegetated with riparian species including willows (*Salix* spp.), river birch (*Betula* spp.), and quaking aspens (*Populus tremuloides*).

Eleven surface water monitoring sites were established within the river-floodplain system (Figure 1b). There were four sites along the river including at the upstream (Inflow) and downstream (Outflow) boundaries of the river-floodplain reach and along two major channels within the river-floodplain system (Main-Mid-01 & Main-Mid-02, see Figure 1). To capture the heterogeneity of aquatic habitats across the floodplain, we included four side channel sites (Side-01 to Side-04), two connected pond sites that had an upstream surface connection to the river (Pond-Con-01 & Pond-Con-02) and one surficially isolated pond (Pond-Iso) with no apparent surface channel connection to the river.

3.2.2 Hydrometric Field Measurements and Conservative Tracer Injection

At all eleven sites, we monitored water level at 15-minute intervals from May 01, 2018 through September 30, 2018 using either TruTrack Capacitance Rods or HOBO U20L Pressure Transducers. To capture relative stage dynamics, we standardized mean daily stage as a z-score by normalizing mean daily stage by the seasonal (i.e., May-September) mean and standard deviation of water levels across the period of record at each individual site. Daily mean stage was used in lieu of sub-daily frequency because surface connectivity dynamics generally occur at seasonal timescales in this system. Floodplain and site elevations were extracted from a USGS 3DEP 1m resolution digital elevation model (Figure 1). Precipitation (2018 water year total: 645 mm) and snow water equivalent (2018 peak: 401 mm) records were obtained from the Wild Basin SNOTEL, #1042, (2914 m), located within the watershed.

To determine how river-floodplain surface connectivity changed as a function of streamflow we conducted instantaneous NaCl injection experiments at high (June 13, 2018) and low flows (July 30, 2018). We injected NaCl into the main stem of the river, 125m upstream from Inflow, and monitored the change in specific conductance (SC) over time (i.e., the breakthrough curve, BTC) at six downstream locations (Table 1) using Campbell CS547A-L conductivity loggers. We calculated modal velocity (V_m) as the time to peak (TTP) divided by the flow path distance from the injection site ($DIST_i$) to the monitoring site.

3.2.3 Incorporating Microbial Indicators of Hydrologic Connectivity

One emerging field-based approach that may provide new insights into connectivity is utilizing hydrologic information contained in microbiomes. Recent work has demonstrated that analysis of microorganisms can be a valuable tool in hydrologic research because membership of aquatic microbiomes are intimately coupled with hydrologic transport (Good et al., 2018; Martínez-Carreras et al., 2015; Pfister et al., 2009). Microorganisms are passive dispersers in aquatic systems and dispersal effects are primarily driven by the directional flow of water (Nemergut et al., 2013). As a result, membership of downstream aquatic microbiomes have been shown to be similar to the microbiomes within shallow soils (Crump et al., 2012) and deeper groundwaters (Amalfitano et al., 2014) that generate streamflow. However, as surface water ecosystems become disconnected and residence times of aquatic systems increase, community assembly is increasingly affected by ecological dynamics (e.g., competition, predation) that result in changes in membership of the site-specific microbiome (Crump et al., 2012; Lindström et al., 2006). At any one point in time, aquatic microbiome membership is the balance between immigration and emigration, which are primarily regulated by hydrologic connectivity, and microbial growth and mortality, which are affected by *in situ* environmental parameters (e.g., resources and temperature) (Crump & Hobbie, 2005; Read et al., 2014; Savio et al., 2015). As hydrologic flow states and aquatic network structure also influence hydrologic connectivity, the membership of

aquatic microbiomes has the potential to reflect connectivity status. The recent formalization of analytical techniques and bioinformatic pipelines to characterize microbiome membership have made analyses of environmental microbiomes more affordable and accessible to non-specialists (Thompson et al., 2017). These increasingly routine analyses of microbiome membership, coupled with the ubiquity of microorganisms in aquatic ecosystems, make microbial analyses a potentially powerful tool for assessments of hydrologic connectivity.

3.2.4 Field Sample Collection and Lab Analysis

At all sites, we collected water samples from May 05, 2018 to September 25, 2018 at approximately weekly intervals for a total of 21 sampling events. A total of 228 water samples were collected for aqueous geochemistry, filtered within 24 hours with a 0.45- μ m PVDF filter (Millipore, HVLP04700) and frozen until analysis for major ions using a Dionex ICS-3000 ion chromatograph at the US Forest Service Rocky Mountain Research Station in Fort Collins, Colorado. A subset of 215 water samples were collected in sterile 60 mL falcon tubes for 16S rRNA amplicon analysis, kept cold until filtered within 12 hours onto a white polycarbonate GTTP 0.2- μ m filter (Millipore, GTTP02500), flash frozen with liquid nitrogen and then stored in a -80°C freezer until analyses. To assess within site variability, for a subset of sites (Inflow, Outflow, Side-01, Pond-Con-01, and Main-Mid-01), we collected duplicate samples each week for 16S rRNA analyses. At all other sites, only individual samples were collected. Due to logistical constraints, Side-02 was sampled for 16S rRNA analysis every other week while other sites were sampled weekly.

We extracted DNA from each filter with a MoBio PowerSoil® DNA Isolation Kit using standard protocols. The 16S rRNA gene (V4 region) was amplified using 515F and 806R universal primers with the forward primer barcoded following the Earth Microbiome Project protocols (Caporaso et al., 2011). The

forward primer 515F included the unique sample barcode following Parada et al. (2016) and both primers included degeneracies as described in Parada et al. (2016) and Apprill et al. (2015). For each sample, we ran a 50 μ L PCR reaction using an Invitrogen Platinum™ Hot Start PCR Master Mix with 10 μ L of DNA. The PCR product was quantified and then combined into a single pool in equimolar concentrations and cleaned using a MinElute® PCR Purification kit. Cleaned, pooled DNA was sequenced with a MiSeq reagent v2 500 cycle kit on the Illumina MiSeq platform at the Colorado State University Next Generation Sequencing Core facility. Sequence reads were analyzed using MOTHUR (Schloss et al., 2009) and OTU counts defined at a 97% similarity of the sequence using the OptiClust algorithm. Generated OTUs were then aligned to a SILVA reference file (Quast et al., 2013). We then removed samples with limited sequences (<1000 reads), trimmed operational taxonomic units (OTUs) to remove samples not observed more than 3 times in 20% of the samples, and relativized OTU counts by the total OTUs in the sample. All 16S amplicon analyses were conducted using the phyloseq package in R (McMurdie & Holmes, 2013). Due to lack of duplication at all sites, we further merged duplicate samples into mean values to simplify subsequent analyses.

3.2.5 Connectivity Strength Metrics

To quantify hydrologic connectivity, we identified a source site (Inflow) and considered the magnitude of connectivity between this source and multiple target sites. We first analyzed surface connectivity information using relative stage dynamics. To do so, we used a graphical analysis approach by plotting the mean daily Inflow stage against the relative stage as represented by stage z-scores (described in section 2.2) at the target sites. Strongly co-varying stage levels between source and target may suggest the presence of connectivity while inflection points in source-target stage relationships can help identify thresholds at which connectivity dynamics shift (Cabezas et al., 2011). At the spatial scale of our study system, streamflow fluctuations propagate out into the floodplain rapidly and hydrologic

response lags are generally on the order of minutes to hours. Thus, using covariance in daily mean stage is appropriate for seasonal connectivity dynamics because time lags can be assumed to be minimal at daily or longer timescales. To identify inflection points in source-target stage relationships and identify inflection thresholds at Inflow (I_{stage}), we fit broken line linear regression models using the *segmented* package in R, which identifies a user-defined number of inflection points (Muggeo, 2008). At two sites, where hysteresis was observed in the source-target relationship, we removed the rising limb from the inflection point identification process. We constrained the analysis to test models from zero to two inflection points and used the segmented algorithm in the *segmented* R package to automatically chose the final number of inflection points based on Davie's test (Muggeo, 2020). In all cases, models with one or two inflection points were chosen over the linear fit. However, because broken-stick regression can be prone to over-fitting, we then removed any inflection point where the change in slope was less than 0.005. It should be noted that while coherent hydrologic fluctuations between sites can be a useful tool for confirming connectivity, it can also be subject to false positives when other factors act similarly on both sites (Rinderer et al., 2018).

We developed an approach to more explicitly evaluate the magnitude of connectivity between source and target sites using both geochemical and microbial indicators. For both metrics, we quantified the magnitude, defined hereafter as connectivity strength (σ), as a continuous variable ranging from 0 and 1. Connectivity strength denotes the degree of influence of the source on the target. To measure connectivity strength, we assumed that when strong surface hydrologic connectivity was present, source and target water compositions would be more similar than when connectivity was weak or absent. This is a commonly used assumption embedded in source water mixing approaches which use aqueous geochemistry to assess hydrologic connectivity (Cabezas et al., 2009; Jones et al., 2014). For microbial communities, we expected that when hydrologic connectivity was strong, the membership of the water column microbiome would be more similar because the target community would be strongly

influenced by immigration from the source community. Conversely, when surface hydrologic connectivity was weak/absent, we expected inter-species interactions would be the dominant influence on microbiome membership and the source and target would become less similar over time.

To calculate connectivity strength using aqueous geochemistry (σ_g), we first normalized ion concentrations by their mean and standard deviations and conducted a principle component analysis (PCA) on all major ions present including sodium, chloride, calcium, magnesium, potassium and sulfate ions. Analytical results included several outlying values for chloride and potassium that were removed due to suspected contamination. To maintain a balanced dataset, we replaced the removed outliers by linearly interpolating reported values from the previous and subsequent weeks at the same site. Interpolation was appropriate because other solutes at the same site followed similar linear patterning during the weeks where outliers were replaced. We examined PCA eigenvalues and eigenvectors (Figure 1, Table S1), and based on variable loadings chose to include two principle components (PCs) for further analysis that represented two major water source components. At each sampling date, within the 2-dimensional PC space (PC1 and PC2), the log transformed Euclidean distance was calculated between a given target site geochemical composition and the geochemical composition at Inflow (i.e., source site) (Eq. 2). This value was then rescaled to between 0 and 1 using a min-max normalization and reversed to calculate a chemical similarity score as follows (Eqs. 1 & 2).

$$ED_i = \log \left(\sqrt{(PC1_{s_i} - PC1_{t_i})^2 + (PC2_{s_i} - PC2_{t_i})^2} \right) \quad (\text{Eq. 1})$$

$$\sigma_{g_i} = 1 - \left(\frac{ED_i - \min(ED)}{\max(ED) - \min(ED)} \right) \quad (\text{Eq. 2})$$

Where ED_i is the logged Euclidian distance within the PCA space on a given sampling date, the subscripts s_i and t_i refer respectively to PC scores at Inflow (i.e., the source) and a target site, σ_{g_i} is the connectivity strength at site i on a given sampling date and ED is the complete dataset.

To calculate connectivity strength using microbiome membership (σ_m), on each sample date, we calculated a similarity score using the Bray-Curtis similarity index (BC) between microbiome membership at a given target site and Inflow (i.e., the source), as follows (Eq. 3).

$$\sigma_{mi} = BC_{st} = \frac{2C_{st}}{S_s + S_t} \quad (\text{Eq. 3})$$

Where C_{st} is the sum of the lower of the two counts of each OTU found at both sites while S_s is the total number of sequence reads at Inflow and S_t is the total number of sequence reads at the target site. We also conducted a principle coordinate analysis (PCOA) using the BC dissimilarity index to visualize microbiome membership in lower dimensional space (Figure 1c). As BC ranges from 0 to 1, we did not perform a min-max normalization on the result.

To identify the relationship between Inflow stage and site-level connectivity, at each site, we fit natural cubic spline regression equations with a single knot between Inflow stage and surface connectivity strength for both geochemical and microbial metrics using the *splines* package in R (R Core Team, 2016). Spline fits were used to best capture the non-linearity of these relationships. As with relative stage (i.e., stage z-scores), hysteresis was observed at two sites. At those two sites, we fit two different functions, using values collected before and after May 30th, 2018, which was the date that stage data suggested a change occurred in the source-target relationship. Samples were collected at Inflow stages ranging from 259 to 683 mm, which spanned 88% of the full range of observed daily stage at Inflow in 2018 which ranged from 235 to 715 mm. At Inflow stages that were outside the range of values when connectivity strength was measured in the field, we assigned a constant value for connectivity strength equal to the modeled value at the highest or lowest Inflow stage at which sampling occurred. Using these models, we then generated daily time series of connectivity strength at each site using the Inflow stage record for 2018.

3.2.6 Metric Evaluation

We evaluated the use of geochemical (σ_g) and microbial (σ_m) connectivity strength metrics using several approaches. First, we compared σ_g and σ_m against the conservative tracer (NaCl) injection results including a binary assessment of arrival or no response of the injected tracer. At sites with arrival, we calculated Pearson correlation coefficients between σ_g and σ_m and time to peak of the tracer breakthrough curve (i.e., modal travel time). To compare connectivity strength metrics against the relative stage dataset, we calculated durations of connectivity between source and each target site. For relative stage, connectivity duration was defined as the percent of the study period when Inflow stage was above the determined inflection point in source-target stage relationships as described in section 2.4. For sites with two identified inflection points, we calculate surface connectivity durations using both inflection points to reflect the uncertainty of determining which inflection point best represents the loss of surface connectivity. For σ_g and σ_m , surface connectivity duration was defined as the percent of the study period in which σ_g and σ_m were above 0.5. Pearson correlation coefficients were calculated to compare whether metrics performed similarly across all sites. To explore the sensitivity of results to a chosen connectivity strength threshold, we also calculated the daily number of connected sites using thresholds ranging from the 10th to 90th percentile of σ_m (0.24 to 0.79).

3.2.7 Sensitivity Analysis of Surface Connectivity to Inter-Annual Variability in Streamflow

To assess how sensitive connectivity dynamics are to inter-annual variation in streamflow, we made use of five years of seasonally monitored water levels (May through September) at Inflow, starting in 2016 through 2020. These stage records were collected with TruTrack Capacitance Rods and were summarized to mean daily stage. As several data gaps in the record exist, we imputed gaps using spline regressions with daily streamflow records from a nearby USGS gage at the Big Thompson River below Moraine Park, Colorado (USGS #402114105350101) (Figure S5). As seasonal hysteresis was observed in

the streamflow relationship between the North St. Vrain and Big Thompson rivers, spline regression equations were fit separately for the rising limb and falling limb, which were respectively defined as prior and post peak seasonal flow at the North St Vrain.

From this five year record of Inflow stage, we used the microbial connectivity strength models developed for each target site within the 2018 study period (described above) to predict daily connectivity strength values at seven target sites with intermittent surface connectivity based on all five years from 2016 to 2020 between May 01 and September 30th. This approach explicitly makes the assumption that there is stationarity in source-target structural connectivity and is intended only to test the degree to which inter-annual variation in streamflow may influence surface connectivity given unchanging physical structure. Additionally, as 2018 was a relatively low streamflow year, sampling during the 2018 study period spanned only 69% of the range of Inflow stages observed across all five years (2018: 259 – 683 mm, 2016-2020: 235 – 849 mm), increasing the uncertainty of predictions at higher flows. To address this, we only report the duration of surface connectivity within three categorical groupings of connectivity strength including categories of high connectivity ($\sigma_m \geq 0.6$), intermediate connectivity ($0.4 < \sigma_m < 0.6$), and low connectivity ($\sigma_m \leq 0.4$). Furthermore, all intermittent sites had microbial connectivity strengths above 0.6 at sampling dates during higher observed Inflow stage in 2018. Therefore, given the assumption of stationarity, all sites are treated as maintaining high connectivity at all Inflow stages above the 2018 measured range. Intermediate connectivity was chosen as between $0.4 < \sigma_m < 0.6$ because analysis of the connectivity strength functions suggest that at low connectivity σ_m stabilized between 0.2 to 0.4, and at high connectivity between 0.6 and 0.8.

All analyses and related figures were generated in R version 3.6.1 (R Core Team, 2016).

3.3 Results

3.3.1 Hydrometric Monitoring and Tracer Experiment:

Stream levels in the North St Vrain River followed a snow driven hydrograph with rising streamflow starting in late April, peak flows in late May to early June and falling streamflow throughout the late-summer/early-fall months (June – September) (Figure 1a). Several summer convective storm events occurred in July and August but did not strongly influence the seasonal hydrograph (Figure 1a). Using stage and geochemical patterns at Inflow (Figure 1a), we categorized four distinct hydro-periods: (I) rising limb (May 01, 2018 – May 15, 2018); (II) peak flow (May 16, 2018 – June 18, 2018); (III) falling limb (June 19, 2018 – July 10, 2018); and (IV) recession (July 11, 2018 – Sept 30, 2018) (Figure 1).

Analysis of patterns between Inflow stage and relative stage (i.e., stage z-scores) at target sites indicated that target sites generally followed the broad seasonal pattern of streamflow at Inflow but also demonstrated site-specific behavior (Figures 2 & 3). We used inflection points in source-target stage relationships to infer changes or thresholds in hydrologic connectivity between Inflow and floodplain sites. The stage at which inflection points (I_{st}) in source-target stage relationships occurred varied between sites and spanned a range of Inflow stages from 285 to 667 mm (Figures 2 & 3, Table S1). At the major channel sites Main-Mid-01 and Outflow, relative stage was strongly coherent with Inflow stage throughout the study period and no inflection points with slope changes larger than ± 0.005 were identified (Figure 2). At Main-Mid-02, two inflection points were identified at lower inflow stages (I_{st1} : 301 mm & I_{st2} : 406 mm) suggesting a shift in connectivity at lower mainstem flows.

At side channel sites, relative stage generally followed patterns similar to Inflow stage with the exception of Side-01 that exhibited hysteretic behavior with higher stage relative to the Inflow during the rising limb compared to the falling limb and recession (Figure 3: panels Side-01, -02, -03 and -04). Inflection points were identified across a wide range of streamflows ranging from the lowest at Side-01 (I_{stage} : 285 mm) to the highest at Side-03 (I_{stage} : 612 mm).

Both of the surface connected ponds (Pond-Con-01 & Pond-Con-02) and the isolated pond (Pond-Iso) had high water levels starting in the rising limb that did not fluctuate strongly as a function of Inflow stage (slopes - 0.002 to 0.003). At all three ponds, water levels declined rapidly relative to Inflow stage below the inflection point (Figure 3). The inflection point occurred during the falling limb at Pond-Con-02 (I_{stage} : 613 mm), and at much lower flows during the recession at Pond-Con-01 (I_{stage} : 366 mm) and Pond-Iso (I_{stage} : 389 mm) (Figure 3). Like Side-01, Pond-Con-02 exhibited hysteretic behavior with higher stage relative to the Inflow on the rising limbs than on the falling limb. The high water levels in all pond sites during the rising limb suggest sampling began after ponds had mostly filled with groundwater, local snowmelt, and streamwater. Pond-Con-01 and Pond-Con-02 went dry in mid-September while at Pond-Iso, levels dropped below our water level logger in early September and the pond went completely dry in late September (Figure 3).

The hysteretic behavior observed at Side-01 and Pond-Con-02, which are connected to each other by a surface channel (Figure 1b), may be related to a failure of a beaver dam during peak flows. While we did not identify the specific failed dam, multiple beaver dams were observed in that region of the floodplain and other such failures have been observed in the system at high streamflow. Elsewhere, beaver dam failures have been shown to change the thresholds in river stage at which floodplain features have surface connections (C. J. Westbrook et al., 2011).

The tracer injection experiments conducted during high (June 13, 2018, Inflow stage: 635 mm) and low flows (July 30, 2018, Inflow stage: 384 mm) demonstrated the presence or absence of surface water connectivity between Inflow and a subset of target sites (Table 1). While tracers can also move through sub-surface flowpaths, the instantaneous tracer injection cannot detect flowpaths with very long residence times, and as such tracer arrival primarily reflects surface connectivity within our system. We did not observe arrival of injected tracer at Pond-Iso during either experiment, providing evidence of a lack of strong surface connectivity between Inflow and this site (Table 1). Tracer arrivals at other sites

were variable, and we only observed tracer arrival during both the high and low flow injections at the Major Channel sites (Table 1). During the high flow tracer injection, tracer arrival was first observed at Main-Mid-01 with a time to peak (TTP) of 22.5 minutes, followed by Side-01 (TTP: 35 min), Outflow (TTP: 46 min) and a more delayed arrival at Pond-Con-02 (TTP: 101 min) and Pond-Con-01 (TTP: 196 min) (Table 1). Modal velocity, which is defined as the most common velocity along a flowpath, was highly variable at connected sites (range: 0.09 - 0.87 m s⁻¹, Table 1) indicating variable residence times along connected flow pathways. During the low flow tracer, the tracer arrival was only observed at the Main-Mid-01 site (TTP: 40.8 min, Vel_m: 0.48 m s⁻¹) and Outflow site (TTP: 85 min, Vel_m: 0.43 m s⁻¹). Given the limits of detecting tracers at high residence times noted above, the lack of response at Side-01, Pond-Con-01 and Pond-Con-02 during the low flow injection cannot confirm a complete absence of surface connectivity. However, these results demonstrate that during the low flow experiment, Side-01, Pond-Con-01 and Pond-Con-02 were not strongly connected with the Inflow site.

3.3.2 Seasonal Dynamics in Aqueous Geochemistry and Microbiome Membership

Using a principal component analysis, we identified which geochemical indicators were most representative of connectivity and generated a reduced dimensional space with uncorrelated components. The primary principal component (PC1) corresponded to bulk ionic strength and explained 62.2% of the variance in water chemistry and the secondary principal component (PC2) explained 17.8% of variance and was strongly driven by SO₄²⁻ concentrations (Figure 1c, Table S2). All ion concentrations were negatively related to PC1 with Na⁺, Ca²⁺, Cl⁻, Mg²⁺, and K⁺ having moderate loadings (between -0.39 to -0.48). SO₄²⁻ had a strong positive loading on PC2 (0.84) while Ca²⁺ and Mg²⁺ had moderate negative loadings (-0.36 and -0.30, respectively).

Seasonal geochemical patterns at Inflow followed a snowmelt dilution pattern where geochemical ion concentrations (e.g., Na^+) were lowest during peak flows (Figure 1, S2 & S3). This geochemical pattern propagated strongly to sites with surface connections to the river during high flows resulting in high geochemical connectivity strength (σ_g) (Figures 2 & 3). As stage declined, geochemical composition diverged between Inflow and most floodplain target sites, resulting in lower σ_g values (Figure 2 & 3). Floodplain target sites crossed the 0.5 σ_g value across a wide range of Inflow stages (I_{geo}) from 337 to 657 mm, demonstrating substantial heterogeneity in connectivity dynamics across the river-floodplain system. Connectivity strength at Main-Mid-01 and Outflow never declined below 0.5 while Pond-Iso had distinct geochemistry from Inflow throughout the season resulting in low σ_g across the study period that never exceeded 0.5. A sharp decline in σ_g at Pond-Iso was observed at low Inflow stages during the period that the pond was going dry, which may be the result of evapo-concentration increasing salinity (Figure 3).

Using a principal coordinates analysis (PCOA), we explored seasonal dynamics in microbiome membership and examined the potential to utilize microbiome membership as an indicator of connectivity. The PCOA of microbiome membership identified a major axis PCOA-1 that explained 32.5% of the variance in microbiome membership and a secondary axis that explained 15.9% of the variance (Figure 1c). All additional axes explained less than 10% of the variance. Microbial membership at Inflow was relatively stable between the rising limb and falling limb, with more shifts in membership at Inflow observed during the recession period (Figure 1c, S3 & S4). During peak flows, sites with structural surface connections to the river had microbiomes similar to Inflow, resulting in high microbial connectivity strength (σ_m) values (Figure 2 & 3). Major channel sites maintained their similarity to Inflow for most of the study period with some divergence at the lowest flows later in hydrograph recession. At side channels and connected pond sites, microbiome membership started diverging from the seasonal pattern at Inflow in either the falling limb or recession hydro-period, resulting in lower σ_m values later in

the season (Figure 2 & 3). Floodplain target sites crossed the 0.5 σ_m value at Inflow stages (I_{micro}) ranging from 306 to 589 mm. As with the geochemical metric, the model fit for σ_m at Main-Mid-01 and Outflow never declined below 0.5 while Pond-Iso had distinct microbial membership from Inflow with low σ_m across the study period that never exceeded 0.5.

3.3.3 Comparison of Connectivity Metrics

Both geochemical and microbial connectivity strength metrics performed well in discriminating between sites that were connected as determined by tracer injections compared to sites where we did not observe arrival of injected tracer (Table 1, Figure 4). Across both injections, sites with observed tracer arrival had higher connectivity strength values (σ_g : 0.67 (mean) ± 0.02 (SE), σ_m : 0.77 ± 0.03) than did sites with no observed tracer arrival (σ_g : 0.33 ± 0.06 , σ_m : 0.31 ± 0.03). At sites with observed tracer arrival, σ_m was strongly negatively correlated ($R = -0.90$, p -value < 0.01) with time to peak (TTP) of the breakthrough curve, while σ_g was only moderately negatively correlated with TTP ($R = -0.62$, p -value = 0.16) suggesting σ_m may be more responsive to residence time than σ_g . Because Pond-Con-01 had high leverage in the correlation analysis, we also ran the analysis without Pond-Con-01 and found that σ_m was still negatively correlated with TTP ($R = -0.74$, p -value = 0.09), however there was no longer any correlation between σ_g and TTP ($R = -0.15$, p -value = 0.96).

In comparing the surface connectivity duration above 0.5 (C_{dur}) for each site, σ_m and σ_g generated similar results across sites ($R = 0.98$) but were more moderately correlated with C_{dur} as measured with relative stage (σ_m : $R = 0.71$; σ_g : $R = 0.71$) (Figure 5a & 5b). All three metrics identified stable connected conditions (100% C_{dur}) at Main-Mid-01 and Outflow. However, while σ_m and σ_g identified stable disconnected conditions at Pond-Iso (0% C_{dur} , Figure 5c), the source-target stage relationship analysis identified connectivity inflection points at Pond-Iso (55% C_{dur} , see Figure 5a & b). Despite strong correlations between C_{dur} derived from σ_m and σ_g , there were several sites with

substantively different C_{dur} between metrics including Pond-Con-01 ($\sigma_m = 57.5\%$, $\sigma_g = 47.7\%$), Side-01 ($\sigma_m = 49.7\%$, $\sigma_g = 35.9\%$) and Side-04 ($\sigma_m = 24.8\%$, $\sigma_g = 12.4\%$).

3.3.4 Connectivity Regimes

Across the 2018 study period, sites identified as stable ($C_{dur} = 0\%$ or 100% ; Outflow, Main-Mid-01, & Pond-Iso) had generally unimodal distributions of connectivity strength with modes at high or low values (Figure 6). In contrast, distributions of connectivity strength at the remaining seven sites with intermittent connectivity, had wide spread and generally a dominant mode at lower connectivity values and a secondary mode at high connectivity values (Figure 6). Within the intermittent target sites, some sites such as Side-03 and Side-04 exhibited rapid shifts between modes in σ_g & σ_m with few observed sample dates with intermediate connectivity strength while others such as Pond-Con-01 exhibited more gradual behavior with intermediate connectivity strength values for a larger proportion of the study period (Figures 3 & 6).

Aggregating site specific results to the river-floodplain system reveals transitions in system surface connectivity. At high flows, conditions are more homogenous and there is relatively high connectivity across the entire river-floodplain system (Figure 7a & b). Conversely, there was a bimodal distribution of river-floodplain connectivity at intermediate flows with some sites remaining connected and others becoming disconnected from Inflow. The mean value of σ_g and σ_m across the river-floodplain system was positively related to Inflow stage (Figure 7c), whereas the variance in connectivity, as derived from the standard deviation of σ_g and σ_m , was highest during intermediate flows (Figure 7d). Hysteresis was observed in the relationship between mean σ_g and σ_m and Inflow Stage, reflecting hysteretic source-target relationships at Side-01 and Pond-Con-02.

At the river-floodplain system scale, we also found that defining binary σ_m surface connectivity thresholds to describe the system-wide behavior can be sensitive to the chosen σ_m threshold value (Figure 8). We varied the threshold between the 10th to 90th percentiles of σ_m and observed the effect on exceedance probabilities of how many sites are connected in the 2018 study period. Varying σ_m thresholds between 0.4 to 0.6 generated small shifts in the exceedance probabilities distributions. Outside that range, exceedance probability distributions exhibited larger changes in their shape (Figure 8).

3.3.5 Sensitivity of Floodplain Surface Connectivity to Inter-Annual Variability in Streamflow

Our modeled river-floodplain system connectivity dynamics (using only σ_m) differed across the hydrographs of five years reflecting the influence of inter-annual variability in the timing and magnitude of seasonal snowmelt hydrographs (Figure 9). To measure the inter-annual variability (termed total sensitivity) at each intermittently connected target site, we calculated the range in duration (% of period) within three connectivity categories: high ($\sigma_m > 0.6$), intermediate ($0.4 < \sigma_m < 0.6$) and low connectivity ($\sigma_m < 0.4$) (Figure 9, Table S4). Total sensitivity ranged between 15 to 21% for duration of high connectivity, 6 to 18% for intermediate connectivity, and 12 to 20% for low connectivity (Figure 9a). Along with generally lower total sensitivity for intermediate connectivity, the duration that sites spent in intermediate connectivity was also relatively low, with intermediate connectivity duration ranging between 7% to 32% of the study period across all intermittently connected target sites and years (Figure 9a, Table S4). This sensitivity is also reflected in the exceedance probabilities (% of period) of the percent of intermittent sites in high, intermediate and low connectivity categories. As one would expect, when examining hydrographs from higher streamflow years, connectivity at intermittent sites remained

high longer, while hydrographs from low streamflow years yield longer durations of low connectivity (Figure 9b).

3.4 Discussion

Coupling hydrometric measurements such as stage with measures of connectivity strength derived from geochemical and microbial indicators is useful for describing spatiotemporal patterns in surface connectivity at both specific target sites and at river-floodplain system scales. At the target site specific level, source-target stage relationships reveal patterns of hydrologic response to both shifting river flows and subsurface groundwater levels. While high water levels are associated with higher connectivity, source-target stage relationships are sensitive to both shifts in connectivity type and the site-level geomorphic controls on water level. However, these relationships do not necessarily contain information about the type of connectivity present (surface vs subsurface) without additional contextual information. For example, in our study both Pond-Con-01 and Pond-Iso demonstrated similar source-target stage relationships with Inflow throughout the hydrograph even though Pond-Iso likely had little to no surface connection with Inflow, whereas Pond-Con-01 did have surface connectivity. As such, source-target stage relationships did not reveal differences in surface connectivity between Pond-Con-01 or Pond-Iso and Inflow. However, our connectivity metrics derived from geochemical (σ_g) and microbial (σ_m) indicators did identify differences in connectivity between Pond-Con-01 and Pond-Iso and Inflow. Specifically, both σ_g and σ_m revealed low connectivity between Inflow and Pond-Iso but higher connectivity strength values between Inflow and Pond-Con-01 during high flows, both of which match our visual field observations. Accordingly, source-target stage relationships alone did not provide insight to functional connectivity defined by the observed influence of the source site on the target site, whereas geochemical and microbial indicators did. For this reason, in the discussion we focus on the σ_g

and σ_m connectivity strength metrics to describe spatial and temporal patterns of surface connectivity within the river-floodplain system.

3.4.1 Connectivity Strength as a Continuous Measure

Treating connectivity as a continuous value successfully enabled the development of connectivity functions that described site specific behavior in response to fluctuations in stage at Inflow. The site specific connectivity functions allowed us to predict surface connectivity at each target site daily throughout the main study period (May 01, 2018 through September 01, 2018). This approach also enabled us to assess the sensitivity of surface connectivity regimes across variable seasonal hydrographs using Inflow stage measurements from five years (2016 through 2020).

Using daily connectivity predictions for the 2018 study period, we identified three major surface water connectivity regimes during the study period (Figure 6). Sites were observed to have: high σ values and low spread for the majority of the study period, low σ values and spread, or intermittently connected with a wide range of σ values that varied with Inflow stage (Figures 5 & 6). Sites that had high σ for a large proportion of the study period were those located along the main stem of the river. At very low streamflows, these sites did exhibit evidence of a shift toward decreased σ_g and σ_m (Figures 2 & 5). This shift perhaps reflects increased transit time or alternatively, changes in source water composition within the reach. The only site to demonstrate low σ values throughout the study was Pond-Iso where we observed no surface connection to the main channel. Pond-Iso had a unimodal distribution of low σ values despite being geographically near Inflow (Figure 1b), helping demonstrate that surface connectivity rather than geographic proximity is the primary driver of high connectivity strength. At sites with intermittent surface connectivity, interactions between river flow dynamics and floodplain geomorphic structures generated site-specific variability in connectivity regimes. Distributions

of σ_m and σ_g connectivity strength at all intermittent sites, except at Main-Mid-02 and for σ_m at Pond-Con-01, were characterized by a dominant mode of low connectivity strength and a secondary mode of higher connectivity strength (Figure 6). This reflects that at the majority of floodplain target sites, high connectivity strength values are only maintained at Inflow stages well above the median stage of 424 mm during the 2018 study period.

While this bimodality at intermittently connected target sites could make a case for treating surface connectivity as binary, we observed some sites experience prolonged periods of intermediate connectivity strength. If we consider σ values of $0.4 < \sigma < 0.6$ to be intermediate connectivity, then during the 2018 study period, some sites spent as much as 38% of the study period in a state of intermediate connectivity (ranges: σ_m : 7%-30%; σ_g : 12-38%). Intermediate connectivity strength may reflect conditions when surface flow rates and volume from the main channel have diminished but surface water storage remains relatively high. As such, there is increasing dissimilarity of target site conditions from the source site, which could result from a combination of higher residence times, increased lags in solute and microbial transport and influences from other water sources (i.e. groundwater). Identifying places with longer durations of intermediate surface connectivity is thought to be particularly important for identifying control points (sensu Bernhardt et al., 2017) in a landscape that have disproportionate influence on hydrologic and biogeochemical properties of the ecosystem. In river-floodplain systems, sites with high durations of intermediate connectivity may act as control points because they can have a substantial flux of river water moving through them but also long enough residence times for microbially mediated biogeochemical processes that are distinct enough from those in the main stem river to influence ecosystem properties downstream (Covino, 2017; Lynch et al., 2019).

3.4.2 Microbiomes as complementary sources of connectivity information

While geochemistry and microbiome membership were broadly similar when calculating connectivity metrics such as surface connectivity duration (Figure 5), we also observed key distinctions that illustrate how microbiome membership may provide additional information about connectivity not observed in hydrologic and geochemical metrics. Within our system, σ_m was strongly negatively correlated with time to peak during our tracer experiments suggesting that σ_m is responsive to residence times (Figure 4). In contrast, σ_g was less well correlated with time to peak (Figure 4). This is consistent with known differences in drivers between the two metrics. Geochemistry will reflect mixing of source waters which may or may not be related to residence times. The majority of geochemical solutes used in this study are not likely to be reactive at timescale of surface residence times. Of these, sulfate (SO_4^-) is more reactive but typically only under anoxic conditions which is rare in ecosystems of low residence time. In contrast, ecological theory predicts that microbial communities are shaped not just by dispersal but also by local ecological dynamics that tend to dominate microbiome assembly as residence time becomes greater than growth rate (Lindström et al., 2005). As flow decreases and residence times increase in a water body, selection driven by local environmental conditions is likely to become a larger factor relative to dispersal (i.e. immigration and emigration) in determining microbiome membership (Mayr et al., 2020), which could result in increasing dissimilarity in microbiome membership between a source and target location.

This shift towards a selection driven microbial community assembly may be most observable when residence times increase above a certain threshold, which might help explain the differences we observed at Pond-Con-01 between the microbial and geochemical connectivity metrics (Figure 3 & 5, Table S1). At Pond-Con-01, σ_m had a gradual, mostly linear relationship with Inflow stage with an inflection point at moderate Inflow stage (I_{micro} : 438 mm, see Figure 3). Although σ_m revealed a change in connectivity to Inflow at this stage (438 mm), pond stage remained relatively invariant at these flows (Figure 3). Additionally, σ_g was relatively invariant with Inflow stage until a sudden drop at low Inflow

stage (I_{geo} : 381 mm), which occurred closer to the timing ($I_{\text{stage}} = 366$ mm) at which stage began falling (Figure 3). The surface flowpath between the river and Pond-Con-01 passed through several beaver ponds before reaching the site. As a result, even at peak river flows, water velocities through Pond-Con-01 were low, and travel times were long, relative to other sites (Table 1). As streamflow declined, the water flux into the pond also decreased and residence times increased because pond levels and volume remained stable while velocity decreased. Through this period, the stable levels and persistence of high geochemical connectivity strength suggest a surface flow connection to the river was maintained, but the degree of influence of the river on the pond microbiome declined. Thus, from a functional connectivity perspective, one could either say the site was at different connectivity strengths with the Inflow depending on which metric was examined. This reinforces that functional connectivity is defined by the metric of interest. Select of methods requires consideration what aspects of connectivity are being reflected by each method and which is most useful for different research or management questions (Wohl et al., 2019).

3.4.3 Connectivity Regimes: Scaling from Site to System Scales

Aggregating site dynamics to river-floodplain system scale behavior is critical for understanding how river-floodplain connectivity impacts broader landscapes processes. While our analyses here are limited due to our relatively small sample size of sites, aggregation of site behavior did reveal important distinctions between mean system behavior and spatially distributed behavior. As conceptualized in the flood and flow pulse concepts (Junk et al., 1989; Tockner et al., 2000), mean surface connectivity across the river-floodplain system rose as streamflow increased (Figure 7c). Thus, while threshold-like behavior was observed at many individual sites, mean system behavior followed a continuous gradient because the connectivity thresholds were highly variable among sites. However, it is also clear that the mean is a

poor descriptor of the spatially aggregated behavior, particularly at lower river flows when connectivity strength values across the floodplain had a bimodal distribution with some sites maintaining relatively high surface connectivity while the majority were surficially disconnected. This has important implications for scaling many spatially distributed biogeochemical and ecologic processes impacted by connectivity such as carbon production and storage, nutrient retention, and methane fluxes (Lynch et al., 2019; Roley et al., 2012; Samaritani et al., 2011; Sutfin et al., 2016).

The low variance in connectivity observed at high river flows (Figure 7c) is consistent with the flood homogenization theory that physical and chemical states across floodplains are more similar at high flows (Thomaz et al., 2007). Our results also support the idea that physio-chemical condition at individual sites in floodplains are most different from the river at the lowest flows (low σ values) due to isolation. However, our findings diverge from the homogenization theory in that peak variability in connectivity dynamics was observed at intermediate flows rather than low flows. Thus, while individual sites might be most different from each other at lowest flows due to isolation, the distribution of connectivity dynamics across the floodplain was most variable when river stage was intermediate and some sites were surficially isolated while others remained strongly or moderately connected to the source.

3.4.5 Inter-annual Variability in Connectivity at Site-Specific and River-Floodplain System Scales

In watersheds characterized by a single large snowmelt event, hydrologic variability is often driven by inter-annual variation in snowpack accumulation and melting that regulates the timing and magnitude of streamflow (Hammond et al., 2018). In floodplains within these watersheds, whether surface connectivity regimes are sensitive to this inter-annual variability will depend on the interactions between streamflow hydrographs and the physical structure of river-floodplain connections. Assessing

this sensitivity can inform our understand of variability under current hydro-climate regimes, and can help us predict the implications of forecasted future climate changes including lower snowpack, earlier snowmelt and drier late season conditions (Barnett et al., 2005; Stewart et al., 2005). Here, for simplification we hold physical structure constant, but we also recognize there are interactions between changing climate and dynamic physical structures. Given this assumption of physical stationarity, our analysis for five years at intermittent sites highlight that connectivity regimes are sensitive to streamflow variability with substantial year to year shifts at sites in the duration of high and low connectivity. We also observed that within a given river-floodplain system, there will be spatial variation in sensitivity that will be driven by the river-floodplain physical structure and corresponding stage thresholds, but also can be related to the manner of changes in streamflow hydrographs. This can be observed in our dataset by comparing floodplain surface connectivity based on river flow dynamics from two low flow years: 2018 and 2020. In 2018, we observed the lowest peak flows at Inflow in the five year dataset but 2018 had a longer duration of medium to high flows than was observed in 2020 (Figures 8 & S5). As a result, a majority of sites remained highly surficially connected for longer in 2018 than 2020, while durations of intermediate connectivity were highest in 2020. As such, efforts to understand how climate change will alter floodplain function will need to consider both changes to flow magnitudes and to flow durations.

3.4.6 Limitations and Recommendations for Future Research

While the approach developed in this manuscript successfully describes spatiotemporal connectivity dynamics, there are several assumptions and limitations that future work should consider. Connectivity strength metrics used here enable the development of a continuous value between 0 and 1, however the meaning of the connectivity strength values are dependent on the internal variation

within a system and interpretation may differ among systems. As such, we suggest that when identifying thresholds in different connectivity states, future research should consider a distribution of possible connectivity strength values (see Figure 9). Additionally, in this study we only observe source to target connectivity from a single source which limits our ability to describe surface connectivity between different habitats within the floodplain. While it was outside the scope of this effort, we suggest that future efforts could attempt to consider multiple sources but to do so, one would first need to identify what target sites have structural connections to each source.

An additional limitation is that the empirical connectivity functions we developed assume stationarity in the underlying floodplain structure unless models are explicitly fit to account for hysteretic relationships. Our observations of hysteresis at two sites in 2018 was likely driven by the construction of beaver dams that were subsequently breached by high flows. In beaver-mediated river-floodplains, such hysteresis may actually be a consistent feature of these system as beaver dam construction often occurs at lower flow periods. More broadly, as river-floodplains often have highly dynamic geomorphology, such changes in connectivity thresholds are likely relatively common. However, such assumptions are equally present in all approaches reliant on static physical datasets such as single date LIDAR acquisition or field surveys (Passalacqua et al., 2015). Therefore, we believe our approach is valuable for longer-term studies, but that conditions should be monitored through time and relationships updated similar to how a rating curve used to estimate discharge needs to be updated if the underlying channel morphology is altered during the study period.

While our work demonstrates that aquatic microbiomes can be utilized for inference into hydrologic connectivity, our ability to determine the broad applicability of this technique is limited. This study was conducted in a relatively small river-floodplain system with relatively homogenous surrounding land cover. To apply the microbial connectivity metric more widely, future work will need to assess how residence time thresholds in different systems and at different scales interact with microbial

membership. Further, as investigations move to larger, more heterogeneous landscape scales, it will be necessary to consider how to incorporate more diverse sources of water and microbes into the approach.

3.5 Summary

In this study, we developed and applied an approach to assess the strength of surface hydrologic connections between a source and target sites within a river-floodplain system using field-based indicators. We defined the source as the river at the upstream boundary of the river-floodplain system with target sites both downstream within the river channel and laterally distributed across the floodplain. Using a field-based dataset, we generated empirical models to describe target connectivity strength, and then tested the sensitivity of connectivity regimes to inter-annual variability in streamflow. Within this approach we also tested the use of aquatic microbiomes and geochemistry as metrics of hydrologic connectivity. By examining similarity in microbial membership and geochemical composition, we accurately assessed the presences/absences of surface flows from the source to target sites. We further found that aquatic microbiomes can provide additional information on residence time dynamics along connected surface flow paths.

Our results demonstrate that surface connectivity in aquatic water bodies in the river-floodplain system can either be stable or intermittent. Intermittently connected target sites can differ widely in source connection/disconnection thresholds. While some target sites demonstrate binary connectivity behavior quickly changing between high and low connectivity states, others display gradual behavior with substantial durations at intermediate connectivity levels. When aggregated to the river-floodplain system scale, mean system-scale surface connectivity increased with stage due to the influence of averaging across sites with heterogeneous conditions. However, we demonstrate that mean behavior is

a poor descriptor of river-floodplain system behavior because spatial distributions of surface connectivity across all sites tend toward bimodality at intermediate and lower flows, reflecting conditions when river stage is sufficient to enable surface connectivity for only a portion of the system. As a result, the spatial heterogeneity of connectivity peaked at intermediate river stage values. We also demonstrate that surface connectivity regimes are sensitive to inter-annual variation in streamflow and that while differences in the magnitude of peak flow are important so are changes to the flow duration across the range of differing flow states. Collectively, our findings demonstrate that our approach enables improved observations of hydrologic functioning within a heterogeneous landscape and can serve as a tool for better linking hydrologic process to ecologic and biogeochemical outcomes in river-floodplain systems.

Table 3.1: Results of high and low flow conservative tracer injections. NaCl was injected 125m above Inflow, the source location, and monitored at the 6 target sites listed in the “Target Site” column. NR indicates that no tracer arrival was observed at the target site. There was no observed surface water connection between Inflow (the source) and Pond-Iso, but there were observed surface water connections between Inflow and the remaining 5 sites listed for at least part of the study period (May – October 2018).

Target Site	Site Type	Elevation (m)	Surface Connection to Inflow	Inflow Stage (mm.):	High Flow (June 13, 2018)		Low Flow (July 30, 2018)	
					DISTf ¹ (m)	TTP ² (min)	Vmod ³ (m/s)	TTP ² (min)
					635		384	
Outflow	Major Channel	2529	Yes	2228	46	0.78	85	0.43
Main-Mid-01	Major Channel	2536	Yes	1175	23	0.87	41	0.48
Side-01	Side Channel	2542	Yes	607	35	0.29	NR	NR
Pond-Con-01	Connected Pond	2537	Yes	1040	196	0.09	NR	NR
Pond-Con-02	Connected Pond	2541	Yes	734	101	0.12	NR	NR
Pond-Iso	Isolated Pond	2547	No	-	NR	NR	NR	NR

1) Estimated surface flow path distance from the injection site. Note there is no surface channel connection between Inflow and the Isolated Pond (Pond-Iso)

2) Time to Peak

3) Modal Velocity – calculated as DISTf / TTP

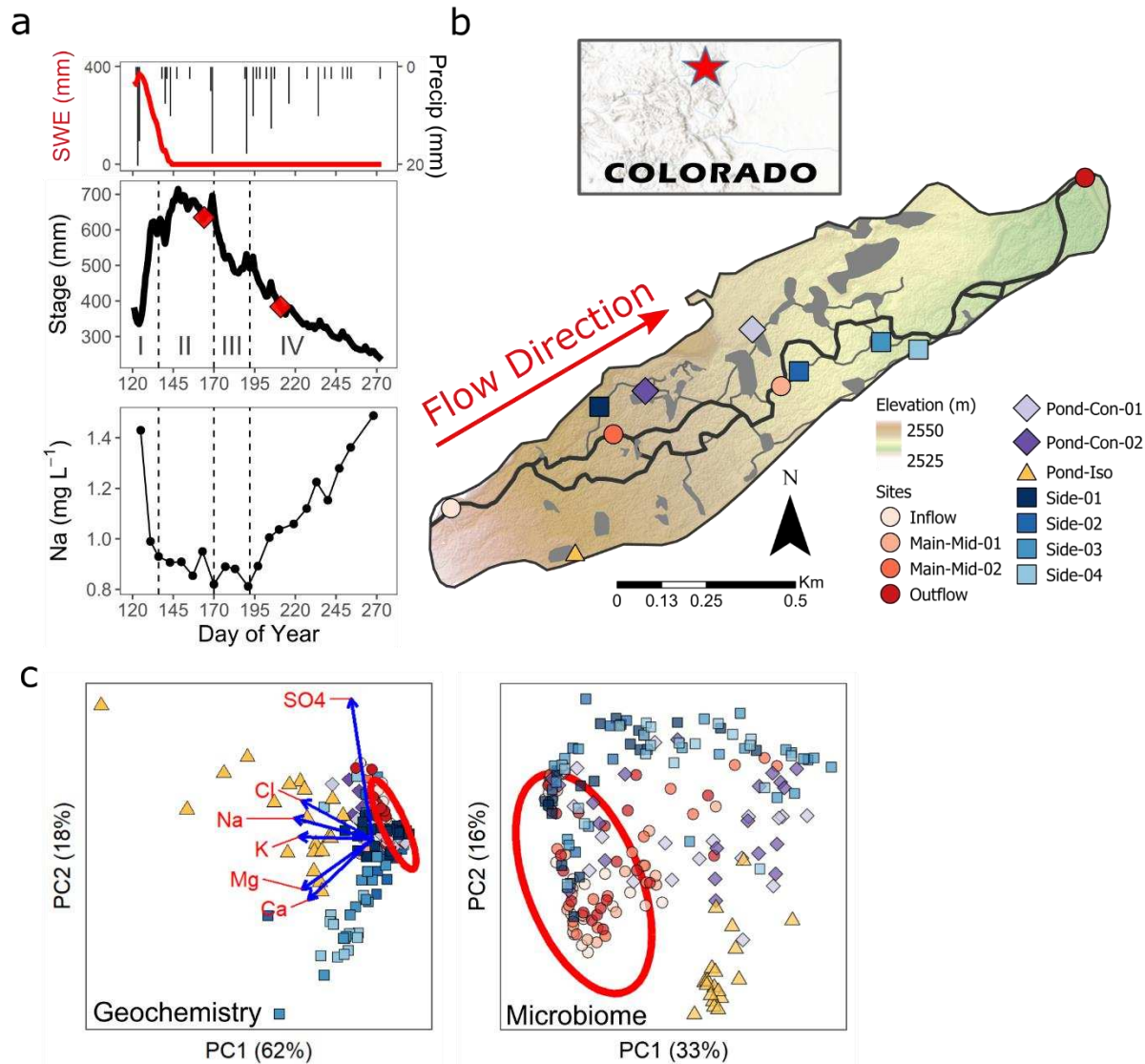


Figure 3.1: (a top) Precipitation and snow water equivalent (SWE) from SNOTEL #1042, (a middle) stage and (a bottom) sodium (Na) concentrations at Inflow, (b) North St Vrain river-floodplain map, and (c left) geochemical PCA and (c right) microbiome PCOAs showing full sampling dataset with axis labels indicating variance explained on each axis. Red line in (a top) is SWE, red diamonds in (a middle) indicate dates of tracer injection experiments. River flow hydro-periods in (a) are categorized as (I) rising limb, (II) peak flows, (III) falling limb, and (IV) recession. Map shows depiction of surface water major river channels (dark grey) and floodplain surface features including ponds, wetlands and side channels (lighter grey). Red circles in (c) are 90% confidence ellipses for Inflow site.

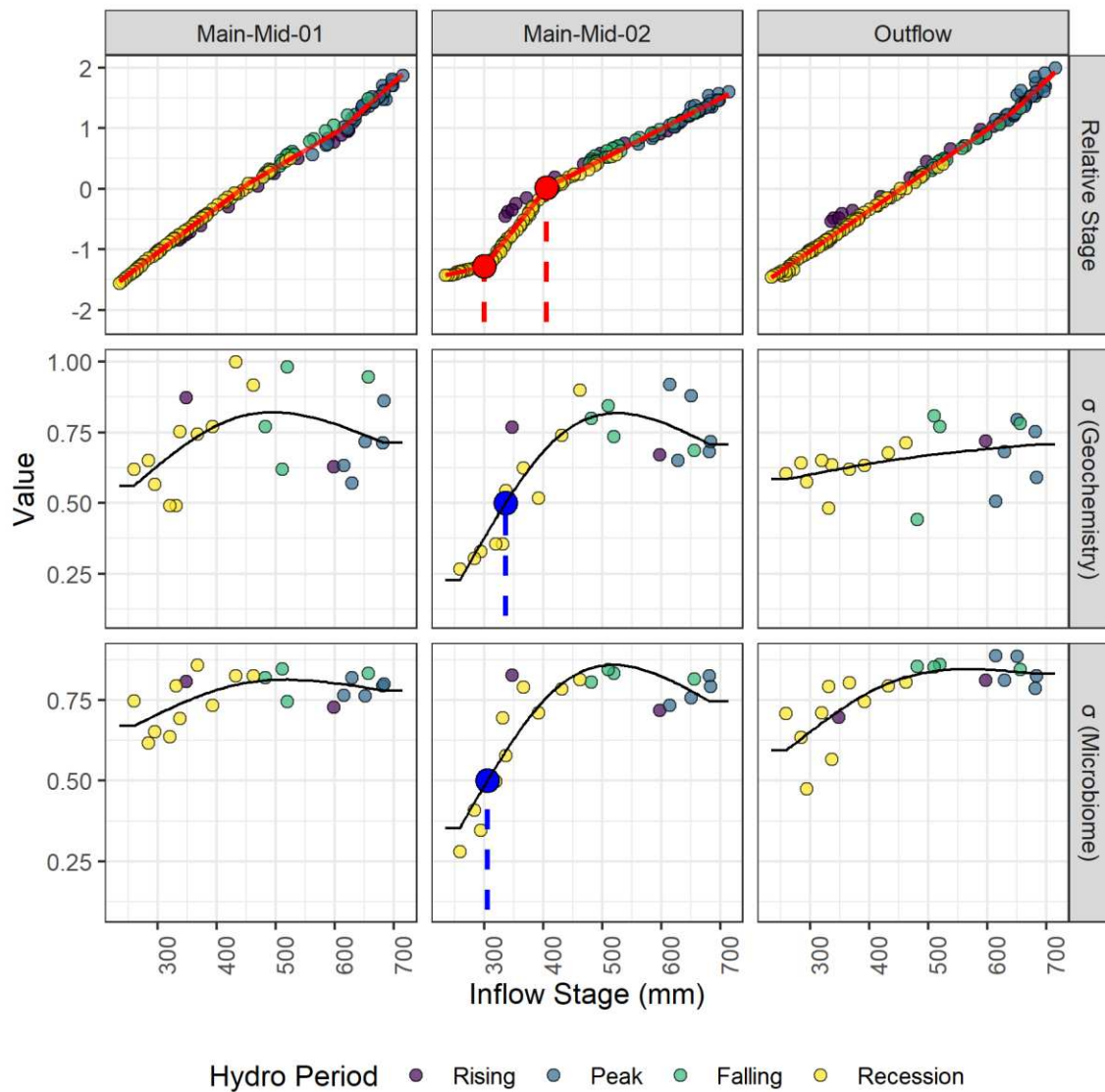


Figure 3.2: Source-target relationships between Inflow stage and major channel target sites for relative stage (i.e., stage z-score, top row), geochemistry surface connectivity strength (middle row), and microbiome surface connectivity strength (bottom row). Red lines in the top row are broken stick regression predictions, and red dots and dashed lines are the identified inflection points in the source-target stage relationships. Black lines in the middle and bottom rows are the spline regression functions for connectivity strength metrics. Blue dots and dashed lines in middle and bottom rows are the Inflow stages at which surface connectivity strength functions are equal to 0.5. Missing blue dots/lines indicate that the surface connectivity strength function remained either above or below the 0.5 threshold for the duration of the study at that particular location.

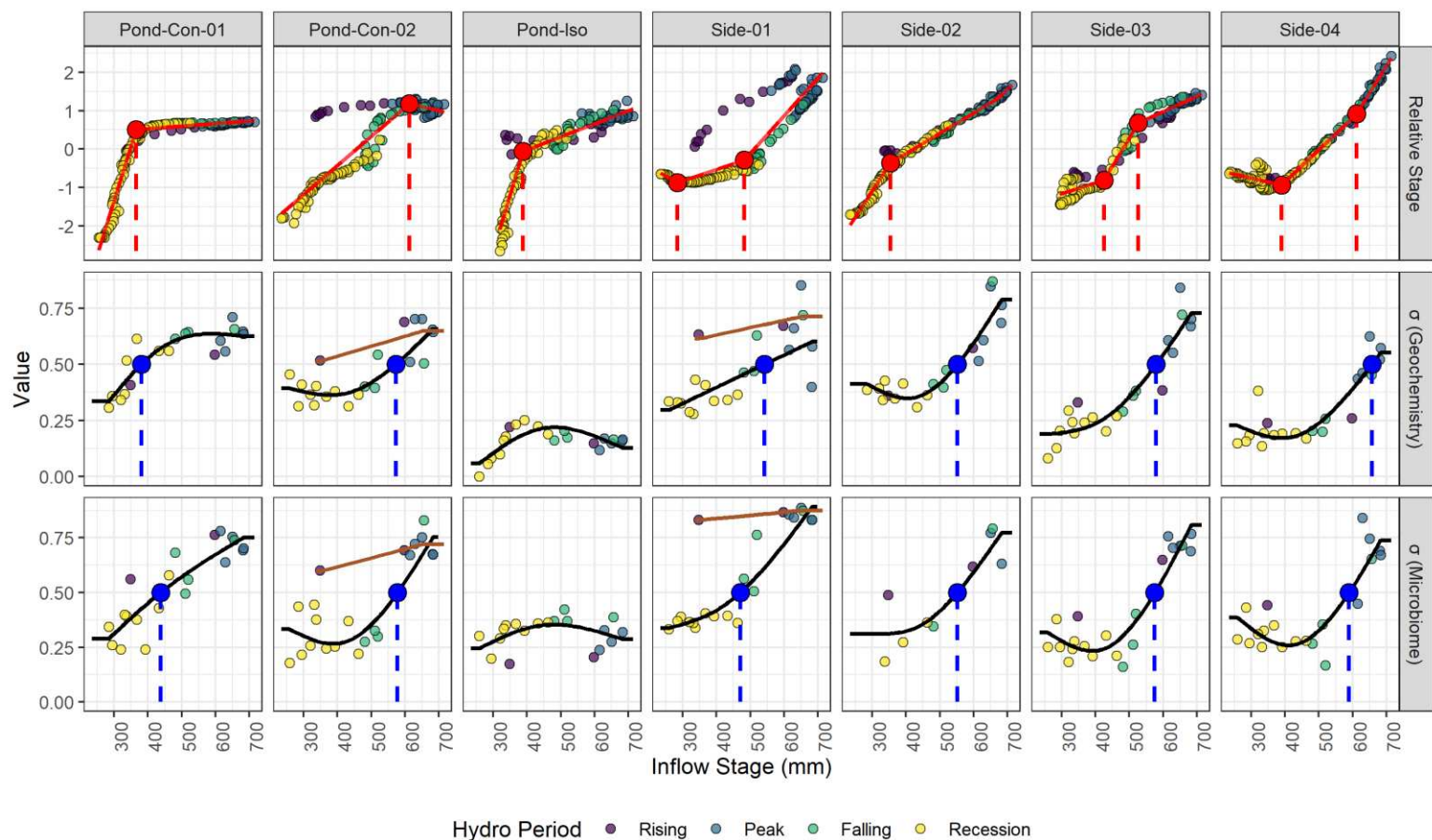


Figure 3.3: Source-target relationships between Inflow stage and floodplain target sites for relative stage (i.e., stage z-score, top row), geochemistry surface connectivity strength (middle row), and microbiome surface connectivity strength (bottom row). Red lines in the top row are broken stick regression predictions, and red dots and dashed lines are the identified inflection points in the source-target stage relationships. Black lines in the middle and bottom rows are the spline regression functions for surface connectivity strength metrics. At sites with hysteric behavior (Side-01 & Pond-Con-02) there are two fits for the rising limb (brown lines) and falling limb (black lines). Blue dots and dashed lines in middle and bottom rows are the Inflow stages at which connectivity strength functions are equal to 0.5. Missing blue dots/lines indicate that the connectivity strength function remained either above or below the 0.5 threshold for the duration of the study at that particular location

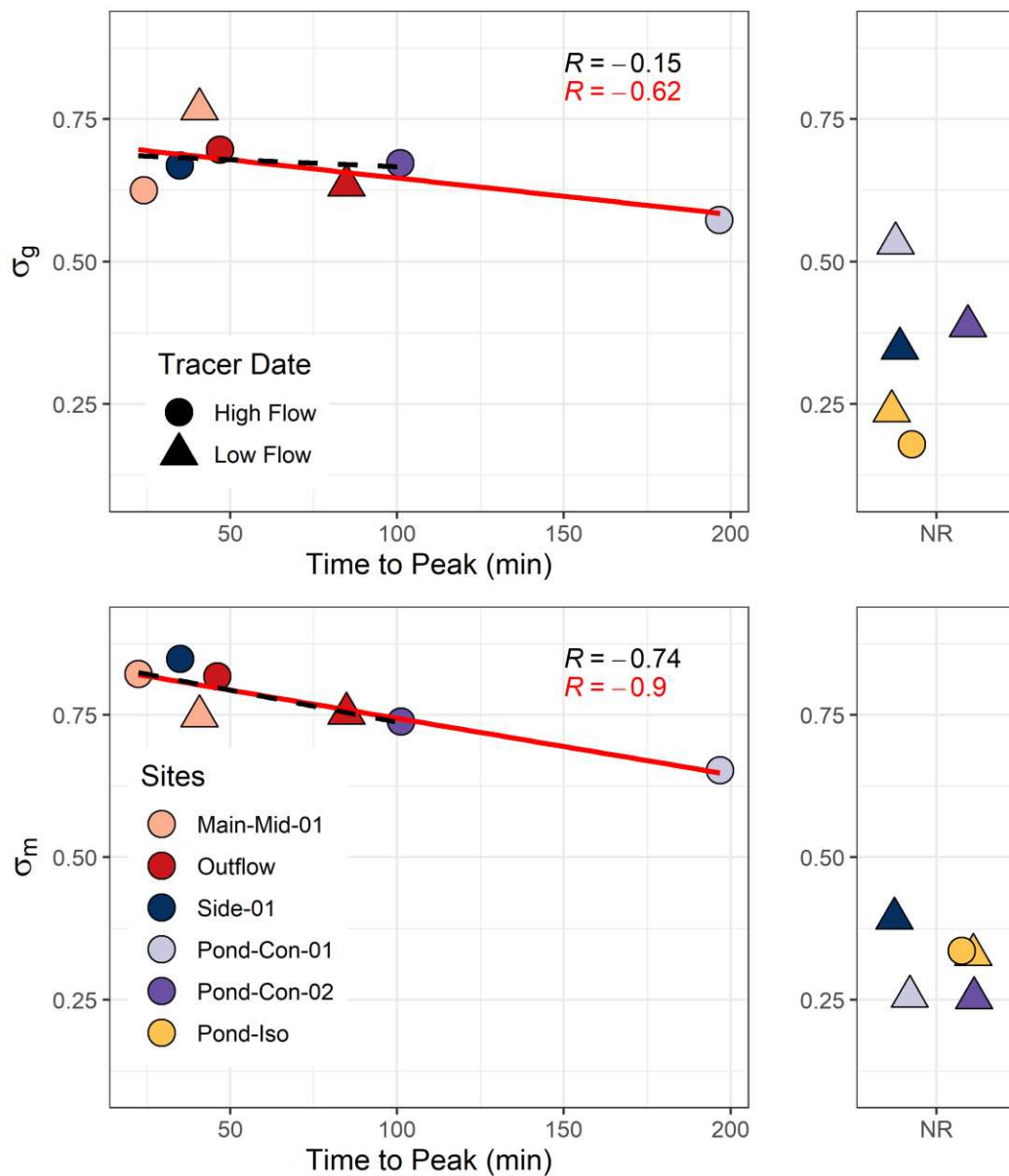


Figure 3.4: Surface connectivity strength metric validation with tracer response and time to peak in minutes (TTP), including results from both high (circle) and low (triangle) flow tracer injections (see Table 1 for tracer injection details). The left panels show sites and dates where we observed tracer arrival. Conversely, the right panels show sites and dates where there was no observed tracer arrival. The x-axis of the left panels is the time to the peak of the injected tracer breakthrough curve, and NR on the x-axis of the right panels indicates no response (i.e., there was no observed arrival of injected tracer). Pearson correlation coefficients were calculated between surface connectivity strength and TTP both including (red) and not including (black) Pond-Con-01 high flow tracer response due to high leverage of that point. Both connectivity strength metrics distinguished well between sites with and without responses. The microbiome connectivity metric (σ_m) correlated more strongly with TTP.

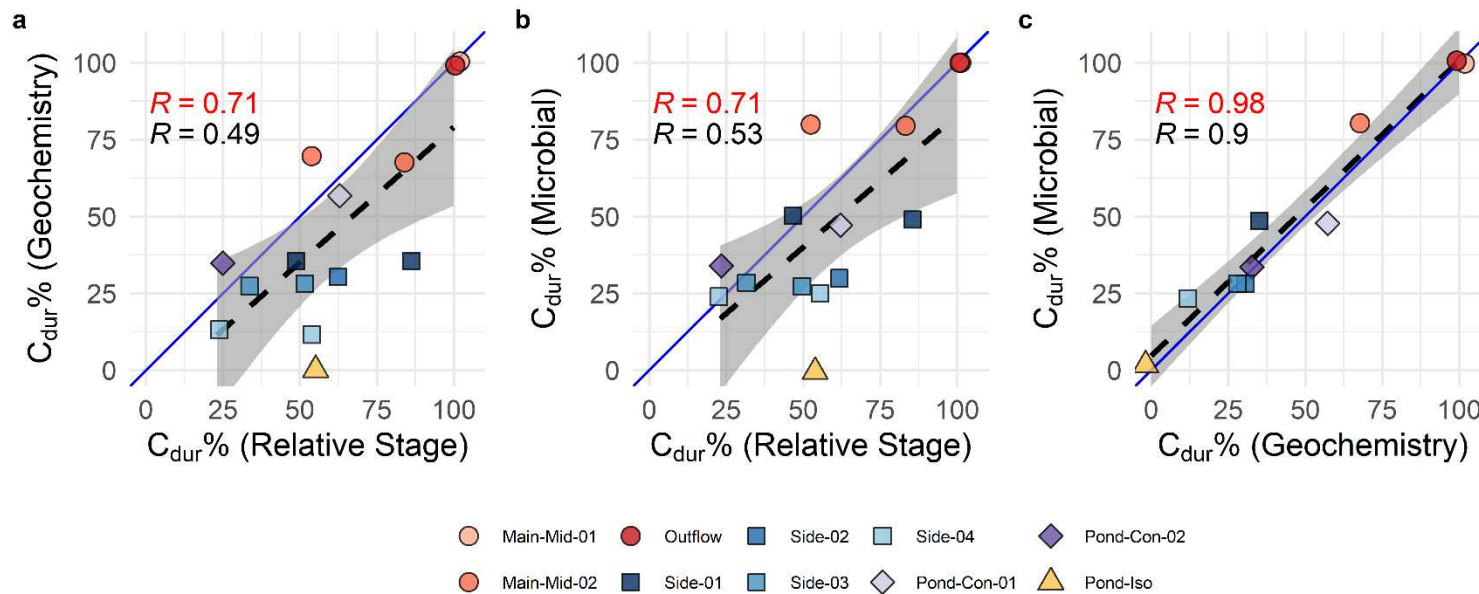


Figure 3.5: Surface connectivity duration (C_{dur}) at each site (as percent of 2018 study period) comparison as calculated with a) relative stage and geochemistry connectivity strength, b) relative stage and microbial connectivity strength and c) geochemistry and microbial connectivity strength. At sites with two identified inflection points in relative stage (see Figures 2 & 3), both inflection points were used for C_{dur} calculations and both C_{dur} values are included in panel (a) and (b). Blue solid line is 1:1 line. Pearson correlation coefficients (R) were calculated for all sites (shown in red font) and at sites with intermittent surface connectivity (excluding Outflow, Main-Mid-01 & Pond-Iso) excluded (shown in black font). Best fit line (black, dashed) includes all sites. Surface connectivity duration derived from relative stage is moderately correlated with other metrics while the two connectivity strength metrics are strongly correlated with each other.

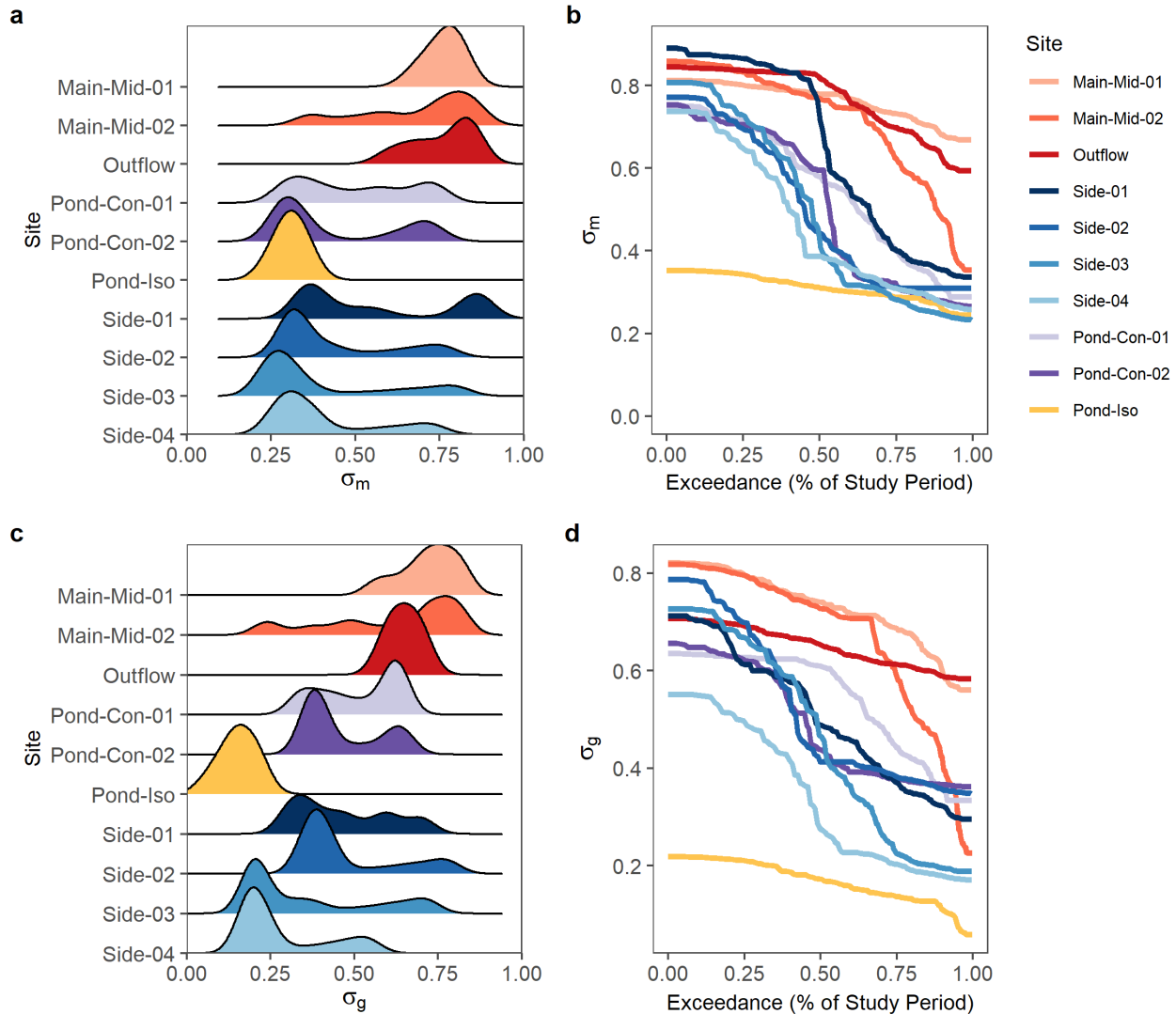


Figure 3.6: Target site-specific surface connectivity distributions during 2018 study period based on modeled daily geochemistry (σ_g) and microbiome surface connectivity strength (σ_m). a & c) Kernel density plots of σ_m & σ_g respectively. b & d) Empirical duration curves of σ_m & σ_g respectively. Sites with stable connectivity exhibit small spread in kernel density plots, while most intermittently connected sites exhibited high spread and a dominant mode at low surface connectivity strength values. Some intermittently connected sites had moderate durations at intermittent connectivity strengths while other sites exhibit rapid shifts between high and low strength values, demonstrated by the slope of lines in panel b & d.

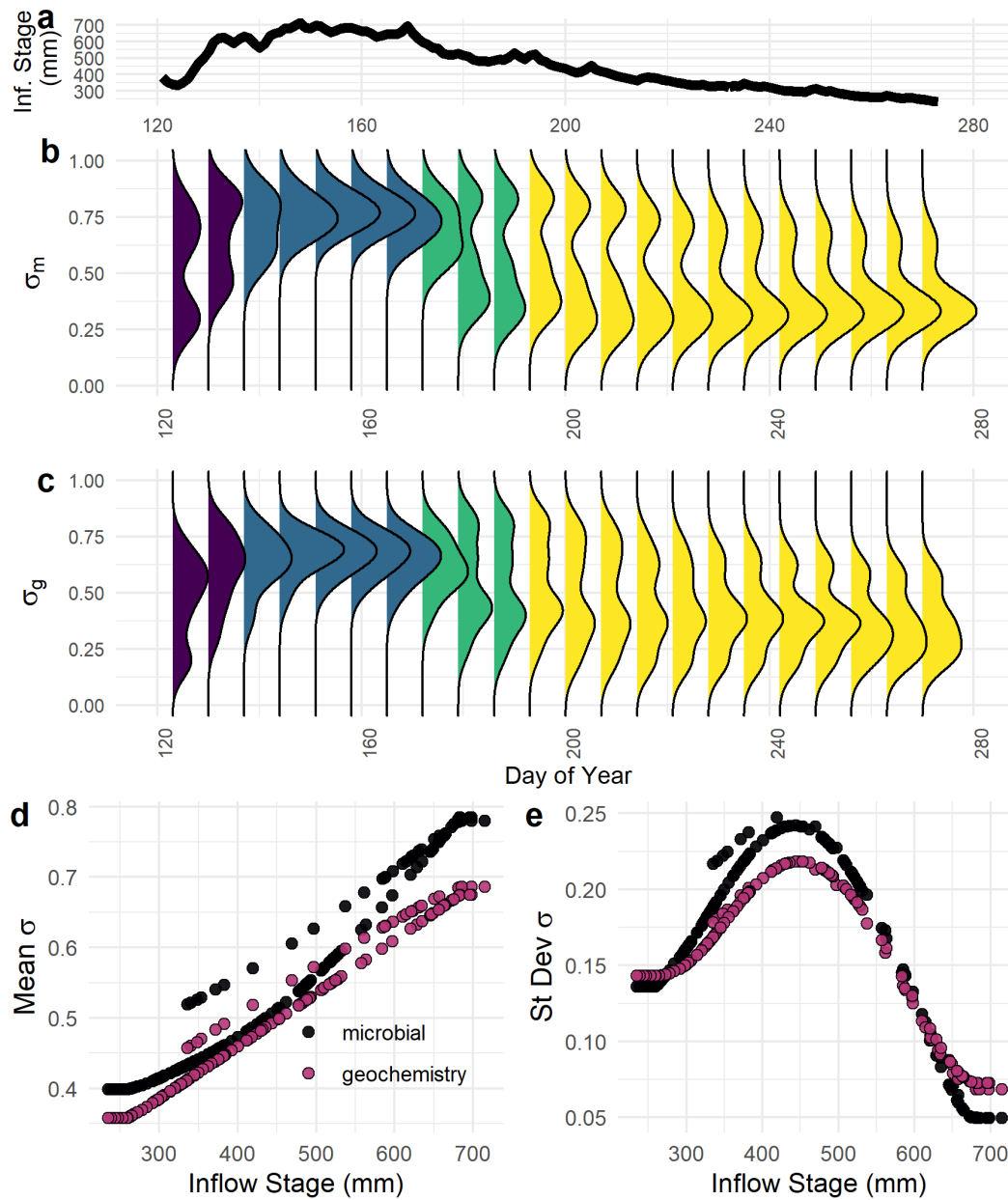


Figure 3.7: Aggregated system scale surface connectivity dynamics for 2018 study period using modeled daily surface connectivity strength (σ_m & σ_g). a) Inflow stage. b & c) Kernel density of weekly mean σ_m and σ_g respectively for sites (excluding Pond-Iso) colored by hydro period: rising (purple), peak (blue), falling (green), and recession (yellow). c) Relationship between daily system mean surface connectivity strength and Inflow stage. d) Relationship between daily standard deviation of surface connectivity strength across the river-floodplain system. Mean system connectivity increases with Inflow stage while variation in system connectivity peaks at moderate Inflow stages. Hysteric behavior in (c) is propagated from hysteresis in inflow-site connectivity functions observed at Side-01 and Pond-Con-02. Flat lines in (c) and (d) at very low and high values are boundary effects caused by making predictions outside the range of Inflow stages that were sampled during study period.

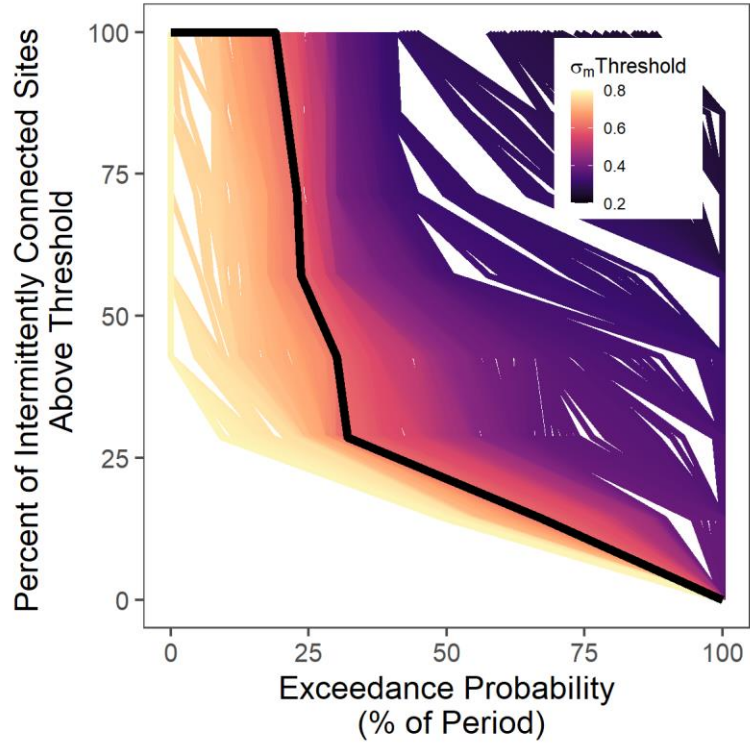


Figure 3.8: Aggregated river-floodplain system scale surface connectivity in 2018 across variable microbial surface connectivity strength (σ_m) thresholds. The threshold is varied between the 10th to 90th percentiles of σ_m . Connectivity strength is calculated with the microbiome metric. Only sites with an observed intermittent connectivity regime in 2018 were included (7 of the 10 target sites). Black line represent 0.5 σ_m threshold value

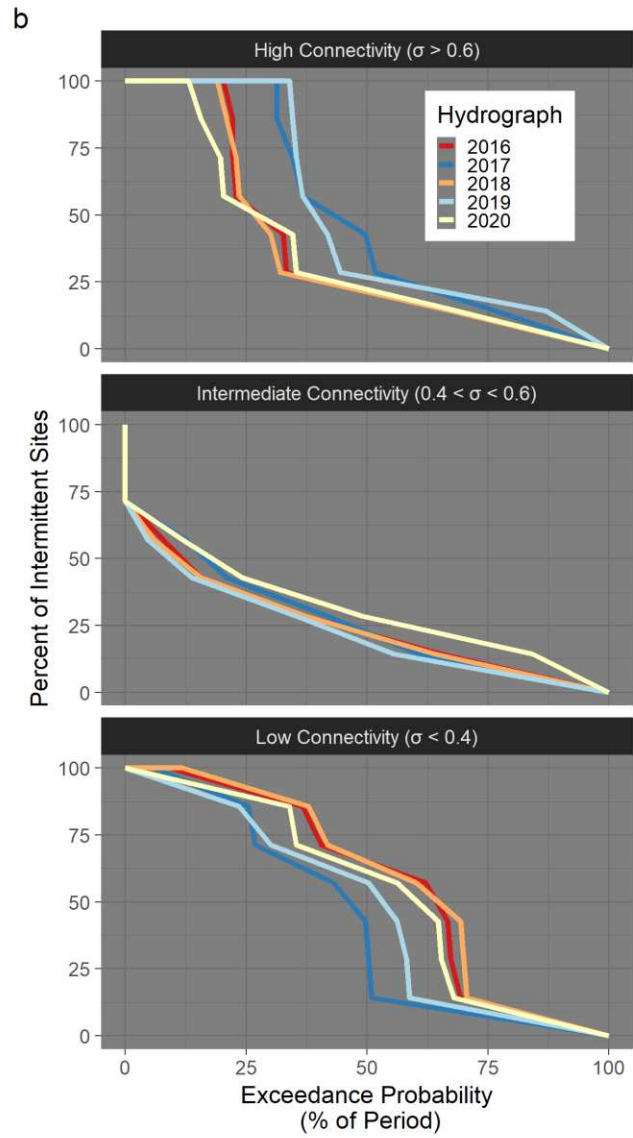
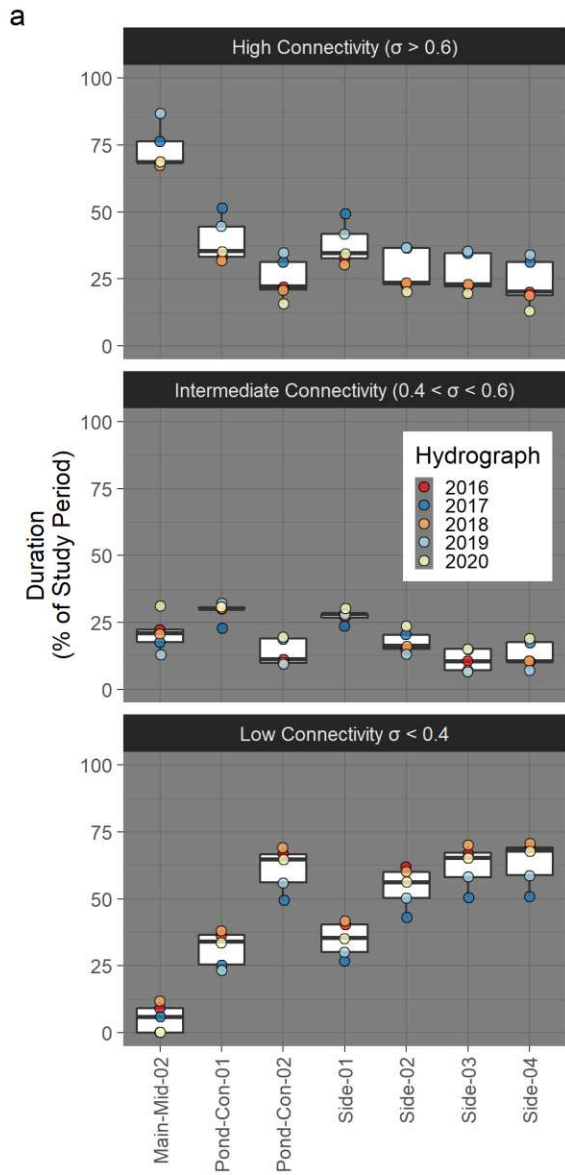


Figure 3.9: Sensitivity of river-floodplain connectivity to variability in season streamflow based on Inflow streamflow records from 2016-2020. Microbial surface connectivity strength (σ_m) is predicted using 2018 site-specific models applied to observed Inflow stage records in each year. This assume homeostatic relationships between connectivity and Inflow stage across years. a) Boxplots of duration of high, intermediate and low connectivity as percent of May-September study period. b) Exceedance probabilities of fraction of sites connected across the study period. Color for each year reflects annual wetness and is ordered from low (red) to high (blue) using annual median Inflow stage. Connectivity strength is calculated using the microbiome metric and only sites with an observed intermittent connectivity regime in 2018 were included (7 of the 10 target sites). The duration of high and low surface connectivity were moderately sensitive to inter-annual streamflow variability across all sites, generating variation in floodplain scale dynamics between high and low flow years. The duration of intermediate surface connectivity was lower overall at most sites, and at several sites these durations were insensitive to inter-annual flow variation, resulting in less sensitivity in intermediate connectivity dynamics across the river-floodplain system.

CHAPTER 4: ECOHYDROLOGY IN THE RIVER CORRIDOR: INVESTIGATING THE INTERDEPENDENT EFFECTS OF WETLANDS, CLIMATE, HUMAN DISTURBANCE AND TOPOGRAPHY ON PRODUCTIVITY AND CLIMATE SENSITIVITY OF VEGETATED MOUNTAIN RIVER CORRIDORS

4.1 Introduction

Globally, human activities have caused widespread wetland loss throughout many of the world's river corridors (Krause et al., 2011; Lee Foote et al., 1996; Rajib et al., 2021; Tockner & Stanford, 2002b). Wetland losses are thought to be magnified in mountainous regions because river corridor wetlands tend to occur in wide, low gradient alluvial valley bottoms which are infrequent within mountain river networks (Salo & Theobald, 2016; Standford et al., 1996). Within mountain river corridors, wetlands were once present even in semi-arid to arid climates, because surface and subsurface connectivity between rivers and their adjacent floodplains maintained sufficiently high water tables throughout growing seasons (Manning et al., 2020; Stanford & Ward, 1993a). However, anthropogenic impacts have caused widespread drying, burial, removal, and degradation of riparian wetlands across the globe (Walter & Merritts, 2015; Wohl et al., 2021). In the mountainous areas of the Western United States, wetland degradation in river corridors has been compounded by both legacy and ongoing impacts including the extirpation of beaver and predators from the landscape (Beschta & Ripple, 2012), flow and sediment regulation (Kuiper et al., 2014), agriculture and ranching (Trimble & Mendel, 1995), placer mining in rivers, development and related infrastructure including levees, ditches, roads and railways (Wohl, 2006). River corridor wetland habitats also face new threats as climate change alters mountain ecosystems with likely reductions of future snowpack and streamflow and increasing frequency of extreme events including floods, wildfires and droughts (Dwire et al., 2018; Perry et al., 2012; Schneider et al., 2017).

Wetlands in river corridor have coupled relationships between vegetation and hydrologic processes that are mutually responsible for vegetation patterning and wetland function (Loheide & Gorelick, 2007). River corridor wetlands are often mosaics containing wetlands with mixed covers of marsh, peatland vegetation and woody wetland species (Cooper et al., 2012). In non-degraded, hydrologically-connected river corridor floodplains of the Southern Rockies Ecoregion, wetland vegetation is typically dominated by willows (*Salix spp*) but also cottonwoods (*Populus angustifolia*) and aspens (*Populus tremuloides*), and emergent wetland species including sedges (*Carex spp*) (Drummond, 2012). River corridors also contain surface water expressions including river channels, ponds and backwaters. Therefore, the presence or absence of wetland or more upland vegetation can be an indicator of the degree of degradation in the river corridor (Karpack et al., 2020; Macfarlane et al., 2016). The presence of willows, in particular, is often dependent on the presences of beavers as the two have a mutualistic relationship. Willows supply forage and dam building materials for beavers while beavers, through their dam building maintain hydrology and geomorphic conditions favorable to willow establishment and growth (Gibson & Olden, 2014; Polvi & Wohl, 2012; C. J. Westbrook et al., 2011; Cherie J. Westbrook et al., 2006). Alternatively, vegetation cover in degraded river corridors may also reflect an alternative stable state dominated by grasslands that occurs from the loss of woody wetland vegetation, over-grazing and/or local extirpation of beavers (Wolf et al., 2007).

In the face of widespread loss of wetlands and a growing interest in restoring functionality in degraded river-floodplain systems (Pollock et al., 2014), there is a need to quantify the current extent of river corridor wetlands and to assess how intact river corridors function differently from river corridors where wetlands have been degraded or lost. Satellite imagery and cloud computing tools provide an opportunity for enhanced monitoring and assessment of riparian integrity and functioning at regional scales (Tomsett & Leyland, 2019). One approach to assessing the integrity of river wetlands using remote sensing is to consider the productivity of river corridor vegetation (Silverman et al., 2019). In

semi-arid areas, river corridor vegetation productivity has been shown to relate to the degree of hydrologic connectivity and been shown to be higher in intact and/or restored river corridor wetlands (Fesenmyer et al., 2018; Silverman et al., 2019).

Previous researchers have suggested that river corridors with wetlands and high geomorphic complexity are more resilient than degraded corridors (Fairfax & Whittle, 2020; Wohl et al., 2017). One way to explore this idea at regional scales is to consider the sensitivity of productivity of river corridor vegetation to inter-annual variability in climate (hereafter referred to as climate sensitivity). In upland vegetation, climate sensitivity is strongly related to land cover type, climatic water deficits, and topographic factors such as hillslope convergence (Hoylman et al., 2019). Yet in riparian zones, where landscapes are broadly convergent, climate sensitivity can also be a function of local water storage capacity and surface and subsurface connectivity between riparian groundwater and adjacent river and hillslope water sources (Albano et al., 2019, 2020).

Here, we use remotely sensed and geospatial datasets to examine spatial patterns in land cover, productivity, and climate sensitivity in river corridors of the Southern Rockies Ecoregion. We first explore how several factors explain observed spatial patterns of wetlands including: regional factors such as elevation and climate; topological factors within river corridors including valley width and proximity to the river; and anthropogenic landscapes. We then assess relationships between wetland cover on river corridor productivity and climate sensitivity across gradients in climatic water availability. Finally, we examine the implications of legacies of human disturbance on river corridor wetlands within a case study of river corridor meadows in Rocky Mountain National Park.

4.2 Methods

4.2.1 Study Region

This study was conducted in riparian corridors within the Southern Rockies Ecoregion, a 138,854 km² mountainous region (elevation range: 1140m to 4400m) encompassing most of central Colorado and parts of Wyoming and New Mexico in the United States (Drummond, 2012). Climate varies widely across the region with precipitation mostly falling as snow (25-100cm) with the most snowfall at higher elevations and on the western side of the Continental divide. The majority of upland areas are forested with dominant species including spruce-fir (*Picea* spp. and *Abies* spp.), lodgepole pine (*Pinus contorta*), and ponderosa pine (*Pinus ponderosa*). Grassland and sagebrush are more common in lower elevation valleys and basins including sagebrush (*Artemisia tridentata*) and oak (*Quercus* spp). Riparian areas with intact vegetation primarily contain mixed willow species (*Salix* spp.).

4.2.2 River Corridor Delineation and Generation of River Corridor Polygon Segments

We delineated river corridors using a hydrologically conditioned USGS 3DEP 1/3 arc-second DEM, National Hydrography Dataset Plus Version 2 (NHDPLUSv2) flowlines and the GFPLAIN tool (see Brooks et al., 2022 (*in review*) for details). In short, GFPLAIN uses a hydro-geometric approach that identifies the spatial extent of flooded area given a scaling relationship between flood height above a stream and watershed area (Nardi et al., 2006, 2019). Parameterization of GFPLAIN was done to delineate regions likely to have the potential for hydrologic connections to a river, which we refer to here as the river corridor (RC). River corridors were then delineated for all river networks in the Southern Rockies Ecoregion with watershed areas above 5 km².

River corridor polygon segments were generated at 200m intervals along the centerlines of river networks in the region (see Brooks et al., 2022 (*in review*) for complete details). Centerlines were extracted from the RC polygon using the RivWidthCloud tool in Google Earth Engine (X. Yang et al., 2020). Once centerlines were extracted, we generated a cross-sectional line at each 200 m across the

river corridor polygon. Cross-sections were buffered by 75 m in each direction to create polygons 150 m long in the longitudinal direction of the centerline. These polygons were intersected with the river corridor polygon to include only areas in the RC. Many polygons had some amount of overlap due to sinuosity of the RC centerline and/or river confluences. To address this, we trimmed any polygon that overlapped with more than 5 other polygons. Due to this trimming process and gaps in centerlines that occur due to RivWidthCloud centerline algorithm, there are some gaps with no polygons, particularly in areas with complex river confluences. Furthermore, because of the 5km² minimum watershed size for river corridor delineation, first-order streams are underrepresented in river segment polygons (Brooks et al. *(in review)*, 2022). RC segment widths were measured as the cross-sectional width at each segment polygon.

4.2.3 Land Cover, Climate and Elevation

We retrieved gridded datasets of regional land cover, climate and elevation and extracted pixels within the river corridor in the region using Google Earth Engine. Land cover was obtained from the 2016 National Land Cover Dataset (NLCD, 30 m resolution) (L. Yang et al., 2018), elevation from the USGS 3DEP 1/3 arc-second digital elevation model (DEM, ~10m resolution) and climate data including precipitation (P) and reference potential evapotranspiration (PET, calculated for Alfalfa) from the daily GRIDMET dataset (~4 km² resolution) (Abatzoglou, 2013). All gridded datasets were downscaled to match the 10m resolution of the DEM using bilinear interpolation. To reduce the number of land cover classes, all developed classes including open space, low, medium, and high intensity development were grouped into a single category termed developed. For some downstream analysis, we also use the category human activities which includes developed classes and agricultural land cover classes including Pasture Hay and Cultivated Crops.

To reflect the climatic conditions of river corridors, we calculated long-term mean water availability (hereafter: climatic water availability) as the water year Standardized Precipitation-Evapotranspiration Index (SPEI), which is the difference between P and PET over a specified timescale, for water years (October - September) between 1986 to 2019. We calculated the mean annual value over the full time stack to reflect long-term climatic conditions. Because of the 4 km² spatial scale of GRIDMET pixels, which are larger than the widths of most observed river corridors in the region, climatic water availability values reflect climatic conditions at a combination of river corridor and some portion of upland environments within watersheds.

We summarized gridded datasets at both HUC12 watersheds and at every river corridor segment polygon. For elevation and climatic water availability, we calculated mean values, while for land cover, we calculated areal coverage and percent cover.

4.2.4 Identifying Trends in River Corridor Land cover Patterning

We identified how the abundance and patterning of land cover relates to geographic factors including climate and river corridor width using beta regression models with a logit link function. Beta regression was conducted for the most common seven land cover types to predict land cover (%) at the HUC12 watershed scale using the *betareg* package in R (Cribari-Neto & Zeileis, 2010). Predictor variables included mean elevation, climatic water availability, and log-transformed RC width. Beta regression was chosen because it can model proportional data that ranges from 0 to 1 (percent cover is a ratio between 0 & 1) and because it allows for flexible non-normal distributions in the response variable, which is common in percent cover datasets (Douma & Weedon, 2019). Because beta regression cannot handle values of exact 0s or 1s, these values were transformed to values close to 0 and 1 with the following equation as suggested by Smithson (2006):

$$(1) p^* = \frac{p(n-1) + 0.5}{n}$$

where p is the percent cover and n is the number of observations in the dataset.

We further sought to understand if explanatory power of vegetation and wetland land cover could be improved if we included percent human activities cover as a predictor variable. We define “Human activities” cover to include all development and agricultural land cover classes. Performance of the model including human activities cover as a predictor variable was compared to the original model using Akaike information criterion (AIC) and Pseudo R^2 values (correlation between linear predictor of the mean and logit link-transformed response value). To further interpret results, we also conducted pairwise analyses using the spearman rank correlation coefficients between individual predictors variables and percent cover for each land cover class.

4.2.5 Productivity and Climate Sensitivity in Wide River Corridors

To measure patterns in productivity and response of vegetation to climate variability in river corridors, we calculated the annual growing season Normalized Difference Vegetation Index (NDVI) and correlations between NDVI and SPEI at yearly time-scales between 1986 and 2019. We use NDVI here as a proxy for productivity and hereafter use the terms interchangeably (Pettorelli et al., 2005). We constrained this portion of the analysis to wider river corridors (RC segment width >90 m) to reflect areas where wetlands are likely to develop and where edge effects in remotely sensed datasets between corridor and upland areas would be reduced.

NDVI was calculated at 30 m pixels using *USGS Landsat Surface Reflectance Tier 1* data sets derived from Landsat 5 to 8 and generated using processing steps and algorithms that are part of the LandTrendr Google Earth Engine module (Kennedy et al., 2018). A single growing season NDVI value was

calculated using the medoid approach for clear high quality Landsat images between July 1st and September 15th with clouds, shadows and snow masked from images. For each pixel, the medoid approach finds the annual median value of every band across the image stack subset for the summer period, which we then used to calculate NDVI for every year at each pixel in the river corridor. Using these yearly summer NDVI values, we then also calculate the mean NDVI for each pixel. To reflect current productivity conditions, mean NDVI for each pixel was calculated only using annual NDVI values from the most recent decade of the study period (2010 to 2019).

Before calculating the sensitivity of NDVI to inter-annual variability in climate, we first generated a detrended (dNDVI) dataset which removed temporal trends from the data. At each pixel, to generate dNDVI, we calculated the residuals of the relationship between year and the fitted prediction using the Sen's slope which is a non-parametric estimator of the slope of the monotonic temporal trend (Sen, 1968). Where there is no trend, this is equivalent to the anomaly from the mean SPEI at that pixel across the time period. Removing the temporal trends in the data can help improve our ability to measure climate sensitivity in systems that might otherwise be obscured by trends in vegetation productivity through the time period.

Adapting approaches from Albano et al. (2020) and Holyman et al. (2019), we measure the climate sensitivity of each Landsat pixel as the standardized regression coefficient (β) between summer dNDVI and water year SPEI. The standardized regression coefficient is formally equivalent in our use case to a Pearson's correlation coefficient because there are only two variables. We use β rather than regression slope to enable cross comparisons of pixels that have different distributions and standard deviations of dNDVI while also preserving the directionality of the fit (Hoylman et al., 2019).

4.2.6 Productivity and Sensitivity in Wetland and Vegetated Non-Wetland RC Segments

To evaluate patterns in productivity and sensitivity in vegetated wide river corridors, we classified each RC segment into six categories. First we summarized results for all vegetated and/or wetland segments (>85% vegetation + wetlands). Then to clarify how land cover class impacts results, we summarized results for segments dominated by a single land cover class (>85% cover) including Woody Wetlands (WW), Emergent Herbaceous Wetlands (EHW), Evergreen Forest, Shrub Scrubs and Grassland Herbaceous.

For each wetland category and each mixed cover subset group, we summarize results by calculating the mean, median, and inter-quartile range (IQR) of mean values for segments in those categories. To analyze patterns across regional river corridor gradients, mean values for each wetland category were calculated after binning segments by both climatic water availability and segment RC width.

As vegetation and resilience in river corridors is also controlled by geomorphology and hydrologic connectivity, we also evaluated the degree that spatial patterns in productivity and sensitivity were present within river corridor segments. We calculated the distance to the river (DTR) for every pixel as distance to the nearest NHDPLUSv2 stream flowline. In areas with multi-thread channels, DTR reflects the distance to the nearest river thread rather than to a single mainstem. To understand how wetlands are configured in relation to other vegetation types, we calculate the river proximity ratio (P_{lc}) for a specified land cover class which is calculated as:

$$P_{lc} = \frac{meanDTR_{lc}}{meanDTR_{all}}$$

Where $meanDTR_{lc}$ is the mean DTR of a pixel with a specific land cover class in a segment and $meanDTR_{all}$ is the mean DTR of all pixels in the segment. Values below one indicate the specified land

cover class is more proximate to the river in the segment relative to an average pixel in the segment while values above one indicate the land cover class is further from the river. We calculated P_{lc} for wide RC segment with at least 10 Landsat pixels and mixed wetland and other vegetated land cover (15% to 85% of either WW or EHW cover).

At every segment, we then used linear regression to find the slope, model significance and R^2 of the relationship between DTR and both NDVI and β . The percent of segments that had significant (model $\alpha < 0.05$) positive and negative slopes were then calculated and results were summarized using the categories described above for dominant and mixed wetland segments and non-wetland segments.

4.2.7 The Role of Compounding Historic Disturbances: A Case Study in Rocky Mountain National Park

One of the challenges of regional scale remote sensing assessments is the lack of field scale context that can help improve inference (Klemas, 2011). Of particular difficulty is assessing the role of historical disturbances that may not be visible from satellite imagery or other geospatial datasets. To examine how land cover, productivity and climate sensitivity are impacted by such disturbances, we conducted a case study at six montane river corridor meadows (hereafter meadows) on the east side of Rocky Mountain National Park with known disturbance histories. Three of the meadows (H1-H3) have high historic disturbance including but not limited to stream incision and/or a lack of beaver activity while the other three (L1-L3) have relatively minimal historic disturbance and have active or recent beaver activity. Meadow elevations and climatic water availability were both in the middle of ranges observed across the region with elevations from 2452 to 2798 masl and climatic water availability ranging between -701 to -1030 mm. At each meadow, we extracted pixel values using meadow polygons to calculate land cover statistics including wetland cover and nearness ratios, mean NDVI and climate

sensitivity. We then explored spatial patterning of NDVI and climate sensitivity by conducting linear regressions between these metrics and distance to the river using pixel-level data. Finally, to explore temporal dynamics, we calculated yearly mean dNDVI and SPEI for each meadow to visualize meadow-scale temporal relationships between water availability and productivity.

4.3 Results

In river corridors (RC) within the Southern Rockies ecoregion, the majority of land cover was classified as vegetation, comprising 74% of the total RC area (Table 1). Non-wetland vegetative cover comprised 45% of the RC area while wetland cover was 32%, including roughly equal areal coverage of Woody Wetlands (WW, 16%) and Emergent Herbaceous Wetlands (EHW, 16%). Of land cover classes indicating human activities, Pasture Hay (11%) was the most common, while Development (3%) was relatively rare as was Cultivated Crops (1%). Open Water comprised 9% of land cover, which primarily reflects the presence of reservoirs but also includes the land area of natural rivers, lakes and ponds. Other land cover types including barren and perennial ice/snow were negligible.

Wider valley segments, with RC widths above 90 m, were more likely to contain mixed land cover types, were generally less forested, and were more likely to be partially comprised of wetland cover and/or human activity cover (Table 1). Evergreen Forests was present (>15% cover) in 37% of narrow segments but in only 13% of wide segments. 65% of wide segments contain some wetlands (wetland cover >15%) compared to only 30% of narrow segments. Wide valley segments also tended to have some amount of human activities cover. Specifically, 23% of wide segments contained some human activities cover (human activities cover >15%) in comparison to 6% of narrow segments. In contrast, relatively few segments were comprised fully (>85% cover) of either wetlands (wide: 9%, narrow: 11%) or human activities cover (wide: 4%, narrow: 2%).

Geographic factors were only moderately predictive of cover for most land cover classes at the HUC12 watershed scale (Figure 1, Table 2). Pairwise spearman rank analysis (ρ) also confirmed that relations were generally weak to moderate between geographic variables and percent cover of individual land cover classes (Figure 2). Wetland cover is associated at least moderately with monotonic gradients in geographic variables. Predictor variables had stronger relationships with EHW (Pseudo R^2 : 0.31) with increasing cover at higher RC widths ($\rho = 0.48$) and slightly weaker positive associations with higher elevation ($\rho = 0.35$) and wetter climatic conditions ($\rho = 0.24$). In contrast, beta model performance was weaker for WW (Pseudo R^2 : 0.21) with increasing cover at wetter climatic conditions ($\rho = 0.42$) and higher elevations ($\rho = 0.32$) and a weak positive association with mean RC width ($\rho = 0.17$). For WW, only climatic water availability and mean RC width were significant coefficients in the beta regression model (Table 2).

We observed different relationships between the human activities cover classes, Pasture Hay and Development, and geographic factors. Specifically, we observed only weak relations between Development and geographic factors but moderate relations between Pasture Hay and geographic factors (Figure 2, Table 2). Pasture Hay cover increased with RC width ($\rho = 0.42$) and while elevation ($\rho = -0.1$) was significant in the model with a negative slope coefficient, this negative association was likely secondary in importance. In fact, additional analysis suggest that Pasture Hay might actually be most associated with river corridors at moderate elevations which is not well described by the linear model (Figure 1). In contrast, development cover appears not to be strongly related to geographic factors (Pseudo $R^2=0.06$) but is slightly more abundant at wider river corridors ($\rho = 0.25$).

Including current human land cover in the beta regression models to predict vegetation and wetland cover had only marginal improvements for models for Grasslands ($\Delta R^2 = 0.05$) and Shrub Scrub ($\Delta R^2 = 0.02$) and no improvement for neither of the wetland cover classes nor for Evergreen Forest (Table 3).

4.3.1 Productivity and Climate Sensitivity in Wide River Corridors

In vegetated RC segments, both productivity (mean segment NDVI = 0.5, IQR = 0.38-0.62) and climate sensitivity (mean segment β = 0.44, IQR = 0.36-0.58) were variable across the region (Figure 3). Mean NDVI was highest at segments with dominant WW (mean NDVI = 0.64), EHW (0.61) and Evergreen Forests (0.61) while Shrub Scrubs (0.35) and Grassland Herbaceous (0.33) dominant segments had lower NDVI values (Figure 3). Nearly all segments, 99.5%, had a positive mean β , reflecting a positive relationship between NDVI and water year SPEI (Figure 3). The degree of climate sensitivity was also linked to land cover class with the lowest climate sensitivity in Evergreen Forest (mean β = 0.28) and WW (mean β = 0.34) dominant segments, and higher climate sensitivity in EHW (mean β = 0.46), Shrub Scrubs (mean β = 0.50) and Grasslands (mean β = 0.50) dominant segments.

Broad regional gradients in climatic water availability influenced both productivity and climate sensitivity in river corridors but the response is modulated by the presence and the type of wetland (Figure 4). Productivity generally rose with increased climatic water availability. This was most acute in non-wetland segments, in which mean NDVI rose from 0.33 to 0.66 between areas with the lowest and highest climatic water availabilities (Figure 4b). This corresponded with a shift in non-wetland vegetation from high Shrub Scrub cover to high Evergreen Forest cover as water availability increased (Figure 4a). In both WW and EHW segments, NDVI also increased with climatic water availability but maintained high mean NDVI even in more arid conditions (Figure 4b).

Climate sensitivity was also influenced by water availability with general downward trends in mean β with increasing climatic wetness (Figure 4c). Non-wetland vegetation again had the strongest patterning with declines from the high mean β in river corridors in more arid areas to low mean β values at river corridors with high water availability. WW had the lowest mean β values but also exhibited a

similar pattern with declines in mean β with increasing water availability. In contrast, EHW segments remained sensitive to climate even in areas with high water availability (Figure 4c).

4.3.2 River Distance Structuring of Wetlands, Productivity and Climate Sensitivity in Wide River Corridors at Segment Scales

In wide segments with mixed vegetation and wetland land covers, wetlands were generally more proximate to rivers than other vegetated land covers (Table 4). We evaluated the degree of this spatial patterning using the river proximity ratio (P) in which values below 1 indicate the wetland pixels are closer to the stream than pixels with other land cover classes in a particular segment. This clustering near the river was much larger for WW than EHW pixels. Across segments median river proximity ratios for WW (P_{ww}) was 0.79 with an IQR of 0.57 to 1. Emergent Herbaceous Wetlands had median proximity ratios (P_{ehw}) of 0.94 with an IQR of 0.70 – 1.17.

Across the region, significant linear relationships between DTR and productivity (using significance threshold of $\alpha < 0.05$) were observed in 54% of the 31,027 wide, vegetated segments used for this analysis (Table 4). 39.3% of all segments were observed to have significant negative regression slopes (NDVI is lower further from the river) while only 14.7% of the segments had significant positive slopes (NDVI is higher near the river). Negative relationships between DTR and NDVI were most common in segments with mixed wetlands and other vegetation and least common in segments with dominant WW cover.

Significant relationships between DTR and climate sensitivity were somewhat less common, occurring in 39.7% of segments (Table 4). Significant positive regression slopes were slightly more common with β significantly increasing with DTR at 22.7% of segments while negative regression slopes were observed at 17% of segments. Positive relationships between DTR and β were also more common

in segments with mixed wetlands and other vegetation but were least common in non-wetland segments.

4.3.3 Rocky Mountain National Park Case Study

Within our case study in Rocky Mountain National Park, montane river corridor meadows with high disturbance (H1 – H3) differed in wetland land cover, productivity and climate sensitivity as compared to meadows (L1 – L3) with low disturbance (Figure 5 & 6). Known disturbance histories include loss of beaver, overgrazing, water diversions, roads, ranching, vegetation removal, debris flow from a dam failure, stream incision, gravel mining, and the development of a golf course (Table 5). In highly disturbed meadows, WW areal cover was relatively low (mean (m): 25.1% of meadow area, range (r): 12.5%-49.9%) compared to WW areal cover in low disturbance meadows (m: 68.5%, r: 52.6% – 96.1%). EHW cover was relatively high at highly disturbed meadows (m: 59.6%, r: 23.9% – 81.7%) compared to EHW cover at low disturbance meadows (m 9.9%, r: 0% – 25.2 %) (Figure 7, Table 5). Meadows with high disturbance also all had lower mean productivity (m: 0.63) compared to low disturbance meadows (m: 0.71) and substantially higher mean β (m: 0.56) than low disturbance meadows (m: 0.28). Across the five meadows that had mixed land cover (excluding L1), WW were either closer or equidistance to the river than other land covers (P_{ww} range: 0.5 to 1.0) while EHW were equidistant or further away (P_{ehw} range: 1.0 to 1.8) (Table 7, Figure 5). All meadows except L3 had significant negative relationships between NDVI and DTR but slopes of significant relationships were not substantially different between meadows with differing disturbance ranging between -0.04 and -0.06 of NDVI per 100m. In contrast, while all meadows except L2 had significant positive relationships between β and DTR, slopes of significant models were higher at low disturbance meadows (r: 0.12 to 0.20 per 100m) and lower at disturbed meadows (r: 0.01 to 0.08 per 100m).

4.4 Discussion

Our results indicate that the occurrence of wetlands with woody species such as willows are rare throughout river corridors of the Southern Rockies Ecoregion, comprising just a sixth of the river corridor study area, with implications for both river corridor productivity and vegetation resilience to climate variation. Wetlands without woody species, upland vegetation covers including shrubs lands, forests, grasslands; open water often in the form of reservoirs; and human activities including ranching, hayfields and development are all found in areas that once were likely to contain these wetlands. Woody wetland cover is absent (<15% cover) from two-thirds of wider river corridor segments (>90m), which historically were likely to have housed river-wetland complexes. Today, less than 10% of these wider river corridor segments have dominant WW cover (>85%). Within the remaining 28% of wide RC segments with mixed WW and other vegetation covers, WW are strongly clustered in proximity to rivers. This clustering suggests that the eco-hydrologic conditions necessary to maintain these wetlands no longer extend throughout the full corridor width but are more often present in river adjacent areas.

4.4.1 The Implications of Wetland Occurrence on Productivity and Resilience in River Corridors

Our remotely sensed measures enabled us to quantify the patterning of river corridor productivity and climate sensitivity across broad gradients in land cover, climate, elevation and historic disturbance. Our results from the regional analysis demonstrate that the presence of WW cover and their associated eco-hydrologic properties are important for maintaining both vegetation productivity and low climate sensitivity, particularly in vegetated river corridors with climatic water availability below approximately -1000 mm. Similar to findings in upland areas (Hoylman et al., 2019), below this threshold, low productivity, high sensitivity vegetation including shrublands and to a lesser degree

grasslands begin to dominate non-wetland portions of the river corridor. Above this -1000m threshold, high productivity, low sensitivity evergreen forests are increasingly common. Low productivity and high sensitivity is likely a signal of water limitation, which is occurring in these areas despite the river corridor having high topographic convergence. This water limitation is likely a function of both higher atmospheric water demand in lower elevation landscapes, a lack of river-floodplain hydrologic connectivity, and more limited contributions from hillslope groundwater which are not sufficient to alleviate water limitation, especially during drier years.

In WW dominated river corridors, productivity also goes down and sensitivity goes up in drier climatic zones, however these changes were smaller relative to non-wetland zones. This suggests these areas in the river corridor may act as a hydrologic refugia (sensu McLaughlin et al., 2017), buffering vegetation from water limitation during dry years because high groundwater tables enable sufficient soil moisture (Cherie J. Westbrook et al., 2006). In drier climatic zones, hillslope contributions are likely minimal and thus this buffering is likely the result primarily of river-floodplain connectivity. In zones with higher water availability, differences in productivity and sensitivity between wetlands and non-wetland covers become smaller, likely because atmospheric demand is lower and hillslopes contributions provide enough water that non-wetland, forested river corridors experience less water limitation even in drier years.

The relatively high presence of wetlands without woody cover throughout the region (EHW: 17.5% of RC area), matches field-scale studies that show that degradation and historic disturbances can shift river corridors to an altered state that are distinct from upland areas, where herbaceous and grassland species are adapted to grazing and less persistent groundwater tables (Wolf et al., 2007). We should note that the NLCD Emergent Herbaceous Wetland classification might also include some wetland types such as fens and marshes where hydrologic conditions are too wet for woody species to survive. However, based on our case study and observations of satellite imagery, it appears the majority

of EHW cover are in fact more xeric than where WWs are present. Such areas might still retain some, but not all, aspects of the hydrologic, soil and geomorphic properties that define wetlands but have been pushed into an altered state through various disturbances such as overgrazing, beaver loss, and hydrologic alterations. Such shifts were observed in our case study where land cover in high disturbance river corridors had high EHW cover that was not widely abundant in low disturbance river corridors.

The implications of disturbance legacies and resulting EHW cover appears currently to be largely on the climate sensitivity rather than the productivity of river corridor vegetation. In our case study, while mean NDVI in these altered wetlands were on average 10% lower than low disturbance river corridors, mean climate sensitivity in high disturbance river corridors was double that of low disturbance river corridors. At regional scales, similar patterns were observed. Segments dominated by WW had mean NDVI 6% higher, while mean climate sensitivity was 32% lower than segments dominated by EHW. Interestingly, the sensitivity of EHW segments remained high even in areas with higher climatic water availability where non-wetland vegetation has low sensitivity.

This relatively high productivity combined with high climate sensitivity is unique to EHW within land covers observed in this study. We suggest that this occurs in systems where vegetation experiences highly variable soil moisture conditions within seasons and across years that can generate intermittent periods of water limitation. Such limitations might be driven by hydrologic and geomorphic alterations but also by overgrazing that might preclude species that can maintain canopy cover during drought and/or access deeper soil moisture (Polvi & Wohl, 2012). Seasonally, in snow-dominated systems, lateral hydrologic connectivity between the river and floodplain that supports high groundwater tables can depend on streamflow thresholds that initiate lateral surface flow. The period of time where lateral connections are established can be spatially and temporally variable even in more hydrologically connected river-floodplain systems (Brooks et al, 2022 – in review). In more disconnected systems with stream incision, high groundwater and corresponding high soil moisture conditions might be present,

but only for periods of the year with the highest streamflow. In average or wet years, the duration of high soil moisture might be sufficient for high productivity but in dry years, productivity is strongly curtailed by water limitation in hydrologically disconnected river-floodplain systems. Supporting this idea, excluding grazing and raising water tables with in-stream structures both have been shown to increase riparian vegetation productivity and reduce sensitivity within river corridors (Fesenmyer et al., 2018; Silverman et al., 2019).

4.4.2 Spatial Patterning in River Corridors

As river corridors are often complex, heterogeneous landscapes (Poole et al., 2002; Rajib et al., 2021; Wohl & Iskin, 2019), we must also consider spatial patterning within river corridors rather than simply aggregate behavior at segments or larger scales. Our results demonstrate that spatial patterning is common in both wetland cover and in productivity and climate sensitivity. The clustering of WW closer to rivers in the region, suggest that these portions of corridors have been more likely to maintain WW communities. This could be because river proximate areas are more hydrologically connected or because river proximity reduces susceptibility to disturbance. Where wetlands are mixed with other land cover in the river corridor, we observe that significant spatial gradients were more likely for both productivity and climate sensitivity.

As the goal of many river corridor restoration projects is to restore river-floodplain connectivity and wetland habitats, from these findings, we suggest in semi-arid environments, the width of high productivity, low climate sensitivity zones around rivers could be used to monitor the degree of success of floodplain reconnection projects. Similarly, we suggest that long-term tracking of temporal and spatial patterns in river corridor climate sensitivity could be useful for monitoring and detecting changes in wetland states in the future.

4.5 Conclusion

Our results show that productivity and climate sensitivity of river corridors in the Southern Rockies Ecoregion are related to their land cover, disturbance histories, and geographic context. River corridor wetlands, including both those with and without woody cover, comprise around a third of river corridor area throughout the Southern Rockies Ecoregion. These wetlands are highly productivity as measured by NDVI even in drier climatic zones with lower climatic water availability. The remainder of the river corridor area is currently occupied by upland vegetation, human activities such as hay pasture and development, and open water. Only around half of present wetlands are classified as containing woody vegetation. These woody wetlands are on average closer to the river than other land covers, suggesting their establishment and survival has been linked to river-floodplain connectivity and the maintenance of high groundwater and soil moisture. These areas with woody wetlands exhibit low climate sensitivity, thus maintaining high productivity even during drought conditions. The other half of existing wetland cover in the region lack woody species cover, which from our case study in Rocky Mountain National Park, appears to be a signal of historic and/or current ecologic and hydrologic disturbance. These wetlands without woody cover maintain relatively high productivity because they are in convergent, topographically wet areas. However, without high river-floodplain connectivity, they are also sensitive to climate variability, suggesting their productivity is more susceptible to drought and future changes to streamflow and climate. In non-wetland vegetated river corridors, productivity and climate sensitivity is largely driven by land cover and climatic water availability with high productivity, low sensitivity forests in wetter regions and low productivity, high sensitivity shrublands and grasslands in drier climatic zones. Collectively, these results demonstrate that in landscapes with low climatic water availability, river connectivity and maintenance of wetlands with woody species are critical components of maintaining highly productive and resilient habitats within river corridors.

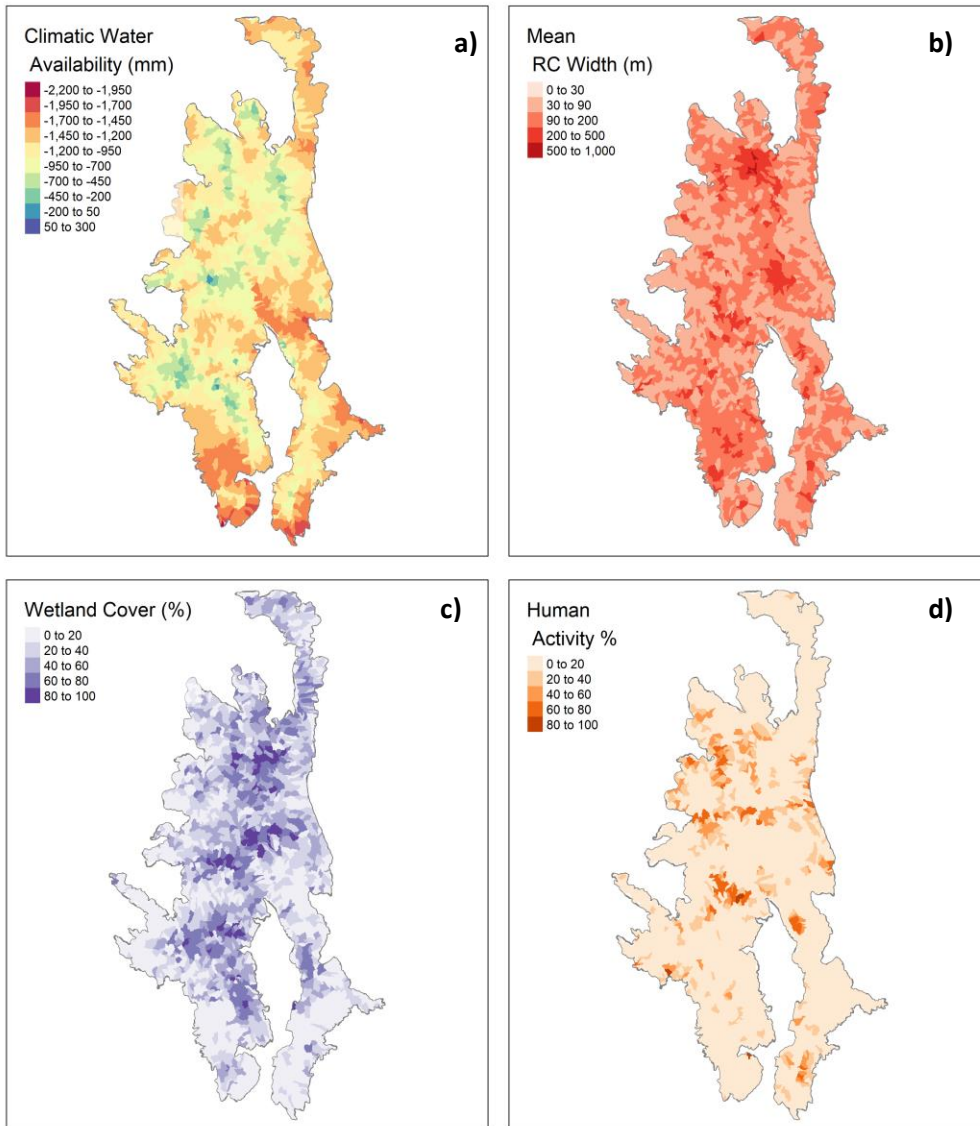


Figure 4.1: River corridor (RC) water availability (a), RC width (b), wetland percent cover (c), and human activity percent cover (d). Each metric is summarized to mean values at HUC12 watersheds and only include river corridors within each HUC12 watershed. Wetland cover includes both Woody Wetlands and Emergent Herbaceous Wetlands class within the 2016 National Land Cover Dataset (NLCD16). Human activity includes all development and agricultural land cover types in NLCD16.

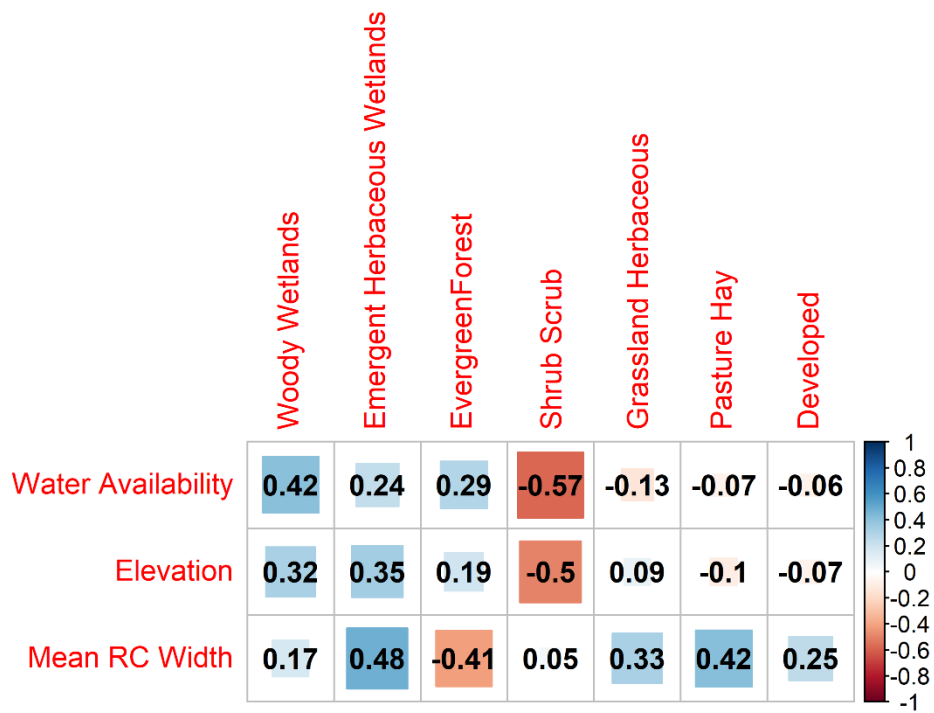


Figure 4.2: Spearman rank correlation coefficients between predictor variables and mean percent cover in river corridors within HUC12 watersheds.

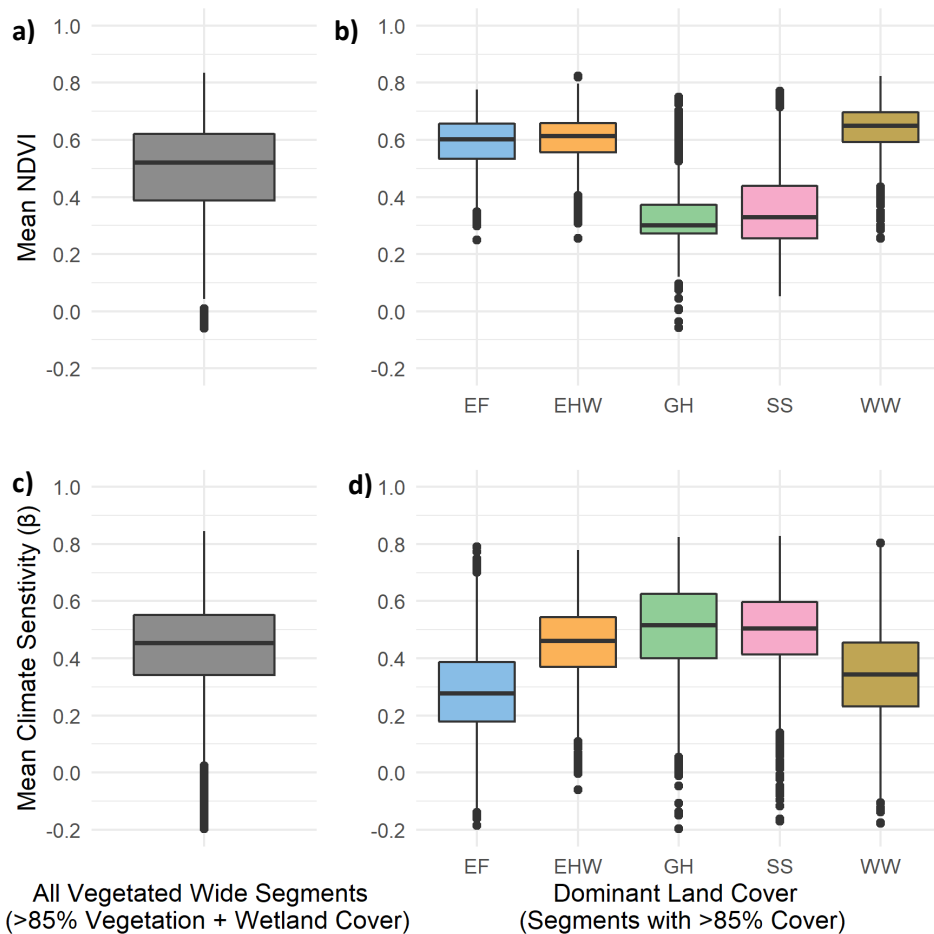


Figure 4.3: Boxplots of Mean NDVI (a, b) and Climate Sensitivity (β , c & d) for all wide vegetated segments (a,c) and wide segments with single dominant land cover classes (b,d) including Evergreen Forest (EF), Emergent Herbaceous Wetlands (EHW), Grassland Herbaceous (GH), Shrubs Scrubs (SS) and Woody Wetlands (WW). NDVI and β values are mean values within each RC segment.

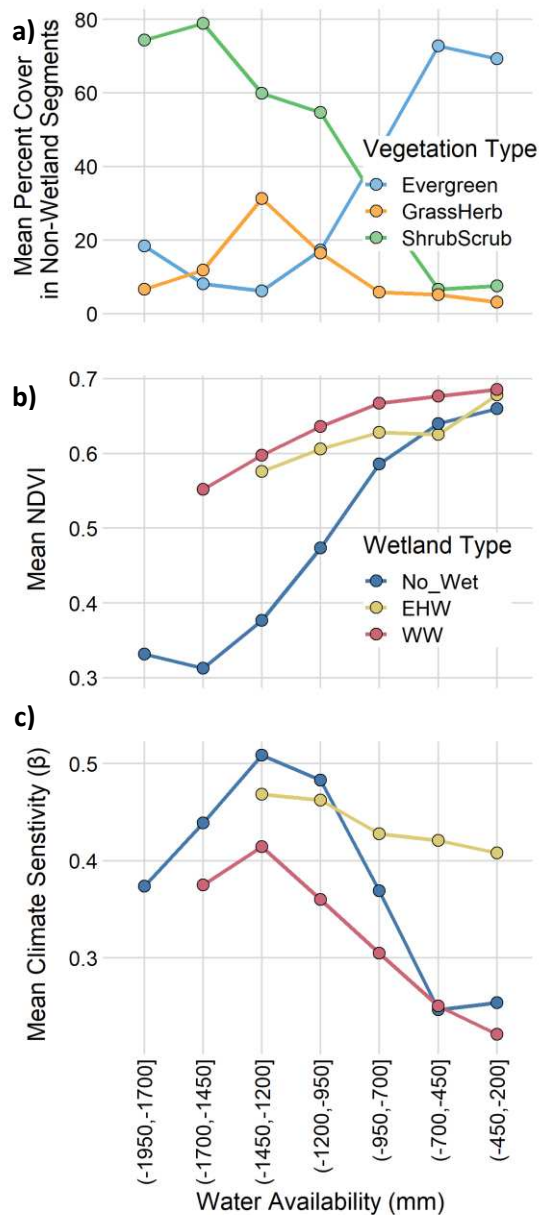


Figure 4.4: (a) Mean percent cover in non-wetland segments (<15% cover WW + EHW), (b) mean NDVI and (c) climate sensitivity (β) of WW and EHW dominant segments (>85% cover) and non-wetland segments across regional gradients in climatic water availability. Mean values were calculated for segments within each land cover category and climatic water availability bins. Mean values for bins with less than 50 segments are not displayed to reduce noise from small sample sizes.

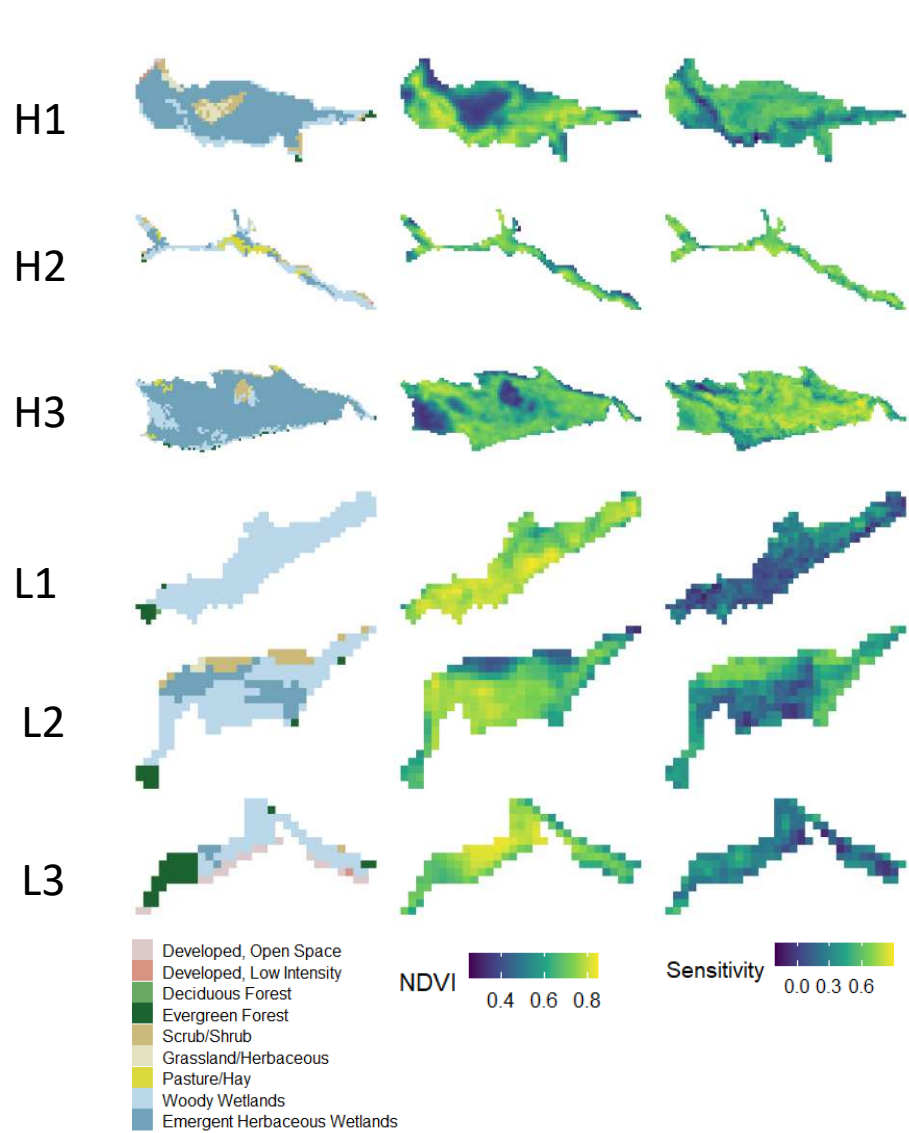


Figure 4.5: Six river corridor meadows in Rocky Mountain National Park used in case study showing spatial patterns of (a) NLCD land cover, (b) NDVI and (c) Climate Sensitivity (β). Based on a priori knowledge of historic disturbances, meadows were classified as having histories of high disturbed (H1 – H3) or low disturbance (L1 – L3).

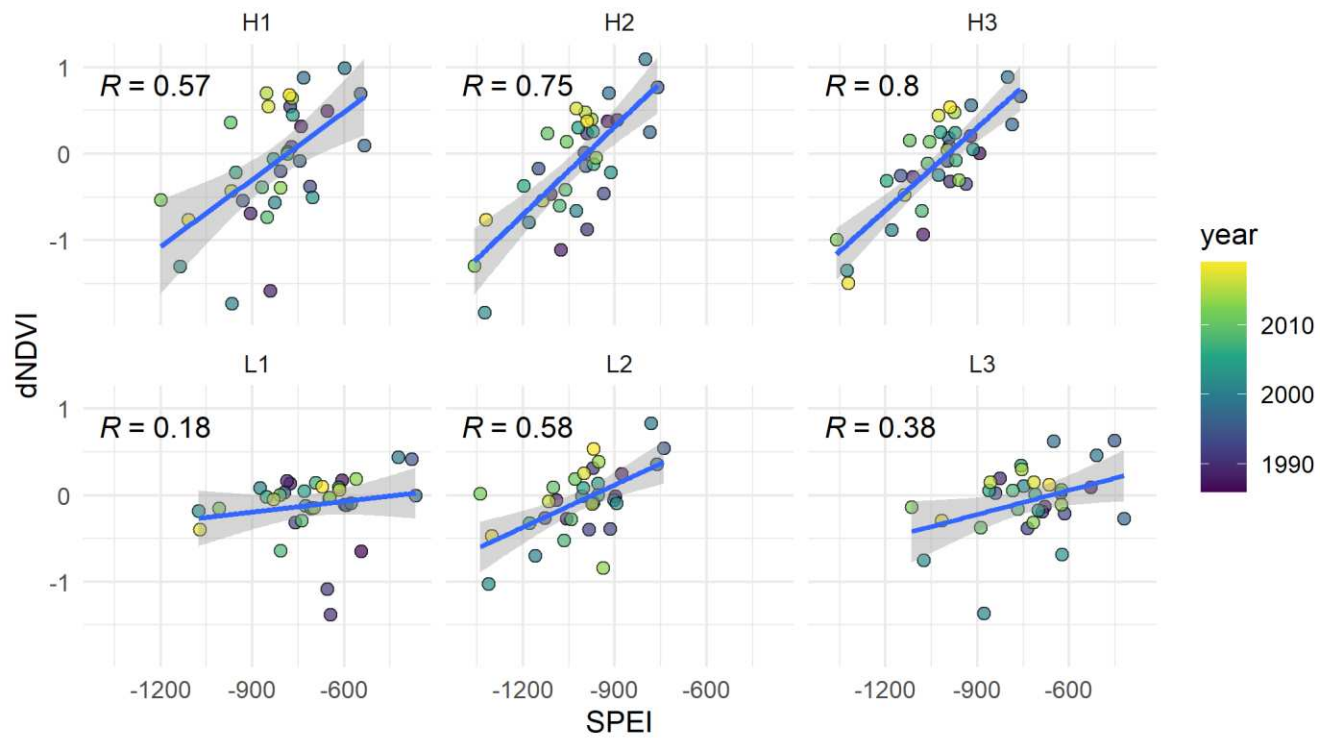


Figure 4.6: Scatterplots between water year SPEI and detrended NDVI (dNDVI) in case study meadows in Rocky Mountain National Park. Points represent spatial yearly means for each meadow from 1986 through 2019. Pearson correlation (R) are included for each meadow with lower R values indicating lower climate sensitivity at the meadow.

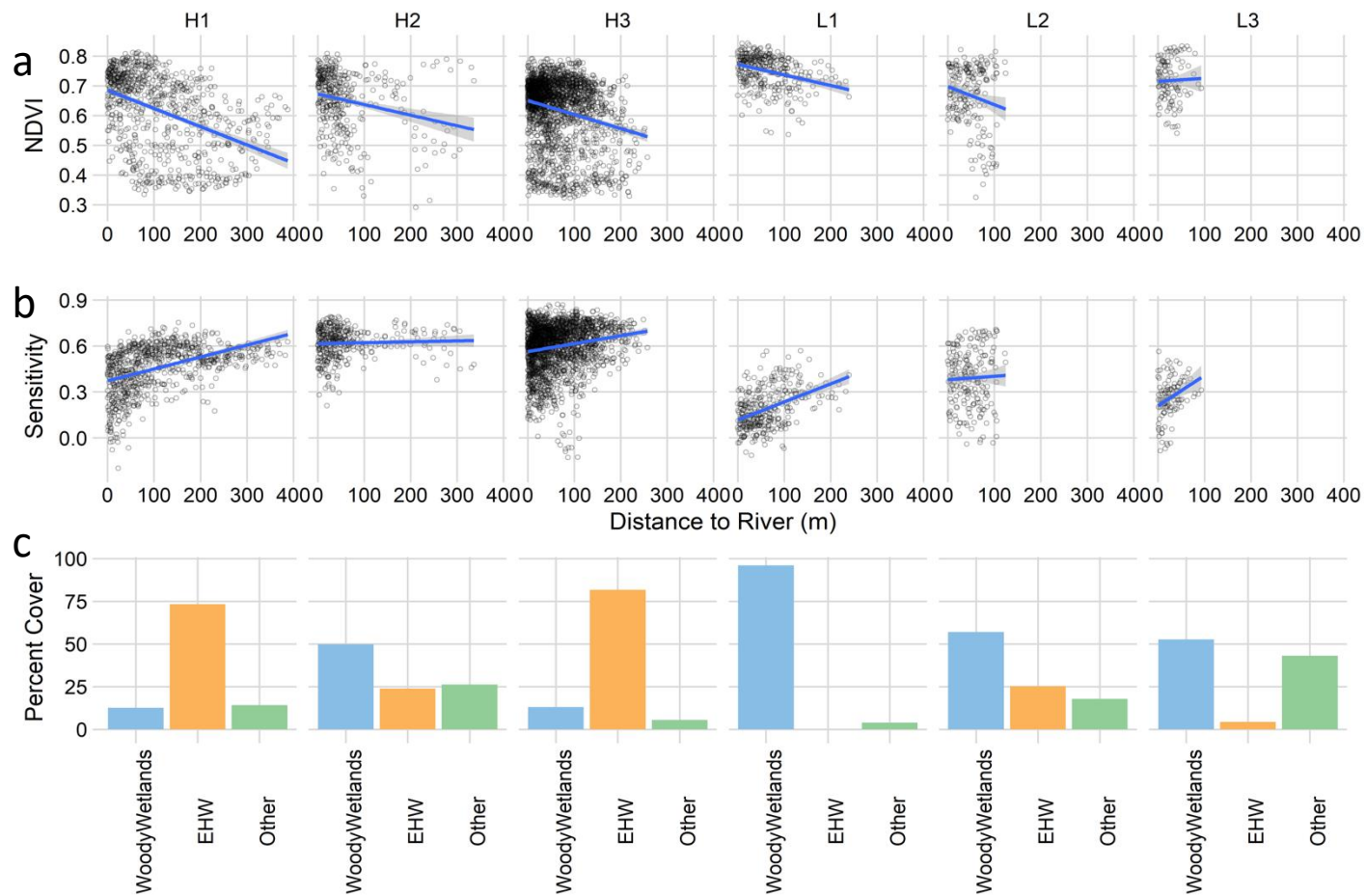


Figure 4.7: Scatterplots of spatial relationships between distance to the river and (a) NDVI and (b) climate sensitivity in case study meadows in Rocky Mountain National Park. Points represent values at each pixel (10m resolution). Percent cover (c) is also included to show wetland land cover percent with other land covers lumped together in the Other category. Blue line in a & b is the best fit linear trend in each relationship.

Table 4.1: NLCD Land Cover in Southern Rockies Ecoregion. Land cover classes are ordered from highest to lowest percent cover by area.

Land Cover	Percent Cover By Area (%)	Percent Cover (%) By Area in Wide Segments (>90 m)	RC Segments with >15% cover (%)		RC Segments with >85% cover (%)	
			Wide (> 90 m)	Narrow (<= 90 m)	Wide (> 90 m)	Narrow (<= 90 m)
Shrub Scrub	24.1	22.8	44.2	38.3	14.2	20.9
Woody Wetlands	16.3	16.2	36.8	21.6	5.1	8.7
Emergent Herbaceous Wetlands	15.8	17.5	27.9	7.9	3.7	2.4
Pasture Hay	10.6	12.4	13.5	1.1	2.2	0.4
Grassland Herbaceous	10.1	10.6	18.3	9.4	3.4	3.8
Open Water	8.5	9.9	6.6	1.1	2.7	0.2
Evergreen Forest	7.5	4.3	12.9	37.1	3.0	23.1
Developed	3.3	3.4	7.8	4.5	0.8	1.3
Deciduous Forest	2.6	1.7	5.3	12.9	0.6	6.3
Cultivated Crops	0.7	0.8	1.2	0.1	0.1	0.1

Table 4.2: Beta regression results for mean percent cover in river corridors at HUC12 scale. Models were fit separately for each land cover class. Stars represent coefficient significance at <0.05 (*), <0.01 (**), and <0.001 (***) p-value thresholds. Significant regression coefficients (p-value < 0.05) are in bold.

Land Cover Class	Intercept	Water Availability	Mean RC Width (log transformed)	Mean RC Elevation	Phi	Pseudo R ²
Developed	-4.07	0	0.3006***	-0.0001	5.51	0.06
Emergent Herbaceous Wetlands	-9.30	0.0003*	1.0472***	0.0011***	4.61	0.31
Evergreen Forest	2.20	0.0007***	-0.7268***	0.0002	2.15	0.2
Grassland Herbaceous	-7.34	-0.0008***	0.4427***	0.0008***	3.41	0.11
Pasture Hay	-4.83	0.0002	0.6565***	-0.0003***	4.18	0.19
Shrub Scrub	-2.29	-0.0018***	0.0799	-0.0004***	1.95	0.27
Woody Wetlands	-2.15	0.0017***	0.4967***	0	3.69	0.21

Table 4.3: Comparison between beta regression models predicting percent cover including and excluding human land cover as model predictor. Red font indicated improvement over original model. Human land cover includes all agricultural and development land cover classes.

	Including Human Land Cover %		Original Model	
	<i>AIC</i>	<i>Pseudo R2</i>	<i>AIC</i>	<i>Pseudo R2</i>
Emergent Herbaceous Wetlands	-7075	0.31	-7074	0.31
Evergreen Forest	-4591	0.2	-4592	0.2
Grassland Herbaceous	-9051	0.16	-9001	0.11
Shrub Scrub	-2292	0.29	-2219	0.27
Woody Wetlands	-4028	0.21	-4025	0.21

Table 4.4: Spatial Patterning of Land Cover, Productivity and Climate Sensitivity within River Corridor Segments. Proportion of segments with positive spatial trend are in black and negative trends are in red.

Land cover Category	Description	Segment Count	Proximity Ratio (P_{IC})		Significant relationships (% of Segments)	
			Median	IQR	NDVI	Climate Sensitivity
WW_Mixed	All vegetated wide segments with between 15% and 85% Woody Wetland cover	10702	P_{ww} : 0.79	P_{ww} : 0.57 - 1.0	14.6% (P) 39.5% (N)	27.8% (P) 14.5% (N)
EHW_Mixed	All vegetated wide segments with between 15% and 85% Emergent Herbaceous Wetland cover	9374	P_{ehw} : 0.94	P_{ehw} : 0.70 - 1.17	13.1% (P) 44.8% (N)	26.7% (P) 18.2% (N)
Woody Wetland Dominant	All wide segments with >85% Woody Wetlands	1798	-	-	22.2% (P) 21.9% (N)	25.4% (P) 9.7% (N)
EHW Dominant	All wide segments with >85% Emergent Herbaceous Wetlands	1809	-	-	15.3% (P) 37.8% (N)	23.2% (P) 20.8% (N)
All Non-Wetland Vegetated Segments	All wide segments with >85% vegetation cover and <15% wetland cover	12536	-	-	15.3% (P) 36.9% (N)	17.3% (P) 18.3% (N)

Table 4.5: Case study results showing geographic context, disturbance history, land cover, productivity and climate sensitivity dynamics within six meadows in Rocky Mountain National Park.

Site	Location Name	Mean Elevation	Climatic Water Availability (mm)	Study Meadow Area (m ²)	Known Disturbance History	Woody Wetland (% Cover)	EHW (% Cover)	P _{ww}	P _{ehw}	NDVI			Climate Sensitivity		
										Mean NDVI	Y Intercept	Slope (per 100m)	Mean Sensitivity	Y Intercept	Slope (per 100m)
H1	Horseshoe Park	2595	-825	724,087	Loss of Beaver, Incision, Sediment disturbance from upstream dam failure, Overgrazing	12.5	73.3	0.5	1.0	0.62	0.69	-0.06	0.46	0.37	0.08
H2	Beaver Meadows	2536	-1030	398,047	Loss of Beaver, Incision, Overgrazing, Water Diversion (historic)	49.9	23.9	0.9	1.1	0.65	0.67	-0.04	0.62	0.61	0.01
H3	Moraine Park	2452	-1030	2,085,968	Loss of Beaver, Incision, Overgrazing, Vegetation Removal, Ranching & Golf Course, Road	13.0	81.7	1.0	1.0	0.62	0.65	-0.05	0.60	0.56	0.05
L1	North St Vrain Meadow	2542	-701	334,915	Active Beaver Meadow, Water Diversion (active), Gravel Pits (historic)	96.1	0.0	NA ¹	NA ¹	0.75	0.77	-0.04	0.19	0.12	0.12
L2	Horseshoe Park	2556	-1010	204,919	Active Beaver Meadow, Historic Structures (removed)	56.9	25.2	0.9	1.0	0.67	0.70	-0.06	0.39	0.38	0.00
L3	Hidden Valley Meadow	2798	-732	123,771	Loss of Beaver (recent), Road	52.6	4.3	0.8	1.8	0.72	0.72	0	0.26	0.21	0.20

1) P_{ww} and P_{ehw} was not calculated for L1 because the proximity ratio is not relevant when WW cover was nearly 100% of all landcover.

CHAPTER 5 – CONCLUSION

This dissertation presents novel techniques to describe the network configuration of river beads in river basins, quantify hydrologic connectivity in a river-floodplain system, and analyzed the role of climate, topography, human disturbance and wetland cover on river corridor vegetation productivity and climate sensitivity.

5.1 Key findings and implications

In chapter two, I developed and demonstrated an approach to identify river beads along river network segments. I then analyzed their network configuration in a case study of twenty basins in the Southern Rockies Ecoregion. Quantifying the configuration of river beads is a first step toward understanding and restoring network-scale hydrological and ecological function of river corridors. The result that there is high variability in the topology of river beads across both network position and between basins suggests that future work to understand interactive effects of river corridors in networks will need to consider a range of topologies to capture the observed variability across basins. These results also suggest that river beads along lower-order rivers are smaller and more widely spaced than in higher-order rivers but might have relatively larger influences because ratios of bead area to streamflow are higher. New metrics are suggested in this research that can help describe a river bead's network context and may reflect the potential of restoration within a river bead to improve hydrologic and ecosystem services.

In chapter three, I developed a field based approach to measure the strength of surface hydrologic connections between the river and aquatic sites within an intact beaver-influenced river-floodplain system. I demonstrated for the first time in river-floodplain systems that monitoring aquatic microbiomes can accurately depict patterns in presence/absence of surface flows from the source to

target sites. I further found that microbial memberships contained information on residence time dynamics along connected surface flow paths, suggesting that microbiomes could be useful tool for future hydrologic research. The developed metrics enabled the treating of connectivity as a continuous variable, thus improving our capability to describe spatiotemporal connectivity dynamics and identify characteristics of connectivity regimes such as the duration and timing of connectivity states. This advance may be useful for better linking hydrologic process to both site-level and system-wide ecologic, biogeochemical and physical dynamics such as biodiversity, nutrient uptake, and carbon cycling. The observation that peak system-wide variability in connectivity occurred at intermediate streamflow suggest heterogeneity in floodplain conditions may not always follow monotonic relationships with streamflow but rather can have nonlinearities that reflect interacting physical thresholds and hydrologic processes. The results also suggest that surface connectivity in these systems may be sensitive to changes to streamflow duration resulting from a changing climate.

In chapter four, I investigated the influence of geographic context, land cover, topography and disturbance history on the productivity and climate sensitivity of vegetation in river corridors throughout the Southern Rockies Ecoregion and in a case study in Rocky Mountain National Park. I found that wetlands, which comprise today only around a third of river corridor area, maintain high productivity even in river corridor segments within water limited landscapes. However, around half of existing wetland cover in the region lacked woody species cover. Based on the case study in Rocky Mountain National Park, wetlands without woody cover appeared to be a signal of historic and/or current ecologic and hydrologic disturbance. I demonstrated that this lack of woody cover in wetlands is linked across the region to higher sensitivity to inter-annual climate variability, suggesting productivity in these areas is more susceptible to drought and future changes to streamflow and climate. Wetlands with woody cover were clustered in proximity to rivers and maintain relatively low climate sensitivity. This was in the case even in landscapes with low climatic water availability, suggesting that river

connectivity is a critical component of maintaining highly productive and resilient habitats within river corridors.

5.2 Opportunities for Future Research

Restoring river corridor functions has increasingly been presented as a potential scalable solution with multiple ecologic and water resource benefits. Yet because of the complexity inherent in these systems, we remain surprisingly limited in our ability to measure, predict and model the hydrologic, geomorphic and ecologic influence of river corridors on the river network. This dissertation advances our understanding by introducing techniques for identifying river beads in the network in chapter two and for describing the complexity of their hydrologic regimes at field scales in chapter three. However, there remains many opportunities and gaps that need to be filled to advance our understanding on these topics. One clear need is to identify how network position and configuration of river beads impacts the role of river corridors in regulating key processes. River bead network topologies and the contextual network metrics for river beads suggested in chapter two could underpin hypothesis driven work to better understanding the role of these river beads in network processes. Observational studies, modeling and/or experimental flume-based studies would all be useful to study the effects on a process of interest (e.g., sediment retention, carbon fluxes or hydrologic storage) across gradients of network position (i.e., ratios of river bead size to streamflow) or within networks with diverging river bead network configurations.

A second research need is to connect hydrologic functioning in river-floodplains to ecologic and biogeochemical processes that influence the fluxes of water, nutrients and carbon through a river-floodplain system. A major advance would be to couple hydrologic measurements of connectivity developed in chapter three with in-out budgets of water, solutes, and in-situ measurement of biogeochemical processing across multiple river-floodplain systems. Because of the difficulties in scaling

such work, field based measurement would ideally be focused on informing and validating model development of coupled hydrologic and biogeochemical models that could be applied to make predictions across multiple river-floodplains within a network. A critical consideration in developing such field and model approaches is that hillslope contributions need also be included in flux budgets. Without such efforts, it can be difficult or impossible to isolate the impact of river-floodplains from those of their contributing areas.

As research in this field continues to develop, it will need to continue to contend with the challenges of measuring and modeling systems whose beneficial ecosystem functions emerge from highly dynamic behavior that varies widely in time and space and that is influenced by both internal behavior such as lateral hydrologic connectivity and external forcing such as climate variability and watershed scale processes. Thus, it is essential to begin to develop approaches that can consider behavior at both individual river corridor segments but also account for network and watershed influences across scales.

REFERENCES

- Abatzoglou, J. T. (2013). Development of gridded surface meteorological data for ecological applications and modelling. *International Journal of Climatology*, *33*(1), 121–131. <https://doi.org/https://doi.org/10.1002/joc.3413>
- Albano, C. M., McClure, M. L., Gross, S. E., Kitlasten, W., Soulard, C. E., Morton, C., & Huntington, J. (2019). Spatial patterns of meadow sensitivities to interannual climate variability in the Sierra Nevada. *Ecohydrology*, *12*(7), 1–20. <https://doi.org/10.1002/eco.2128>
- Albano, C. M., McGwire, K. C., Hausner, M. B., McEvoy, D. J., Morton, C. G., & Huntington, J. L. (2020). Drought Sensitivity and Trends of Riparian Vegetation Vigor in Nevada, USA (1985–2018). *Remote Sensing*, *12*(9), 1362. <https://doi.org/10.3390/rs12091362>
- Ali, G., Oswald, C., Spence, C., & Wellen, C. (2018). The T-TEL Method for Assessing Water, Sediment, and Chemical Connectivity. *Water Resources Research*, pp. 634–662. <https://doi.org/10.1002/2017WR020707>
- Allen, G. H., & Pavelsky, T. M. (2015). Patterns of river width and surface area revealed by the satellite-derived North American River Width data set, 395–402. <https://doi.org/10.1002/2014GL062764>. Received
- Amalfitano, S., Del Bon, A., Zoppini, A., Ghergo, S., Fazi, S., Parrone, D., ... Preziosi, E. (2014). Groundwater geochemistry and microbial community structure in the aquifer transition from volcanic to alluvial areas. *Water Research*, *65*, 384–394. <https://doi.org/10.1016/j.watres.2014.08.004>
- Amoros, C., & Bornette, G. (2002). Connectivity and biocomplexity in waterbodies of riverine floodplains. *Freshwater Biology*, *47*(4), 761–776. <https://doi.org/10.1046/j.1365-2427.2002.00905.x>
- Annis, A., Nardi, F., Morrison, R. R., & Castelli, F. (2019). Investigating hydrogeomorphic floodplain mapping performance with varying DTM resolution and stream order. *Hydrological Sciences Journal*, *64*(5), 525–538. <https://doi.org/10.1080/02626667.2019.1591623>
- Van Appledorn, M., Baker, M. E., & Miller, A. J. (2019). River-valley morphology, basin size, and flow-event magnitude interact to produce wide variation in flooding dynamics. *Ecosphere*, *10*(1). <https://doi.org/10.1002/ecs2.2546>
- Apprill, A., McNally, S., Parsons, R., & Weber, L. (2015). Minor revision to V4 region SSU rRNA 806R gene primer greatly increases detection of SAR11 bacterioplankton. *Aquatic Microbial Ecology*, *75*(2), 129–137. Retrieved from <https://www.int-res.com/abstracts/ame/v75/n2/p129-137/>
- Barnett, T. P., Adam, J. C., & Lettenmaier, D. P. (2005). Potential impacts of a warming climate on water availability in snow-dominated regions. *Nature*, *438*(7066), 303–309. <https://doi.org/10.1038/nature04141>
- Bellmore, J. R., & Baxter, C. V. (2014). EFFECTS OF GEOMORPHIC PROCESS DOMAINS ON RIVER ECOSYSTEMS: A COMPARISON OF FLOODPLAIN AND CONFINED VALLEY SEGMENTS. *River Research and Applications*, *30*(5), 617–630. <https://doi.org/10.1002/rra.2672>
- Belmont, P. (2011). Floodplain width adjustments in response to rapid base level fall and knickpoint migration. *Geomorphology*, *128*(1–2), 92–102. <https://doi.org/10.1016/j.geomorph.2010.12.026>
- Bernhardt, E. S., & Palmer, M. (2011). River Restoration : The Fuzzy Logic of Repairing Reaches to Reverse Catchment Scale Degradation River restoration : the fuzzy logic of repairing reaches to reverse catchment scale degradation, *21*(September), 1926–1931. <https://doi.org/10.2307/41416628>
- Bernhardt, E. S., Blaszcak, J. R., Ficken, C. D., Fork, M. L., Kaiser, K. E., & Seybold, E. C. (2017). Control Points in Ecosystems: Moving Beyond the Hot Spot Hot Moment Concept. *Ecosystems*. <https://doi.org/10.1007/s10021-016-0103-y>

- Beschta, R. L., & Ripple, W. J. (2012). The role of large predators in maintaining riparian plant communities and river morphology. *Geomorphology*, 157–158, 88–98. <https://doi.org/10.1016/j.geomorph.2011.04.042>
- Blodgett, D. (2018). nhdplusTools: Tools for Accessing and Working with the NHDPlus, version 0.3. 8.
- Bracken, L. J., & Croke, J. (2007). The concept of hydrological connectivity and its contribution to understanding runoff-dominated geomorphic systems. *Hydrological Processes*, 21(13), 1749–1763. <https://doi.org/10.1002/hyp.6313>
- Bracken, L. J., Wainwright, J., Ali, G. A., Tetzlaff, D., Smith, M. W., Reaney, S. M., & Roy, A. G. (2013). Concepts of hydrological connectivity: Research approaches, Pathways and future agendas. *Earth-Science Reviews*, 119, 17–34. <https://doi.org/10.1016/j.earscirev.2013.02.001>
- Brierley, G. J., & Fryirs, K. (2000). River styles, a geomorphic approach to catchment characterization: Implications for river rehabilitation in Bega catchment, New South Wales, Australia. *Environmental Management*, 25(6), 661–679.
- Briggs, M. A., Wang, C., Day-lewis, F. D., Williams, K. H., Dong, W., & Lane, J. W. (2019). Science of the Total Environment Return flows from beaver ponds enhance floodplain-to-river metals exchange in alluvial mountain catchments. *Science of the Total Environment*, 685, 357–369. <https://doi.org/10.1016/j.scitotenv.2019.05.371>
- Bywater-Reyes, S., Wilcox, A. C., & Diehl, R. M. (2017). Multiscale influence of woody riparian vegetation on fluvial topography quantified with ground-based and airborne lidar. *Journal of Geophysical Research: Earth Surface*, 122(6), 1218–1235. <https://doi.org/10.1002/2016JF004058>
- Cabezas, A., Garcia, M., Gallardo, B., Gonzalez, E., Gonzalez-Sanchis, M., & Comin, F. A. (2009). The effect of anthropogenic disturbance on the hydrochemical characteristics of riparian wetlands at the Middle Ebro River (NE Spain). *Hydrobiologia*, 617(1), 101–116. <https://doi.org/10.1007/s10750-008-9531-9>
- Cabezas, A., Gonzalez-Sanchis, M., Gallardo, B., & Comin, F. A. (2011). Using continuous surface water level and temperature data to characterize hydrological connectivity in riparian wetlands. *Environmental Monitoring and Assessment*, 183(1–4), 485–500. <https://doi.org/10.1007/s10661-011-1934-9>
- Caporaso, J. G., Lauber, C. L., Walters, W. A., Berg-Lyons, D., Lozupone, C. A., Turnbaugh, P. J., ... Knight, R. (2011). Global patterns of 16S rRNA diversity at a depth of millions of sequences per sample. *Proceedings of the National Academy of Sciences*, 108(Supplement 1), 4516 LP – 4522. <https://doi.org/10.1073/pnas.1000080107>
- Cheng, F. Y., & Basu, N. B. (2017). Biogeochemical hotspots: Role of small water bodies in landscape nutrient processing. *Water Resources Research*, 53(6), 5038–5056. <https://doi.org/10.1002/2016WR020102>
- Cohen, M. J., Creed, I. F., Alexander, L., Basu, N. B., Calhoun, A. J. K., Craft, C., ... Walls, S. C. (2016). Do geographically isolated wetlands influence landscape functions? *Proceedings of the National Academy of Sciences of the United States of America*, 113(8), 1978–1986. <https://doi.org/10.1073/pnas.1512650113>
- Collins, B. D., Montgomery, D. R., Fetherston, K. L., & Abbe, T. B. (2012). The floodplain large-wood cycle hypothesis: A mechanism for the physical and biotic structuring of temperate forested alluvial valleys in the North Pacific coastal ecoregion. *Geomorphology*, 139–140, 460–470. <https://doi.org/10.1016/j.geomorph.2011.11.011>
- Cooper, D. J., Chimner, R., & Merrit, D. (2012). Western mountain wetlands. In D. P. Batzer & A. H. Baldwin (Eds.), *Wetland Habitats of North America: Ecology and Conservation Concerns* (pp. 313–328).
- Covino, T. (2017). Hydrologic connectivity as a framework for understanding biogeochemical flux through watersheds and along fluvial networks. *Geomorphology*, 277, 133–144. <https://doi.org/10.1016/j.geomorph.2016.09.030>

- Cribari-Neto, F., & Zeileis, A. (2010). Beta regression in R. *Journal of Statistical Software*, *34*, 1–24.
- Crump, B. C., & Hobbie, J. E. (2005). Synchrony and seasonality in bacterioplankton communities of two temperate rivers. *Limnology and Oceanography*, *50*(6), 1718–1729. <https://doi.org/10.4319/lo.2005.50.6.1718>
- Crump, B. C., Amaral-zettler, L. A., & Kling, G. W. (2012). Microbial diversity in arctic freshwaters is structured by inoculation of microbes from soils, *6*(9), 1629–1639. <https://doi.org/10.1038/ismej.2012.9>
- Csardi, G., Nepusz, T., & others. (2006). The igraph software package for complex network research. *InterJournal, Complex Systems*, *1695*(5), 1–9.
- Doughty, M., Sawyer, A. H., Wohl, E., & Singha, K. (2020). Mapping Increases in Hyporheic Exchange from Channel-Spanning Logjams. *Journal of Hydrology*, 124931. <https://doi.org/10.1016/j.jhydrol.2020.124931>
- Douma, J. C., & Weedon, J. T. (2019). Analysing continuous proportions in ecology and evolution: A practical introduction to beta and Dirichlet regression. *Methods in Ecology and Evolution*, *10*(9), 1412–1430. <https://doi.org/10.1111/2041-210X.13234>
- Drummond, B. M. A. (2012). Southern Rockies Ecoregion.
- Dwire, K. A., Mellmann-Brown, S., & Gurrieri, J. T. (2018). Potential effects of climate change on riparian areas, wetlands, and groundwater-dependent ecosystems in the Blue Mountains, Oregon, USA. *Climate Services*, *10*(November 2017), 44–52. <https://doi.org/10.1016/j.cliser.2017.10.002>
- Fairfax, E., & Whittle, A. (2020). Smokey the Beaver: beaver-dammed riparian corridors stay green during wildfire throughout the western United States. *Ecological Applications*, *30*(8), 1–8. <https://doi.org/10.1002/eap.2225>
- Ferguson, R. I., Cudden, J. R., Hoey, T. B., & Rice, S. P. (2006). River system discontinuities due to lateral inputs: generic styles and controls. *Earth Surface Processes and Landforms: The Journal of the British Geomorphological Research Group*, *31*(9), 1149–1166.
- Fesenmyer, K. A., Dauwalter, D. C., Evans, C., & Allai, T. (2018). Livestock management, beaver, and climate influences on riparian vegetation in a semi-arid landscape. *PLoS One*, *13*(12), e0208928.
- Frissell, C. A., Liss, W. J., Warren, C. E., & Hurley, M. D. (1986). A hierarchical framework for stream habitat classification: Viewing streams in a watershed context. *Environmental Management*, *10*(2), 199–214. <https://doi.org/10.1007/BF01867358>
- Fritz, K. M., Schofield, K. A., Alexander, L. C., McManus, M. G., Golden, H. E., Lane, C. R., ... Pollard, A. I. (2018). Physical and Chemical Connectivity of Streams and Riparian Wetlands to Downstream Waters: A Synthesis. *JAWRA Journal of the American Water Resources Association*. <https://doi.org/10.1111/1752-1688.12632>
- Fryirs, K. A., Wheaton, J. M., & Brierley, G. J. (2016). An approach for measuring confinement and assessing the influence of valley setting on river forms and processes. *Earth Surface Processes and Landforms*, *41*(5), 701–710. <https://doi.org/10.1002/esp.3893>
- Gallant, J. C., & Dowling, T. I. (2003). A multiresolution index of valley bottom flatness for mapping depositional areas. *Water Resources Research*, *39*(12). <https://doi.org/10.1029/2002WR001426>
- Gangodagamage, C., Barnes, E., & Fofoula-Georgiou, E. (2007). Scaling in river corridor widths depicts organization in valley morphology. *Geomorphology*, *91*(3–4), 198–215. <https://doi.org/10.1016/j.geomorph.2007.04.014>
- Garbin, S., Celegon, E. A., Fanton, P., & Botter, G. (2019). Hydrological controls on river network connectivity. *Royal Society Open Science*, *6*(2). <https://doi.org/10.1098/rsos.181428>
- Gendaszek, A. S., Magirl, C. S., & Czuba, C. R. (2012). Geomorphic response to flow regulation and channel and floodplain alteration in the gravel-bedded Cedar River, Washington, USA. *Geomorphology*, *179*, 258–268.

<https://doi.org/10.1016/j.geomorph.2012.08.017>

- Gibson, P. P., & Olden, J. D. (2014). Ecology, management, and conservation implications of North American beaver (*Castor canadensis*) in dryland streams. *Aquatic Conservation: Marine and Freshwater Ecosystems*, 24(3), 391–409. <https://doi.org/10.1002/aqc.2432>
- Gilbert, J. T., Macfarlane, W. W., & Wheaton, J. M. (2016). The Valley Bottom Extraction Tool (V-BET): A GIS tool for delineating valley bottoms across entire drainage networks. *Computers and Geosciences*, 97, 1–14. <https://doi.org/10.1016/j.cageo.2016.07.014>
- Good, S. P., Urycki, D. R., & Crump, B. C. (2018). Predicting Hydrologic Function With Aquatic Gene Fragments. *Water Resources Research*, 54(3), 2424–2435. <https://doi.org/10.1002/2017WR021974>
- Grau, J., Liang, K., Ogilvie, J., Arp, P., Li, S., Robertson, B., & Meng, F. (2021). Improved Accuracy of Riparian Zone Mapping Using Near Ground Unmanned Aerial Vehicle and Photogrammetry Method.
- Hammond, J. C., Saavedra, F. A., & Kampf, S. K. (2018). How Does Snow Persistence Relate to Annual Streamflow in Mountain Watersheds of the Western U.S. With Wet Maritime and Dry Continental Climates? *Water Resources Research*, 54(4), 2605–2623. <https://doi.org/10.1002/2017WR021899>
- Harvey, J., & Gooseff, M. (2015). River corridor science: Hydrologic exchange and ecological consequences from bedforms to basins. *Water Resources Research*, 51(9), 6893–6922. <https://doi.org/10.1002/2015WR017617>
- Hauer, F. R., Locke, H., Dreitz, V. J., Hebblewhite, M., Lowe, W. H., Muhlfield, C. C., ... Rood, S. B. (2016). Gravel-bed river floodplains are the ecological nexus of glaciated mountain landscapes. *Science Advances*, 2(6). <https://doi.org/10.1126/sciadv.1600026>
- Helton, A. M., Poole, G. C., Payn, R. A., Izurieta, C., & Stanford, J. A. (2014). Relative influences of the river channel, floodplain surface, and alluvial aquifer on simulated hydrologic residence time in a montane river floodplain. *Geomorphology*, 205, 17–26. <https://doi.org/10.1016/j.geomorph.2012.01.004>
- Herdrich, A. T. (2016). *Effects of habitat complexity loss on eastern slope Rocky Mountain Brook Trout populations. ProQuest Dissertations and Theses*. Colorado State University, Ann Arbor. Retrieved from <https://ezproxy2.library.colostate.edu/login?url=https://www.proquest.com/dissertations-theses/effects-habitat-complexity-loss-on-eastern-slope/docview/1832312924/se-2?accountid=10223>
- Hijmans, R. J. (2021). Geographic Data Analysis and Modeling [R package raster version 3.4-10].
- Hoylman, Z. H., Jencso, K. G., Hu, J., Holden, Z. A., Allred, B., Dobrowski, S., ... Seielstad, C. (2019). The Topographic Signature of Ecosystem Climate Sensitivity in the Western United States. *Geophysical Research Letters*. <https://doi.org/10.1029/2019GL085546>
- Hughes, R. M., Kaufmann, P. R., & Weber, M. H. (2011). National and regional comparisons between Strahler order and stream size. *Journal of the North American Benthological Society*, 30(1), 103–121.
- Hunt, L. J. H., Fair, J., & Odland, M. (2018). Meadow Restoration Increases Baseflow and Groundwater Storage in the Sierra Nevada Mountains of California. *Journal of the American Water Resources Association*, 54(5), 1127–1136. <https://doi.org/10.1111/1752-1688.12675>
- Hynes, H. B. N. (1975). The stream and its valley. *SIL Proceedings, 1922-2010*, 19(1), 1–15. <https://doi.org/10.1080/03680770.1974.11896033>
- Jones, C. N., Scott, D. T., Edwards, B. L., & Keim, R. F. (2014). Perirheic mixing and biogeochemical processing in flow-through and backwater floodplain wetlands. *Water Resources Research*, 50(9), 7394–7405. <https://doi.org/10.1002/2014WR015647>
- Junk, W., Bayley, P. B., & Sparks, R. E. (1989). The flood pulse concept in river-floodplain-systems. *Canadian Journal of Fisheries and Aquatic Sciences*, 106(September 2014), 110–127.

<https://doi.org/10.1371/journal.pone.0028909>

- Karpack, M. N., Morrison, R. R., & McManamay, R. A. (2020). Quantitative assessment of floodplain functionality using an index of integrity. *Ecological Indicators*, *111*(December 2019), 106051. <https://doi.org/10.1016/j.ecolind.2019.106051>
- Khan, S., Fryirs, K. A., & Ralph, T. J. (2021). Geomorphic controls on the diversity and patterns of fluvial forms along longitudinal profiles. *Catena*, *203*(March), 105329. <https://doi.org/10.1016/j.catena.2021.105329>
- Klemas, V. (2011). Remote sensing of wetlands: case studies comparing practical techniques. *Journal of Coastal Research*, *27*(3), 418–427.
- Krause, B., Culmsee, H., Wesche, K., Bergmeier, E., & Leuschner, C. (2011). Habitat loss of floodplain meadows in north Germany since the 1950s. *Biodiversity and Conservation*, *20*(11), 2347–2364. <https://doi.org/10.1007/s10531-011-9988-0>
- Kuiper, J. J., Janse, J. H., Teurlincx, S., Verhoeven, J. T. A., & Alkemade, R. (2014). The impact of river regulation on the biodiversity intactness of floodplain wetlands. *Wetlands Ecology and Management*, *22*(6), 647–658. <https://doi.org/10.1007/s11273-014-9360-8>
- Laurel, D., & Wohl, E. (2019). The persistence of beaver-induced geomorphic heterogeneity and organic carbon stock in river corridors. *Earth Surface Processes and Landforms*, *44*(1), 342–353. <https://doi.org/10.1002/esp.4486>
- Lee Foote, A., Pandey, S., & Krogman, N. T. (1996). Processes of wetland loss in India. *Environmental Conservation*, *23*(1), 45–54. <https://doi.org/10.1017/s0376892900038248>
- Leibowitz, S. G., Wigington, P. J., Schofield, K. A., Alexander, L. C., Vanderhoof, M. K., & Golden, H. E. (2018). Connectivity of Streams and Wetlands to Downstream Waters: An Integrated Systems Framework. *Journal of the American Water Resources Association*, *54*(2), 298–322. <https://doi.org/10.1111/1752-1688.12631>
- Lindsay, J. B. (2018). WhiteboxTools user manual. *Geomorphometry and Hydrogeomatics Research Group, University of Guelph, Guelph, Canada*, 20.
- Lindström, E. S., Forslund, M., Algesten, G., & Bergström, A. K. (2006). External control of bacterial community structure in lakes. *Limnology and Oceanography*, *51*(1 1), 339–342. <https://doi.org/10.4319/lo.2006.51.1.0339>
- Lindström, E. S., Kamst-Van Agterveld, M. P., & Zwart, G. (2005). Distribution of typical freshwater bacterial groups is associated with pH, temperature, and lake water retention time. *Applied and Environmental Microbiology*, *71*(12), 8201–8206. <https://doi.org/10.1128/AEM.71.12.8201-8206.2005>
- Lining, K. B., Wohl, E., Rose, J. R., & Leisz, S. J. (2019). Significant Floodplain Soil Organic Carbon Storage Along a Large High-Latitude River and its Tributaries. *Geophysical Research Letters*, *46*(4), 2121–2129. <https://doi.org/10.1029/2018GL080996>
- Livers, B., & Wohl, E. (2016). Sources and interpretation of channel complexity in forested subalpine streams of the Southern Rocky Mountains. *Water Resources Research*, *52*(5), 3910–3929. <https://doi.org/10.1002/2015WR018306>
- Loheide, S. P., & Gorelick, S. M. (2007). Riparian hydroecology: A coupled model of the observed interactions between groundwater flow and meadow vegetation patterning. *Water Resources Research*, *43*(7), 1–16. <https://doi.org/10.1029/2006WR005233>
- Lynch, L. M., Sutfin, N. A., Feghel, T. S., Boot, C. M., Covino, T. P., & Wallenstein, M. D. (2019). River channel connectivity shifts metabolite composition and dissolved organic matter chemistry. *Nature Communications*, *10*(1). <https://doi.org/10.1038/s41467-019-08406-8>

- Macfarlane, W. W., Gilbert, J. T., Jensen, M. L., Gilbert, J. D., Hough-Snee, N., McHugh, P. A., ... Bennett, S. N. (2016). Riparian vegetation as an indicator of riparian condition: Detecting departures from historic condition across the North American West. *Journal of Environmental Management*, (November). <https://doi.org/10.1016/j.jenvman.2016.10.054>
- Manning, A., Julian, J. P., & Doyle, M. W. (2020). Riparian vegetation as an indicator of stream channel presence and connectivity in arid environments. *Journal of Arid Environments*, 178(August 2019), 104167. <https://doi.org/10.1016/j.jaridenv.2020.104167>
- Martínez-Carreras, N., Wetzel, C. E., Frentress, J., Ector, L., McDonnell, J. J., Hoffmann, L., & Pfister, L. (2015). Hydrological connectivity inferred from diatom transport through the riparian-stream system. *Hydrology and Earth System Sciences*, 19(7), 3133–3151. <https://doi.org/10.5194/hess-19-3133-2015>
- Mayr, M. J., Besemer, K., Sieczko, A., Demeter, K., & Peduzzi, P. (2020). Bacterial community composition and function along spatiotemporal connectivity gradients in the Danube floodplain (Vienna, Austria). *Aquatic Sciences*, 82(2). <https://doi.org/10.1007/s00027-020-0700-x>
- McLaughlin, B. C., Ackerly, D. D., Klos, P. Z., Natali, J., Dawson, T. E., & Thompson, S. E. (2017). Hydrologic refugia, plants, and climate change. *Global Change Biology*, 23(8), 2941–2961. <https://doi.org/10.1111/gcb.13629>
- McManamay, R. A., & Derolph, C. R. (2019). Data descriptor: A stream classification system for the conterminous United States. *Scientific Data*, 6, 1–18. <https://doi.org/10.1038/sdata.2019.17>
- McMurdie, P. J., & Holmes, S. (2013). phyloseq: An R Package for Reproducible Interactive Analysis and Graphics of Microbiome Census Data. *PLOS ONE*, 8(4), e61217. Retrieved from <https://doi.org/10.1371/journal.pone.0061217>
- Montgomery, D. R. (1999). Process domains and the river continuum 1. *JAWRA Journal of the American Water Resources Association*, 35(2), 397–410.
- Muggeo, V. (2008). Segmented: an R package to fit regression models with broken-line relationships. *R News*, 8(1), 20–25.
- Muggeo, V. (2020). *Selecting number of breakpoints in segmented regression: implementation in the R package segmented*. <https://doi.org/10.13140/RG.2.2.12891.39201>
- Nardi, F., Morrison, R. R., Annis, A., & Grantham, T. E. (2018). Hydrologic scaling for hydrogeomorphic floodplain mapping: Insights into human-induced floodplain disconnectivity. *River Research and Applications*, 34(7), 675–685. <https://doi.org/10.1002/rra.3296>
- Nardi, F., Vivoni, E. R., & Grimaldi, S. (2006). Investigating a floodplain scaling relation using a hydrogeomorphic delineation method. *Water Resources Research*, 42(9), 1–15. <https://doi.org/10.1029/2005WR004155>
- Nardi, F., Annis, A., Baldassarre, G. Di, Vivoni, E. R., & Grimaldi, S. (2019). GFPLAIN250m, a global high-resolution dataset of earth's floodplains. *Scientific Data*, 6, 1–6. <https://doi.org/10.1038/sdata.2018.309>
- Nemergut, D. R., Schmidt, S. K., Fukami, T., O'Neill, S. P., Bilinski, T. M., Stanish, L. F., ... Ferrenberg, S. (2013). Patterns and Processes of Microbial Community Assembly. *Microbiology and Molecular Biology Reviews*, 77(3), 342–356. <https://doi.org/10.1128/mubr.00051-12>
- Notebaert, B., & Piégay, H. (2013). Multi-scale factors controlling the pattern of floodplain width at a network scale: The case of the Rhône basin, France. *Geomorphology*, 200, 155–171. <https://doi.org/10.1016/j.geomorph.2013.03.014>
- O'Brien, G. R., Wheaton, J. M., Fryirs, K., Macfarlane, W. W., Brierley, G., Whitehead, K., ... Volk, C. (2019). Mapping valley bottom confinement at the network scale. *Earth Surface Processes and Landforms*, 44(9), 1828–1845. <https://doi.org/10.1002/esp.4615>

- Opperman, J. J., Luster, R., McKenney, B. A., Roberts, M., & Meadows, A. W. (2010). Ecologically functional floodplains: Connectivity, flow regime, and scale. *Journal of the American Water Resources Association*, 46(2), 211–226. <https://doi.org/10.1111/j.1752-1688.2010.00426.x>
- Parada, A. E., Needham, D. M., & Fuhrman, J. A. (2016). Every base matters: assessing small subunit rRNA primers for marine microbiomes with mock communities, time series and global field samples. *Environmental Microbiology*, 18(5), 1403–1414. <https://doi.org/10.1111/1462-2920.13023>
- Passalacqua, P., Belmont, P., Staley, D. M., Simley, J. D., Arrowsmith, J. R., Bode, C. A., ... Wheaton, J. M. (2015). Analyzing high resolution topography for advancing the understanding of mass and energy transfer through landscapes: A review. *Earth-Science Reviews*, 148, 174–193. <https://doi.org/10.1016/j.earscirev.2015.05.012>
- Pebesma, E. J. (2018). Simple features for R: standardized support for spatial vector data. *R J.*, 10(1), 439.
- Pekel, J.-F., Cottam, A., Gorelick, N., & Belward, A. S. (2016). High-resolution mapping of global surface water and its long-term changes. *Nature*, 540(7633), 418–422.
- Perry, L. G., Andersen, D. C., Reynolds, L. V., Nelson, S. M., & Shafroth, P. B. (2012). Vulnerability of riparian ecosystems to elevated CO₂ and climate change in arid and semiarid western North America. *Global Change Biology*, 18(3), 821–842. <https://doi.org/10.1111/j.1365-2486.2011.02588.x>
- Pettorelli, N., Vik, J. O., Mysterud, A., Gaillard, J.-M., Tucker, C. J., & Stenseth, N. C. (2005). Using the satellite-derived NDVI to assess ecological responses to environmental change. *Trends in Ecology & Evolution*, 20(9), 503–510.
- Pfister, L., McDonnell, J. J., Wrede, S., Matgen, P., & Fenicia, F. (2009). The rivers are alive : on the potential for diatoms as a tracer of water source and hydrological connectivity, 2845(June), 2841–2845. <https://doi.org/10.1002/hyp>
- Pinay, G., Bernal, S., Abbott, B. W., Lupon, A., Marti, E., Sabater, F., & Krause, S. (2018). Riparian corridors: A new conceptual framework for assessing nitrogen buffering across biomes. *Frontiers in Environmental Science*, 6(JUN), 1–11. <https://doi.org/10.3389/fenvs.2018.00047>
- Pollock, M. M., Beechie, T. J., Wheaton, J. M., Jordan, C. E., Bouwes, N., Weber, N., & Volk, C. (2014). Using beaver dams to restore incised stream ecosystems. *BioScience*, 64(4), 279–290. <https://doi.org/10.1093/biosci/biu036>
- Polvi, L. E., & Wohl, E. (2012). The beaver meadow complex revisited - the role of beavers in post-glacial floodplain development. *Earth Surface Processes and Landforms*, 37(3), 332–346. <https://doi.org/10.1002/esp.2261>
- Poole, G. C. (2002). Fluvial landscape ecology: addressing uniqueness within the river discontinuum. *Freshwater Biology*, 47(4), 641–660.
- Poole, G. C., Stanford, J. A., Frissell, C. A., & Running, S. W. (2002). Three-dimensional mapping of geomorphic controls on flood-plain hydrology and connectivity from aerial photos. *Geomorphology*, 48(4), 329–347. [https://doi.org/10.1016/S0169-555X\(02\)00078-8](https://doi.org/10.1016/S0169-555X(02)00078-8)
- Quast, C., Pruesse, E., Yilmaz, P., Gerken, J., Schweer, T., Yarza, P., ... Glöckner, F. O. (2013). The SILVA ribosomal RNA gene database project: improved data processing and web-based tools. *Nucleic Acids Research*, 41(Database issue), D590–D596. <https://doi.org/10.1093/nar/gks1219>
- R Core Team. (2016). R: A Language and Environment for Statistical Computing. Vienna, Austria. Retrieved from <https://www.r-project.org/>
- Rains, M. C., Leibowitz, S. G., Cohen, M. J., Creed, I. F., Golden, H. E., Jawitz, J. W., ... Mclaughlin, D. L. (2016). Geographically isolated wetlands are part of the hydrological landscape. *Hydrological Processes*, 30(1), 153–160. <https://doi.org/10.1002/hyp.10610>

- Rajib, A., Zheng, Q., Golden, H. E., Wu, Q., Lane, C. R., Christensen, J. R., ... Nardi, F. (2021). The changing face of floodplains in the Mississippi River Basin detected by a 60-year land use change dataset. *Scientific Data*, 8(1), 1–11. <https://doi.org/10.1038/s41597-021-01048-w>
- Read, D. S., Gweon, H. S., Bowes, M. J., Newbold, L. K., Field, D., Bailey, M. J., & Griffiths, R. I. (2014). Catchment-scale biogeography of riverine bacterioplankton. *The ISME Journal*, 9(2), 516–526. <https://doi.org/10.1038/ismej.2014.166>
- Rinderer, M., Ali, G., & Larsen, L. G. (2018). Assessing structural, functional and effective hydrologic connectivity with brain neuroscience methods: State-of-the-art and research directions. *Earth-Science Reviews*, 178(July 2017), 29–47. <https://doi.org/10.1016/j.earscirev.2018.01.009>
- Roley, S. S., Tank, J. L., Stephen, M. L., Johnson, L. T., Beaulieu, J. J., & Witter, J. D. (2012). Floodplain restoration enhances denitrification and reach-scale nitrogen removal in an agricultural stream. *Ecological Applications*, 22(1), 281–297. <https://doi.org/10.1890/11-0381.1>
- Roni, P., Hall, J. E., Drenner, S. M., & Arterburn, D. (2019). Monitoring the effectiveness of floodplain habitat restoration: A review of methods and recommendations for future monitoring. *Wiley Interdisciplinary Reviews: Water*, 6(4), e1355.
- Roux, C., Alber, A., Bertrand, M., Vaudor, L., & Piégay, H. (2015). “FluvialCorridor”: A new ArcGIS toolbox package for multiscale riverscape exploration. *Geomorphology*, 242, 29–37. <https://doi.org/10.1016/j.geomorph.2014.04.018>
- Salo, J. A., & Theobald, D. M. (2016). A Multi-Scale, Hierarchical Model to Map Riparian Zones. *River Research and Applications*, 32, 1709–1720.
- Samaritani, E., Shrestha, J., Fournier, B., Frossard, E., Gillet, F., Guenat, C., ... others. (2011). Heterogeneity of soil carbon pools and fluxes in a channelized and a restored floodplain section (Thur River, Switzerland). *Hydrology and Earth System Sciences*, 15(6), 1757–1769.
- Savio, D., Sinclair, L., Ijaz, U. Z., Parajka, J., Reischer, G. H., Stadler, P., ... Eiler, A. (2015). Bacterial diversity along a 2600km river continuum. *Environmental Microbiology*, 17(12), 4994–5007. <https://doi.org/10.1111/1462-2920.12886>
- Scheel, K., Morrison, R. R., Annis, A., & Nardi, F. (2019). Understanding the Large-Scale Influence of Levees on Floodplain Connectivity Using a Hydrogeomorphic Approach. *Journal of the American Water Resources Association*, 55(2), 413–429. <https://doi.org/10.1111/1752-1688.12717>
- Schloss, P. D., Westcott, S. L., Ryabin, T., Hall, J. R., Hartmann, M., Hollister, E. B., ... Weber, C. F. (2009). Introducing mothur: Open-Source, Platform-Independent, Community-Supported Software for Describing and Comparing Microbial Communities. *Applied and Environmental Microbiology*, 75(23), 7537 LP – 7541. <https://doi.org/10.1128/AEM.01541-09>
- Schneider, C., Flörke, M., De Stefano, L., & Petersen-Perlman, J. D. (2017). Hydrological threats to riparian wetlands of international importance - A global quantitative and qualitative analysis. *Hydrology and Earth System Sciences*, 21(6), 2799–2815. <https://doi.org/10.5194/hess-21-2799-2017>
- Sen, P. K. (1968). Estimates of the regression coefficient based on Kendall’s tau. *Journal of the American Statistical Association*, 63(324), 1379–1389.
- Silverman, N. L., Allred, B. W., Donnelly, J. P., Chapman, T. B., Maestas, J. D., Wheaton, J. M., ... Naugle, D. E. (2019). Low-tech riparian and wet meadow restoration increases vegetation productivity and resilience across semiarid rangelands. *Restoration Ecology*, 27(2), 269–278. <https://doi.org/10.1111/rec.12869>
- Smithson, M., & Verkuilen, J. (2006). A better lemon squeezer? Maximum-likelihood regression with beta-distributed dependent variables. *Psychological Methods*, 11(1), 54–71. [126](https://doi.org/10.1037/1082-</p>
</div>
<div data-bbox=)

- Sparacino, M. S., Rathburn, S. L., Covino, T. P., Singha, K., & Ronayne, M. J. (2019). Form-based river restoration decreases wetland hyporheic exchange: Lessons learned from the Upper Colorado River. *Earth Surface Processes and Landforms*, *44*(1), 191–203. <https://doi.org/10.1002/esp.4525>
- Stanford, J. A., WARD, J. V., LISS, W. J., FRISSELL, C. A., WILLIAMS, R. N., LICHTOWICH, J. A., & COUTANT, C. C. (1996). A General Protocol for Restoration of Regulated Rivers. *Regulated Rivers: Research & Management*, *12*(45), 391–413. [https://doi.org/10.1002/\(SICI\)1099-1646\(199607\)12:4/5<391::AID-RRR436>3.3.CO;2-W](https://doi.org/10.1002/(SICI)1099-1646(199607)12:4/5<391::AID-RRR436>3.3.CO;2-W)
- Stanford, J. A., & Ward, J. V. (1993a). An Ecosystem Perspective of Alluvial Rivers: Connectivity and the Hyporheic Corridor. *Journal of the North American Benthological Society*, *12*(1), 48–60. <https://doi.org/10.2307/1467685>
- Stanford, J. A., & Ward, J. V. (1993b). An Ecosystem Perspective of Alluvial Rivers: Connectivity and the Hyporheic Corridor. *Source Journal of the North American Benthological Society J. N. Am. Benthol. Soc.*, *12*(121), 48–6048. <https://doi.org/10.2307/1467685>
- Steiger, J., Tabacchi, E., Dufour, S., Corenblit, D., & Peiry, J. L. (2005). Hydrogeomorphic processes affecting riparian habitat within alluvial channel-floodplain river systems: A review for the temperate zone. *River Research and Applications*, *21*(7), 719–737. <https://doi.org/10.1002/rra.879>
- Stewart, I. T., Cayan, D. R., & Dettinger, M. D. (2005). Changes toward earlier streamflow timing across western North America. *Journal of Climate*, *18*(8), 1136–1155. <https://doi.org/10.1175/JCLI3321.1>
- Sutfin, N. A., Wohl, E. E., & Dwire, K. A. (2016). Banking carbon: A review of organic carbon storage and physical factors influencing retention in floodplains and riparian ecosystems. *Earth Surface Processes and Landforms*, *41*(1), 38–60. <https://doi.org/10.1002/esp.3857>
- Sutfin, N. A., Wohl, E., Feghel, T., Day, N., & Lynch, L. (2021). Logjams and channel morphology influence sediment storage, transformation of organic matter, and carbon storage within mountain stream corridors. *Water Resources Research*, *57*(5), e2020WR028046.
- Tennekes, M. (2018). tmap: Thematic Maps in R. *Journal of Statistical Software*, *84*(1), 1–39.
- Thomaz, S. M., Bini, L. M., & Bozelli, R. L. (2007). Floods increase similarity among aquatic habitats in river-floodplain systems. *Hydrobiologia*, *579*(1), 1–13. <https://doi.org/10.1007/s10750-006-0285-y>
- Thompson, L. R., Sanders, J. G., McDonald, D., Amir, A., Ladau, J., Locey, K. J., ... Consortium, T. E. M. P. (2017). A communal catalogue reveals Earth's multiscale microbial diversity. *Nature*, *551*(7681), 457–463. <https://doi.org/10.1038/nature24621>
- Tockner, K., & Stanford, J. A. (2002a). Riverine flood plains: present state and future trends. *Environmental Conservation*, *29*(3), 308–330. <https://doi.org/10.1017/S037689290200022X>
- Tockner, K., & Stanford, J. A. (2002b). Riverine flood plains: Present state and future trends. *Environmental Conservation*, *29*(3), 308–330. <https://doi.org/10.1017/S037689290200022X>
- Tockner, K., Malard, F., & Ward, J. V. (2000). An extension of the flood pulse concept. *Hydrological Processes*, *14*(16–17), 2861–2883. [https://doi.org/10.1002/1099-1085\(200011/12\)14:16/17<2861::AID-HYP124>3.0.CO;2-F](https://doi.org/10.1002/1099-1085(200011/12)14:16/17<2861::AID-HYP124>3.0.CO;2-F)
- Tockner, K., Malard, F., Uehlinger, U., & Ward, J. V. (2002). Nutrients and organic matter in a glacial river – floodplain system (Val Roseg ,. *Limnology and Oceanography*, *47*(1), 266–277. <https://doi.org/10.4319/lo.2002.47.1.0266>
- Tomscha, S. A., Gergel, S. E., & Tomlinson, M. J. (2017). The spatial organization of ecosystem services in river-floodplains. *Ecosphere*, *8*(3). <https://doi.org/10.1002/ecs2.1728>

- Tomsett, C., & Leyland, J. (2019). Remote sensing of river corridors: A review of current trends and future directions. *River Research and Applications*, 35(7), 779–803. <https://doi.org/10.1002/rra.3479>
- Trimble, S. W., & Mendel, A. C. (1995). The cow as a geomorphic agent—a critical review. *Geomorphology*, 13(1–4), 233–253.
- Turnbull, L., Wainwright, J., & Brazier, R. E. (2008). A conceptual framework for understanding semi-arid land degradation: ecohydrological interactions across multiple-space and time scales. *Ecohydrology*, 1(1), 23–34. <https://doi.org/10.1002/eco.4>
- Vannote, R. L., Minshall, G. W., Cummins, K. W., Sedell, J. R., & Cushing, C. E. (1980). The River Continuum Concept. *Canadian Journal of Fisheries and Aquatic Sciences*, 37(1), 130–137. <https://doi.org/10.1139/f80-017>
- Walter, R. C., & Merritts, D. J. (2015). Natural Streams of Water-Powered and the Legacy Mills. *American Association for the Advancement of Science*, 319(5861), 299–304.
- Ward, A. S., & Packman, A. I. (2019). Advancing our predictive understanding of river corridor exchange. *Wiley Interdisciplinary Reviews: Water*, 6(1), e1327. <https://doi.org/10.1002/wat2.1327>
- Ward, J. V. (1989). The Four-Dimensional Nature of Lotic Ecosystems Author (s): J . V . Ward Source : Journal of the North American Benthological Society , Vol . 8 , No . 1 (Mar . , 1989), Published by : The University of Chicago Press on behalf of the Society for Freshwa. *Journal of the North American Benthological Society*, 8(1), 2–8.
- Ward, J. V., & Stanford, J. A. (1995). The serial discontinuity concept: Extending the model to floodplain rivers. *Regulated Rivers: Research & Management*, 10(2–4), 159–168. <https://doi.org/10.1002/rrr.3450100211>
- Ward, J. V., & Stanford, J. A. (1995). Ecological connectivity in alluvial river ecosystems and its disruption by flow regulation. *Regulated Rivers: Research & Management*, 11(1), 105–119. <https://doi.org/10.1002/rrr.3450110109>
- Westbrook, C. J., Cooper, D. J., & Baker, B. W. (2011). Beaver assisted river valley formation. *River Research and Applications*, 27(2), 247–256. <https://doi.org/10.1002/rra.1359>
- Westbrook, Cherie J., Cooper, D. J., & Baker, B. W. (2006). Beaver dams and overbank floods influence groundwater-surface water interactions of a Rocky Mountain riparian area. *Water Resources Research*, 42(6), 1–12. <https://doi.org/10.1029/2005WR004560>
- Whitaker, S., Stanislawski, L., & Hamann, M. (2002). Automated stream leveling for the high-resolution national hydrography dataset. In *Proceedings of the 22nd Annual ESRI International User Conference, San Diego, CA, USA* (pp. 8–12).
- Wohl, E. (2006). Human impacts to mountain streams. *Geomorphology*, 79(3–4), 217–248. <https://doi.org/10.1016/j.geomorph.2006.06.020>
- Wohl, E. (2013a). Floodplains and wood. *Earth-Science Reviews*, 123, 194–212. <https://doi.org/10.1016/j.earscirev.2013.04.009>
- Wohl, E. (2013b). Landscape-scale carbon storage associated with beaver dams. *Geophysical Research Letters*, 40(14), 3631–3636. <https://doi.org/10.1002/grl.50710>
- Wohl, E. (2014). *Rivers In the Landscape*. Wiley–Blackwell.
- Wohl, E., & Iskin, E. (2019). Patterns of Floodplain Spatial Heterogeneity in the Southern Rockies, USA. *Geophysical Research Letters*, 46(11), 5864–5870. <https://doi.org/10.1029/2019GL083140>
- Wohl, E., & Scott, D. N. (2017). Wood and sediment storage and dynamics in river corridors. *Earth Surface Processes and Landforms*, 42(1), 5–23. <https://doi.org/10.1002/esp.3909>

- Wohl, E., Lininger, K. B., & Scott, D. N. (2017). River beads as a conceptual framework for building carbon storage and resilience to extreme climate events into river management. *Biogeochemistry*, 1–19. <https://doi.org/10.1007/s10533-017-0397-7>
- Wohl, E., Brierley, G., Cadol, D., Coulthard, T. J., Covino, T., Fryirs, K. A., ... Sklar, L. S. (2019). Connectivity as an emergent property of geomorphic systems. *Earth Surface Processes and Landforms*, 44(1), 4–26. <https://doi.org/10.1002/esp.4434>
- Wohl, E., Castro, J., Cluer, B., Merritts, D., Powers, P., & Staab, B. (2021). Rediscovering , Reevaluating , and Restoring Lost River-Wetland Corridors, 9(June), 1–21. <https://doi.org/10.3389/feart.2021.653623>
- Wolf, E. C., Cooper, D. J., & Hobbs, N. T. (2007). Hydrologic regime and herbivory stabilize an alternative state in Yellowstone National Park. *Ecological Applications*, 17(6), 1572–1587. <https://doi.org/10.1890/06-2042.1>
- Yang, L., Jin, S., Danielson, P., Homer, C., Gass, L., Bender, S. M., ... others. (2018). A new generation of the United States National Land Cover Database: Requirements, research priorities, design, and implementation strategies. *ISPRS Journal of Photogrammetry and Remote Sensing*, 146, 108–123.
- Yang, X., Pavelsky, T. M., Allen, G. H., & Donchyts, G. (2020). RivWidthCloud: An Automated Google Earth Engine Algorithm for River Width Extraction from Remotely Sensed Imagery. *IEEE Geoscience and Remote Sensing Letters*, 17(2), 217–221. <https://doi.org/10.1109/LGRS.2019.2920225>

APPENDIX 1 - SUPPLEMENTAL INFORMATION – CHAPTER 2

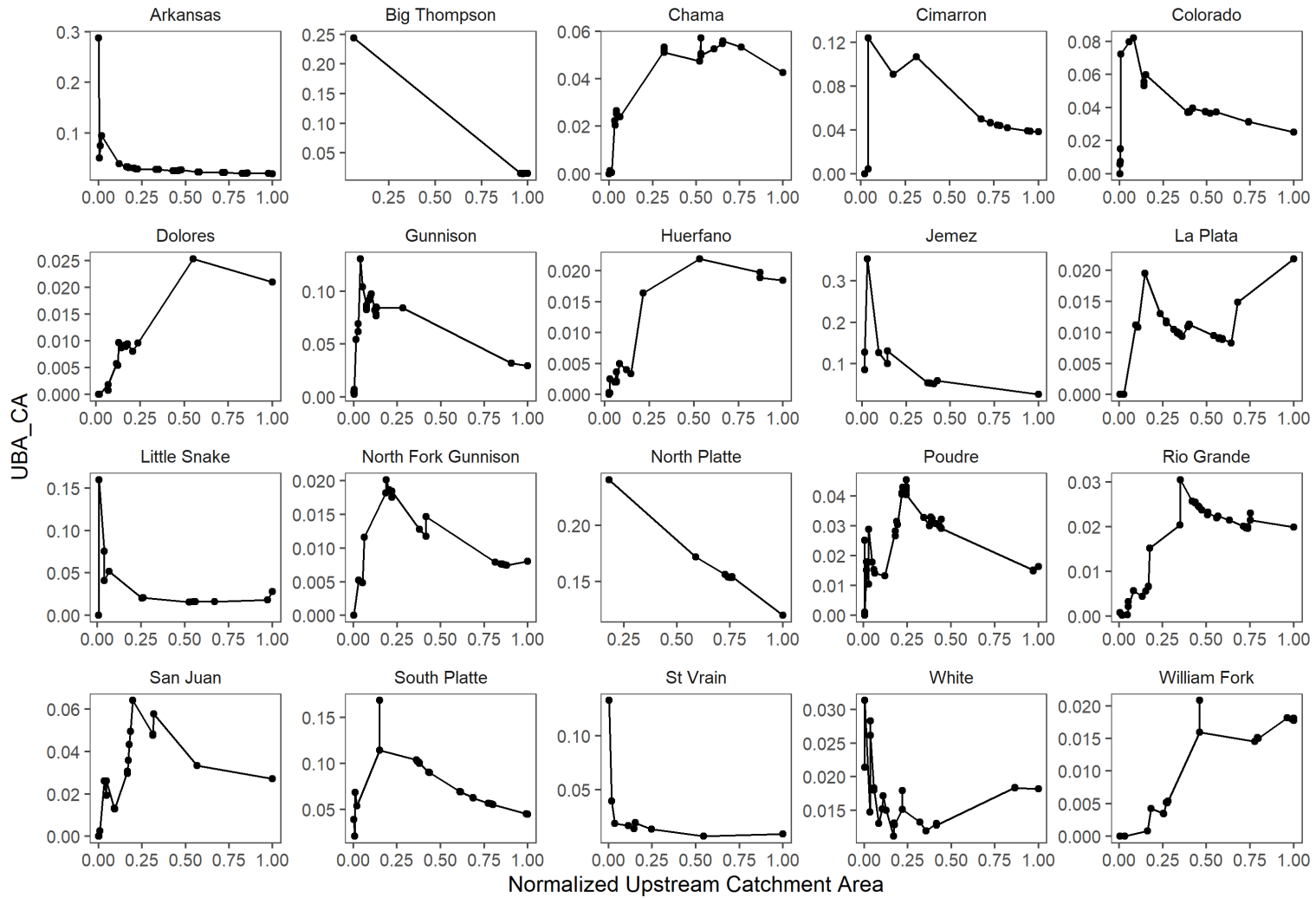


Fig S1: Proportions of up-network accumulated bead area to up-network accumulated catchment area along mainstem segments at study basin. X-axis is the catchment area at mainstem segments normalized by catchment area of the full basin.

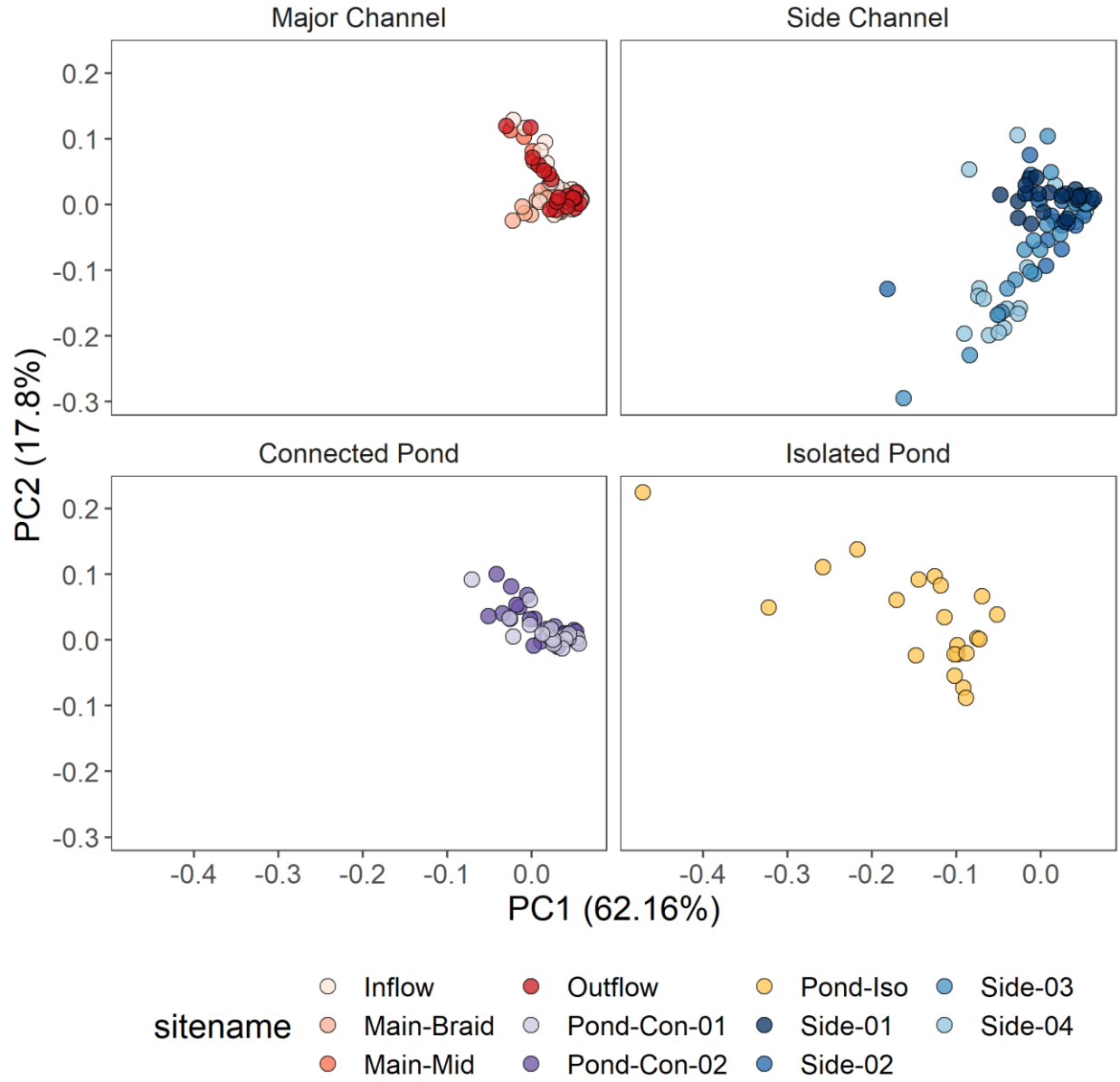


Figure S2: PCA of Geochemical Data by Site Type

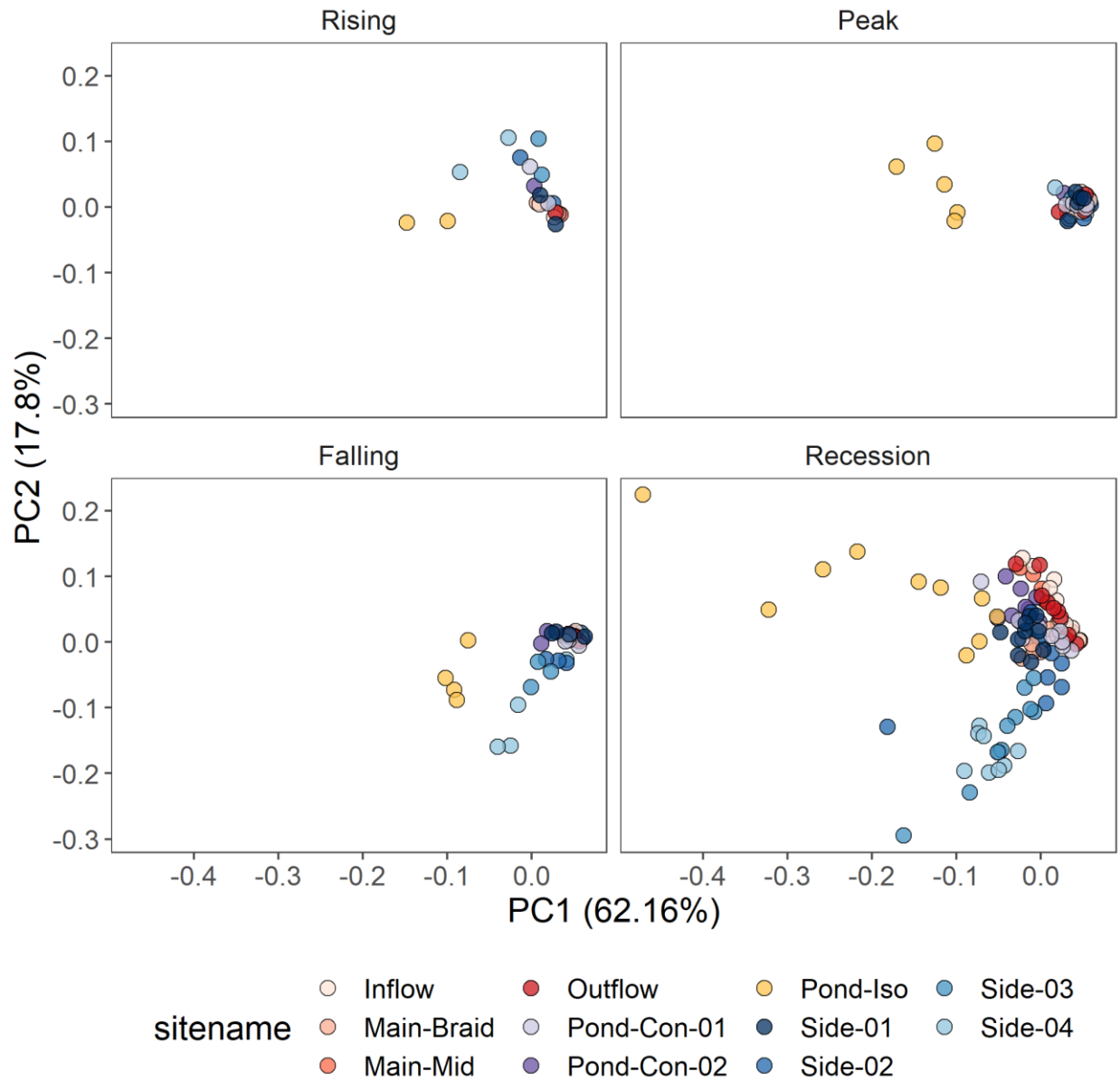


Figure S3: PCA of Geochemical Data by Hydro Period

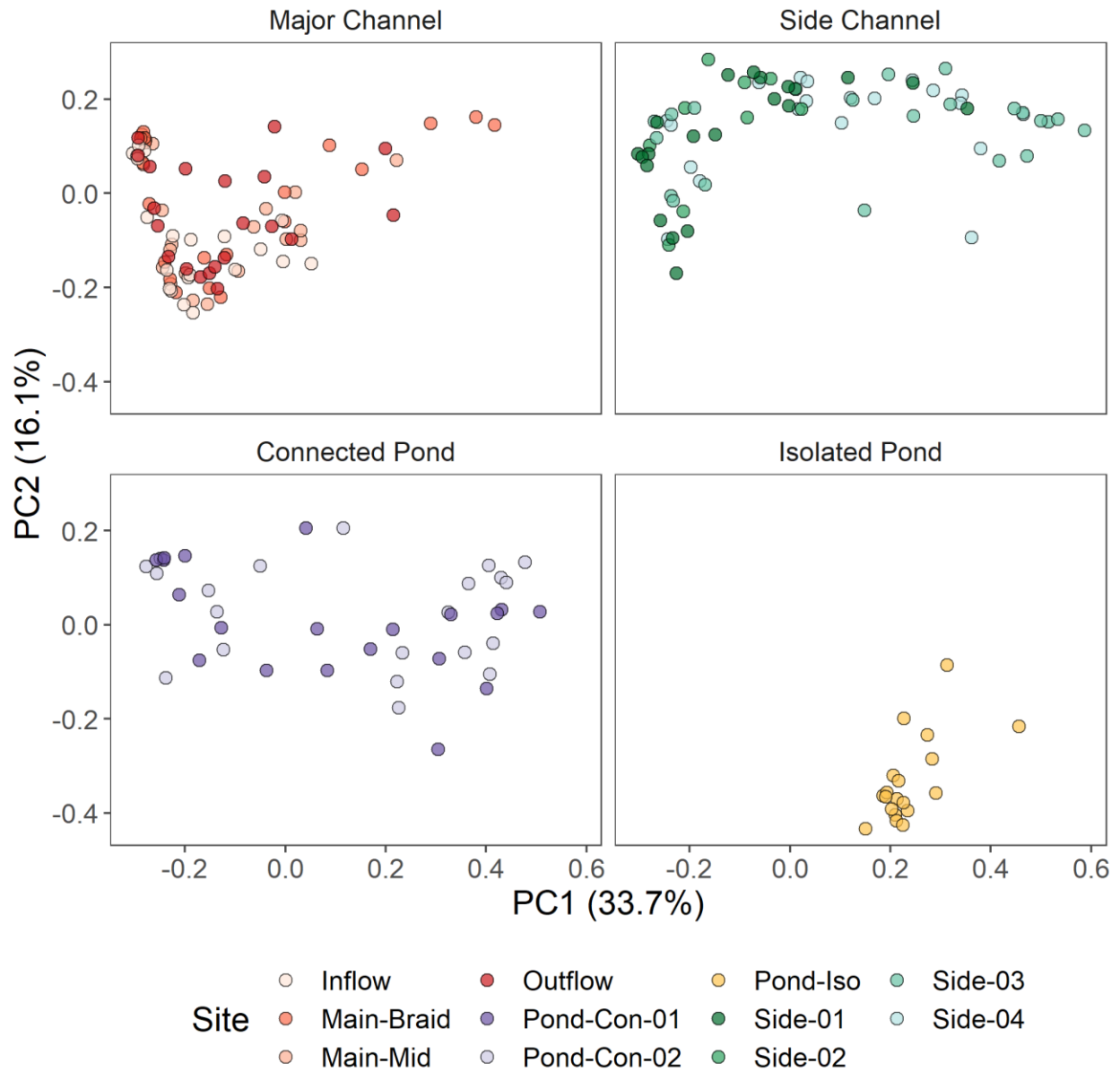


Figure S4: PCOA of Site Microbiomes by Site Type

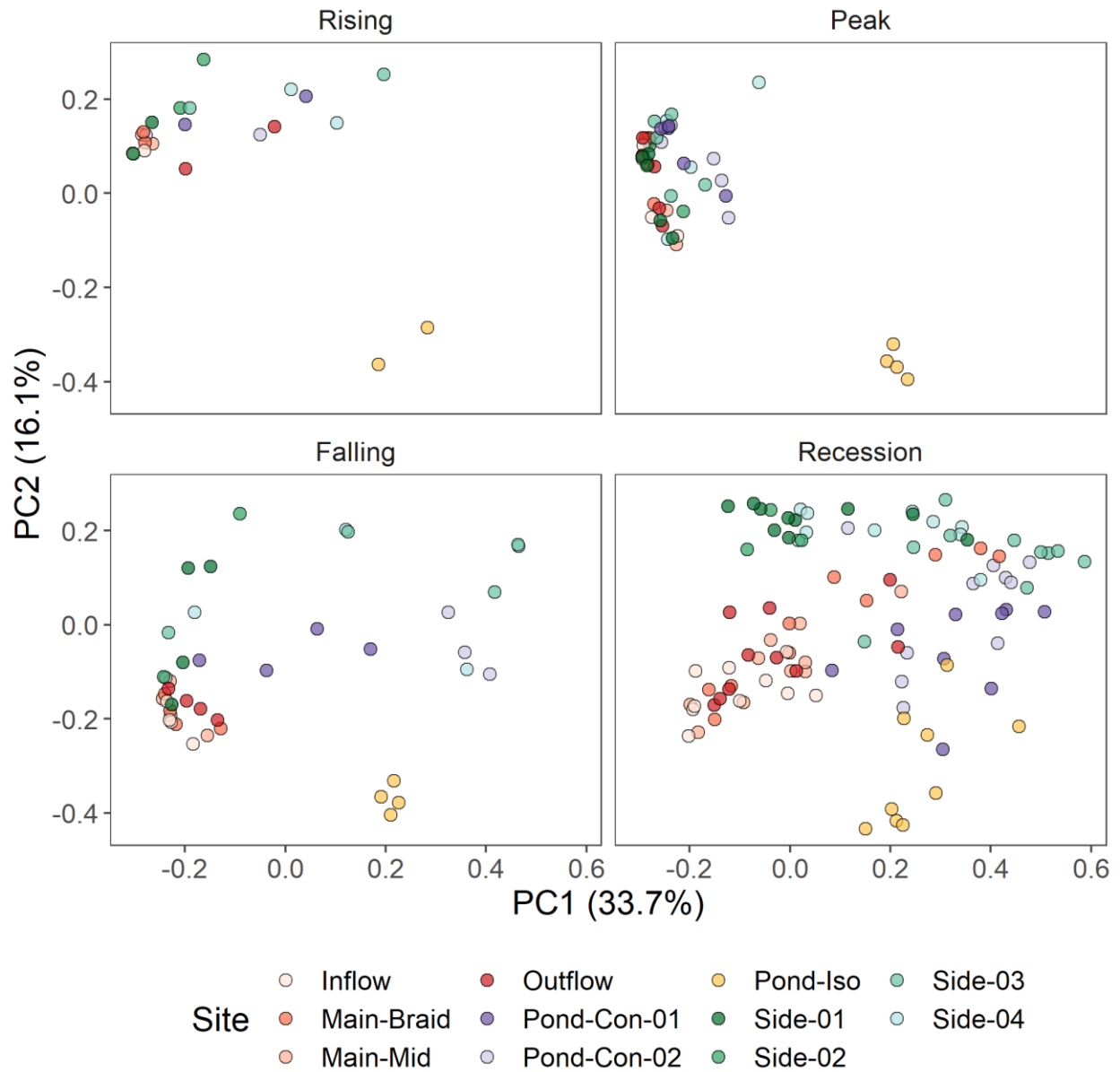


Figure S5: PCOA of Site Microbiomes by Hydro Period

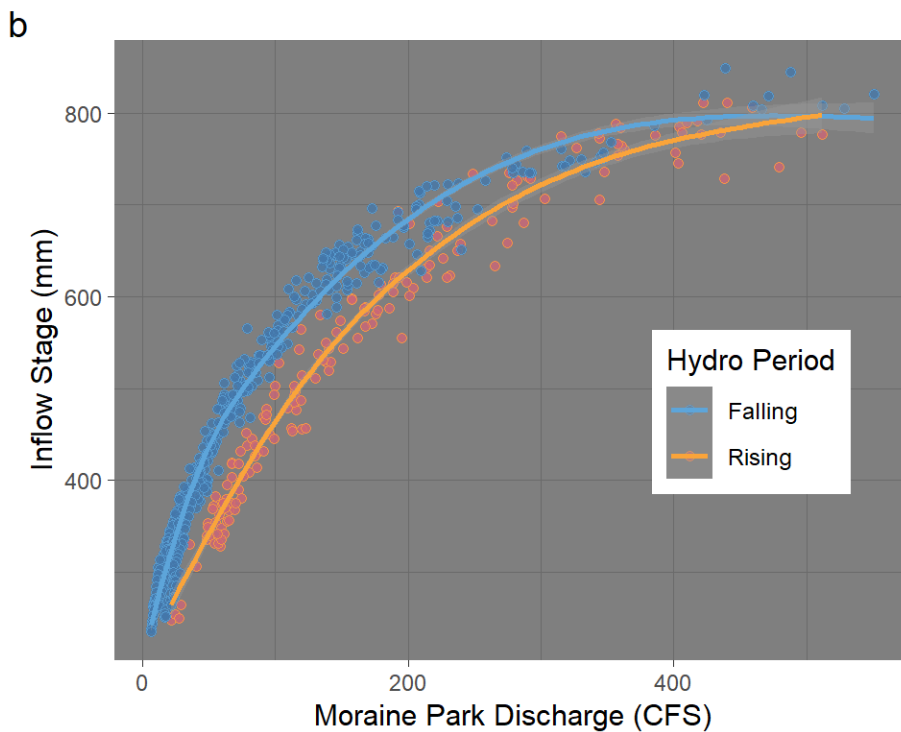
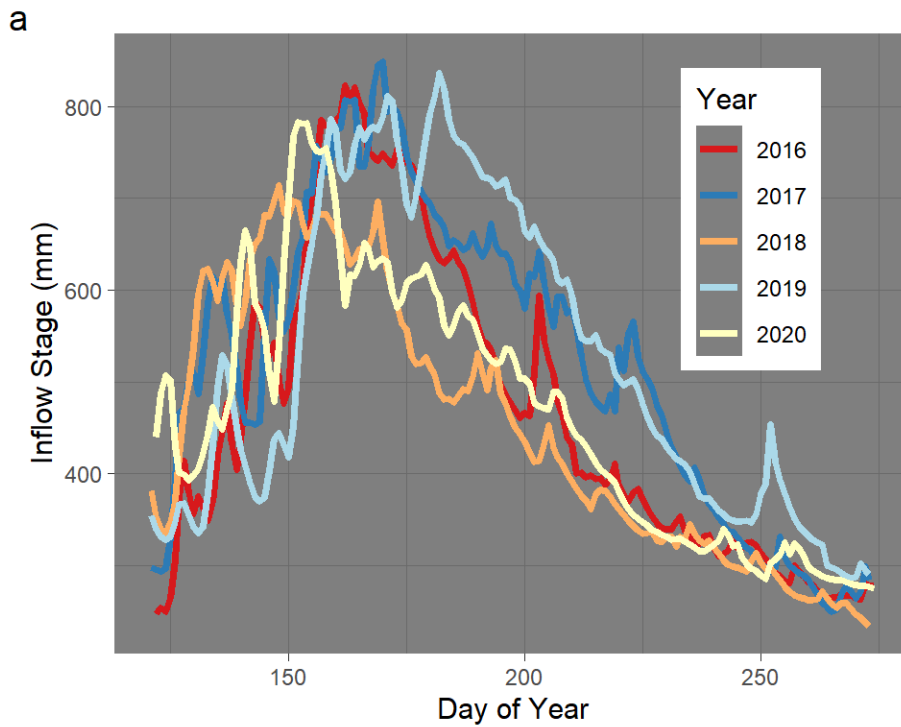


Figure S6: (a) Interpolated Stage for 2016 through 2020 at the Inflow site along the North St Vrain river with gap filling using (b) spline regression between Inflow Stage and nearby USGS gage at Moraine Park. Due to hysteresis between the two sites, two spline fits were generated, one for the rising limb and another for the falling limb.

Table S1. Connectivity thresholds for target sites in 2018 using relative stage, and geochemical and microbial connectivity strength metrics. I_{st} is the Inflow stage at which an inflection point was identified with broken fit regressions between the source site (Inflow) and all target sites. I_{geo} and I_{micro} are the Inflow stage where σ equals 0.5 for geochemistry and microbial metrics respectively. Missing thresholds for I_{geo} and I_{micro} reflect sites where σ never went below or above the 0.5 threshold.

Sitename	<i>Relative Stage Analysis (Broken Line Fit Regression)</i>							<i>Connectivity Strength (σ) (where $\sigma = 0.5$)</i>	
	I_{st1}	I_{st2}	S1	S2	S3	Slope $_{\Delta 1}$	Slope $_{\Delta 2}$	I_{micro}	I_{geo}
Main-Braid	301	406	0.002	0.012	0.005	-0.010	0.007	306	337
Main-Mid	455	610	0.007	0.006	0.009	0.002	-0.003	-	-
Outflow	645		0.007	0.009		-0.003		-	-
Pond-Con-01	366		0.008	- 0.002		0.010		438	381
Pond-Con-02	613		0.008	- 0.002		0.009		578	561
Pond-Iso	389		0.029	0.003		0.026		-	-
Side-01	285	482	- 0.005	0.003	0.010	-0.008	-0.007	471	534
Side-02	354	667	0.014	0.005	0.008	0.008	-0.002	552	553
Side-03	425	526	0.003	0.015	0.004	-0.012	0.011	575	579
Side-04	612		- 0.002	0.008	0.014	-0.010	-0.006	589	657

Table S2: Geochemistry PCA Eigenvectors and % Variance Explained

Ions	PC1	PC2	PC3	PC4	PC5	PC6
Na	-0.48	0.13	-0.01	0.55	-0.30	-0.59
K	-0.46	0.01	0.42	-0.36	0.63	-0.29
Mg	-0.44	-0.30	-0.39	0.41	0.41	0.48
Ca	-0.40	-0.36	-0.44	-0.60	-0.38	-0.11
Cl	-0.44	0.23	0.51	-0.05	-0.42	0.56
SO4	-0.13	0.84	-0.47	-0.18	0.13	0.06
% Variance Explained	0.62	0.18	0.13	0.05	0.02	0.01